Fall 2021

Investigating the transport, fate, and behavior of microplastics in estuarine systems through the application of metal-doped polystyrene analogs using spICP-MS

Robert Rauschendorfer
Western Washington University, rauschr@wwu.edu

Investigating the transport, fate, and behavior of microplastics in estuarine systems through the application of metal-doped polystyrene analogs using spICP-MS

By

Robert Rauschendorfer

Accepted in Partial Completion
of the Requirements for the Degree
Master of Science

ADVISORY COMMITTEE

Dr. Manuel Montaño

Dr. Jenise Bauman

Dr. David Rider

Dr. Ruth Sofield

GRADUATE SCHOOL

David L. Patrick

Master's Thesis

In presenting this thesis in partial fulfillment of the requirements for a master's degree at Western Washington University, I grant to Western Washington University the non-exclusive royalty-free right to archive, reproduce, distribute, and display the thesis in any and all forms, including electronic format, via any digital library mechanisms maintained by WWU.

I represent and warrant this is my original work and does not infringe or violate any rights of others. I warrant that I have obtained written permissions from the owner of any third party copyrighted material included in these files.

I acknowledge that I retain ownership rights to the copyright of this work, including but not limited to the right to use all or part of this work in future works, such as articles or books.

Library users are granted permission for individual, research and non-commercial reproduction of this work for educational purposes only. Any further digital posting of this document requires specific permission from the author.

Any copying or publication of this thesis for commercial purposes, or for financial gain, is not allowed without my written permission.

Robert Rauschendorfer

Date: 11/23/2021

Investigating the transport, fate, and behavior of microplastics in estuarine systems through the application of metal-doped polystyrene analogs using spICP-MS

A Thesis
Presented to
The Faculty of
Western Washington University

In Partial Fulfillment
Of the Requirements for the Degree
Master of Science

by
Robert Rauschendorfer
November 2021

Abstract

Plastics are a group of materials that are mass produced for their unique properties including durability. This has led to plastics becoming a global contaminant as a bulk material and as micro and nano sized particles termed microplastics and nanoplastics (MP/NPs), respectively. As awareness to MP/NPs has grown, these contaminants are found to be ubiquitous yet the risk to environmental systems remained unclear. Toxicity studies have been performed but the transport, fate, and behavior of these contaminants remains limited by the selectivity and sensitivity of the commonly used analytical techniques. To address this deficiency, MP/NP tracers have been developed using isotopic, fluorescent, and metallic labels to enable particle detection in environmental and biological environments. Herein, I describe the application of polystyrene (PS) tracers containing internalized gold nanoparticles to investigate the transport, fate, and behavior of colloidal plastics in an estuarine system. The performed experiments investigated the PS tracers' ability to remain suspended as a function of water chemistry and upon equilibration with sediment. Water chemistry was evaluated through varied salinity and dissolved organic carbon (DOC) concentrations while sediment was collected around Bellingham Bay and paired with synthetic fresh and marine water. Evaluation of the PS tracers was performed on an individual basis using single particle inductively coupled plasma-mass spectrometry (spICP-MS) to determine the quantity of suspended particles. The results from aqueous settling experiments found that salinity quickly increased PS tracer aggregation while DOC was a stabilizing agent at higher concentrations, as statistically evaluated using ANOVA and Tukey's HSD. Likewise, water type and sediment interactions were both significant factors (Welch's ANOVA and ANOVA) in PS tracer capture and deposition resulting in a near total PS tracer capture (approximately 99.5 – 87.0%). This study demonstrated the versatility of MP/NP metallic tracers coupled with spICP-MS for evaluating the transport, fate, and behavior of MP/NPs in complex environments.

Acknowledgements

I would like to thank my advisor, Dr. Manuel Montaño, and the members of my committee, Dr. Jenise Bauman, Dr. David Rider, and Dr. Ruth Sofield, for providing their support and guidance that aided in the completion of this Masters thesis. This gratitude is extended further to the combined research group of Dr. Steven Emory and Dr. David Rider that synthesized the materials required for this study to be performed. In addition, I would like to thank the members of the Huxley College of the Environment for providing assistance, guidance, and equipment that made this study possible. Lastly, I would like to thank my family and friends for their unconditional support through this endeavor and hope this accomplishment serves as a testament to their support.

Table of Contents

Page

Abbreviations

AFM	Atomic Force Microscopy
AuNP	Gold Nanoparticle
BC	Black Carbon
CS	Coarse Sand
CTO	Chemo-thermal Oxidation
DART-MS	Direct Analysis in Real Time-High Resolution Mass Spectrometry
DLS	Dynamic Light Scattering
DLVO Theory	Derjaguin, Landau, Verwey, and Overbeek Theory
DOC	Dissolved Organic Carbon
DOM	Dissolved Organic Matter
EA	Elemental Analyzer
EPA MHW	Environmental Protection Agency Moderately Hard Water
FAAS	Flame Atomic Absorption Spectrometry
Fisher's LSD	Fisher's Least Significant Difference
FS	Fine Sand
FTIR	Fourier-Transformed Infrared
IC	Inorganic Carbon
ICP-MS	Inductively Coupled Mass Spectrometry
IO	Instant Ocean
LC	Labile Carbon
MALDI-TOF MS	Matrix Assisted Laser Desorption Ionization Time of Flight Mass Spectrometry
MP	Microplastic
MP/NP	Micro and Nanoplastic
MS	Medium Sand
NP	Nanoparticle
PA	Polyamide

PE	Polyethylene
PET	Polyethylene Terephthalate
PMMA	Polymethyl Methacrylate
PS	Polystyrene
PS-co-P2VP	Polystyrene-Poly(2-Vinylpyridine) Co-Polymer
PUR	Polyurethane
PVC	Polyvinylchloride
Py-GC-MS	Pyrolysis Gas Chromatography-Mass Spectrometry
SD	Standard Deviation
Sed-FFF	Sedimentation Field Flow Fractionation
SEM	Scanning Electron Microscopy
spICP-MS	Single Particle Inductively Coupled Mass Spectrometry
SRHA	Suwannee River Humic Acid
STEM	Scanning Transmission Electron Microscopy
TC	Total Carbon
TED-GC-MS	Thermal Extraction Desorption Gas Chromatography Mass Spectrometry
TGA	Thermogravimetric Analysis
Tukey's HSD	Tukey's Honest Significant Different
VFS	Very Fine Sand
WWTP	Wastewater Treatment Plant

List of Figures and Tables

Figures

Tables

Appendix: Figures

Chapter 1: Introduction

1.1 Plastic Production and Waste

The emergence of synthetic polymers began with the pursuit of materials that could be molded and their shape retained[1,2]. Bakelite, the first synthetic polymer created in 1907, was quickly followed by the development of other synthetic polymers sparking a technological revolution[1,2]. Plastics are inexpensive, versatile, lightweight, and durable, displacing many conventional materials for use in packaging (35.9% or 146 Mt), building and construction (16.0%; 65 Mt), and textiles (14.5%; 59 Mt) annually as of 2015[3-5]. The growth in plastic production has paralleled global demand while future projections predict a continual increase in production and waste following current trends[5,6].

Plastics soft materials are formed from the linkage of organic monomers produce a polymer chain. For the vast majority of plastic materials, the polymer chains contain a carbon backbone with two associated pendant groups[7,8]. These polymer chains can be expansive affording thousands of linked monomers, while the pendant groups and intermolecular forces between chains give rise to unique chemical properties[8]. From an economic standpoint, the main commercially produced plastics are polyethylene (PE; 38.2% of global plastic production as of 2016), polypropylene (PP; 22.4%), polyvinylchloride (PVC; 12.5%), polyethylene terephthalate (PET; 10.9%), polyurethane (PUR; 8.9%), polystyrene (PS; 4.6%), and polyamide (PA; 2.6%)[3,7,9]. In addition to the plastic, chemical additives can be introduced to plastics that alter the materials' properties to ward off degradative processes. Common additives include plasticizers, antioxidants, heat stabilizers, slip agents, colorants, fillers, metals, and reinforcements that can leach from the plastic[3,10]. From the possible combinations of polymer types and additives, plastics are a complex material suited for a variety of applications and can act as a complex contaminant upon being discarded.

The majority of plastic products are designed for single-use or have a short shelf-life generating considerable strain on maintaining adequate methods for plastic disposal[3,9,11]. The current disposal routes of plastic vary from being recycled, incinerated, stored, or dumped. Recycling is regarded as the most environmentally-conscious method of disposal but for most plastics, this method is not viable. As only certain thermoplastics are economically feasible to be repurposed, it is estimated that less than 10% of plastics could even be considered for recycling[12,13]. The incineration of plastics is another method that accounts for approximately 12% of plastic disposal[14]. With sufficiently high temperatures, plastics may be reduced to mostly carbon dioxide and water, but this requires complete combustion and toxic halogenated compounds that could still be released often as airborne contaminants[3,14]. If incomplete combustion occurs, soot and solid residue ash are produced that are comprised of volatile organic and black carbon compounds that lead to a host of environmental and human health issues[3,14]. As recycling and incineration account for a minority of plastic waste, the majority has amassed in landfills, which have rapidly filled, leading to more plastic waste finding entrance into the environment[3,14]. To address the buildup of plastic waste, several key countries have previously opted for large-scale exportation of plastic waste, often to Asia; but as of 2018, China, the largest acceptor, began rejecting foreign waste[15,16]. All of this amounts to plastic being one of the largest forms of waste and its continual buildup has led to more plastic waste and waste derivatives finding entrance into the environment[14,15].

1.2 Global Plastic Pollution

Plastic waste is a global pollutant that has largely plagued terrestrial and aquatic environments and has been detected in the air, soil, and polar regions[3,6,17,18]. The majority of this mismanaged plastic debris is derived from terrestrial sources and it traverses the environment through our waterways[4,18]. This transport accounts for the emergence of plastic debris into

freshwater and marine environments with an estimated contribution of 80-94% of the total plastic load being ferried by rivers[18]. This has resulted in some the most polluted environments to be coastlines, estuaries, and gyres with increased pollution brought on by urbanization, socioeconomics, and the lack of waste disposal methods[3,9,10,19]. This has led to plastics being continuously produced and disposed, resulting in ecosystems that are saturated in plastic debris that is highly resilient to degradation[10,12,20].

Plastics are a physical blight on ecosystems that impact wildlife through digestive blocking, entanglement, and suffocation[3,6,9,21]. Coupling these actions with the abundance of plastics in marine environments has sparked a social outcry as plastic debris has congregated in masses sized at over 1.6 million km^2 and more than 660 marine species have been placed at risk globally[9,22]. The less visible environmental and biological impacts of bulk plastic debris can occur with the gradual release of chemical additives and continual degradation of the polymers[10,19,23,24]. Migration of additives and monomers from the plastic to the surroundings is dependent on the additive in question, the polymer‘s physical and chemical integrity, and the surrounding environmental conditions[3,10]. Upon release into the environment, additives and monomers are further transformed by biotic and abiotic processes, impacting chemical stability, toxicity, and transport. Likewise, chemicals in the environment can sorb to the polymer’s surface and this sorption capacity is often increased by polymer degradation[10,20,23,24]. These actions illustrate plastics as more than a physical pollutant as they serve as a chemical vehicle and, when associated with aquatic systems, organisms in these environments are likely exposed to these chemicals [10,18,20,23,24].

1.3 The Emergence and Impact of Micro and Nanoplastics

Plastics are highly resilient to degradation as complete mineralization is estimated to take anywhere from decades to centuries[3,6,12,21]. Over this course of time, plastics are subjected to

multiple stressors that contribute to material fragmentation releasing microplastics (MPs) and nanoplastics (NPs)[9,10]. MPs have been classified as polymers with size dimensions below 5mm; while NPs pertain to plastics with nanometer-sized dimensions (< 1 μm), however, no universal definition has been agreed upon for either MPs or NPs[9,10,20,23]. Further classification of MPs and NPs (MP/NPs) distinguishes the particles as being either primary or secondary in origin. The importance of this distinction is between MPs that were intentionally manufactured (primary) or those generated from abrasive processes or environmental weathering (secondary)[9,10,20,25]. Furthermore, distinctions in MP/NP shape, surface chemistry, and spatial and temporal distribution can be assigned that enable a refined approach to address their transport, fate, and behavior.

As pollutants, MP/NPs are initially chemically identical to bulk plastic material, but the physical characteristics play a significant role in their behavior[9]. In tandem with their reduced dimensions, MP/NPs exhibit higher surface area-to-size ratios enabling greater reactivity as it pertains to intermolecular interactions[10,26-28]. The variable surface charge of MP/NPs influences processes such as aggregation, dispersion, and sorption; complicating our understanding of particle transport and ecological impacts[9,10,23].

The global cycling of MP/NPs remains unclear owed to the enhanced mobility of these particles[10,18,23,29]. Environmental concentrations of MP/NPs are highly variable in relation to their various sources and sinks. Wastewater treatment plants (WWTPs) plants have been identified as being a key foci for plastic pollution where the vast majority (95-99%) of MP/NPs that enter a WWTP are retained in biosolids, while the remaining plastics are released with the effluent[10,30,31]. Effluent from WWTPs contribute an estimated 8 trillion plastic particles per day while the vast majority of MP/NPs make their way into biosolids, where they are primarily disposed through agricultural use (51%), landfilling (22%), or incineration (16%) in the United States[10,32].

When biosolids are applied as fertilizer, MP/NPs can gain reentrance into the environment with soil concentrations that rival that of marine environments[31]. Although transport is more inhibited, MP/NPs can still be transported through water to secondary sites via agricultural runoff[30,33]. These processes are further complicated by the dynamic behavior of MP/NPs and provides a mechanism for human and livestock exposure[18,20,33]. This increases the pressure to understand MP/NP toxicity and the associated health risks that come from their exposure through food, water, and air[10,29,34].

In terms of ecosystem dynamics, aquatic species the greatest exposure to MP/NPs[10,24,35]. MP/NPs have been found to accumulate and induce adverse effects in algae and microorganisms up to apex predators with trophic transfer enabling the potential to impact all manner of marine species[10,20,23,36]. For algal species, MP/NPs can act as a stressor that decreases the population and disrupts symbiotic relationships further escalating issues throughout the ecosystem, however, these studies used MP/NP concentrations that exceeded typical environmental relevance[9,23,36]. To invertebrates and vertebrates, MP/NP exposure is often associated with particle adsorption to the gills and accumulation in the gastrointestinal tract where these particles may cause blockage, irritation, and inflammation to the surrounding tissues[9,37,38]. Furthermore, MP/NPs have the potential to cross biological membranes and impact cell signaling disrupting normal biological functions, provoking the immune system, and altering behavior[6,9,25,37]. Ultimately, recurring exposure of MP/NPs have adverse effects on aquatic species that equate to reduced fitness and a cascade of ecological impacts all of which are dependent on polymer concentration[34,36,37,39].

1.4 Transport, Fate, and Behavior of MP/NPs in Aquatic Environments

The spatial and temporal distribution of MP/NPs in aquatic environments is a function of major mechanical forces, particle attributes, environmental factors, and biological

influences[10,18,25,40]. These factors do not exist in isolation; therefore, their interactions and compounding effects all contribute to the unique transport, fate, and behavior of MP/NPs. In regard to their global distribution, advective and turbulent forces greatly aid MP/NP transport leading particles to diffuse, settle, become resuspended, and be deposited in sediments and along shorelines[10,18,41]. Likewise, Brownian motion remains in constant effect for suspended particles and influences localized particle interactions and diffusion. Following these motions, the physical attributes of each particle are of particular importance as these shape the transport, fate, and behavior.

Defining attributes for MP/NPs are their size, shape, density, and topography[10,17,25,38]. As the variability between MP/NPs can be extreme, each of the aforementioned traits adds to uncertainty in particle distribution and behavior[10,18,42]. Of these traits, the role of density is the most apparent in its influence on the vertical distribution of MP/NPs throughout the water column[18,35]. Lighter polymers will reside at the water's surface while heavier polymers are spaced throughout the water column and may ultimately settle in the sediment[18,35]. Likewise, differences in the shape and size of MP/NPs have been found to affect particle distribution where fibers displayed lower settling velocities, compared to spherical particles, and smaller sized particles were more affected by turbulent motions[18].

As water is the predominant media for particle transport, water chemistry is a crucial parameter in relation to MP/NP dispersion and fate. Due to the complexity of natural water systems, the current state-of-knowledge is limited as it pertains to MP/NPs. That said, the role of pH, ionic strength, sediment particles, nanomaterials, dissolved metals, and dissolved organic matter (DOM) have been identified as critical factors in facilitating MP/NP transport, fate, and behavior[10,23,25,26,43]. These factors can influence the transport and fate of MP/NPs through

electrostatic and steric interactions, adsorption, and heteroaggregation that can either reduce or enhance stability[26]. Following the Derjaguin, Landau, Verwey, and Overbeek (DLVO) theory for colloid suspension, pH and ionic strength impact colloidal plastics by compressing the electric double layer thus favoring particle aggregation and deposition[10,26,44,45]. As MP/NPs are largely associated with a negative surface charge, an increased presence of positive counterions associated with higher salinity and more acidic conditions dampens this repulsive force[25,26,43]. As such, a change in environmental conditions such as the transition from freshwater to marine environments, areas afflicted by acid mine drainage, or gastric acid associated with ingestion would alter particle stability and thus the behavior, transport, and fate[26,45]. In each of these situations, particle aggregation and deposition are anticipated based on ion presence causing the compression of the electric double layer leading[25,26,45]. The anticipated result of this would be MP/NPs partitioning with the sediment thus saturating the aquatic environment they are in.

In natural water systems there are a plethora of geogenic particulates and colloids (minerals, carbonates, and oxides) that continually interact and exert electrostatic and steric forces on their surroundings. These particulates largely stem from natural sources but can derive from commercial products and can exhibit profound effects on MP/NPs often associated with adsorption, coagulation, and deposition[10,25,26,43]. The formation of MP/NP heteroaggregates impacts the transport and fate of the colloidal polymers through an increase in size and a measurable disruption to zeta potential[10,30,43]. This will often destabilize the combined particles leading to further aggregation, settling, and deposition[46]. Alternatively, if particle suspension is retained during heteroaggregation, MP/NPs can act as vectors in the transport of secondary particulates particularly iron oxides[43]. In addition to particulates, dissolved metals and organic matter immediately interact with MP/NPs that enter aquatic environments[10,17,23,25]. The attraction

of soluble metals to a particle's surface is influenced by surface chemistry and electrostatic forces, and the capacity for metal adsorption is a function of MP/NP size[23,25,26,47]. Consequently, these colloidal MP/NPs vectors become more complex pollutants with newly altered transport, behavior, and fate.

Alternatively, small organic compounds, such as fulvic and humic substances, are thought to stabilize colloidal plastics with the rational supporting DOM adsorption to the polymer's surface and steric repulsion between the plastics and DOM[10,25,26,35]. The accumulation of DOM to MP/NPs is hypothesized to operate on hydrophobicity and π-π interactions resulting in the formation of a corona, thus retaining particle stability through repulsive forces[25,27]. Likewise, steric repulsion between colloidal plastics and DOM is also possible and has been experimentally supported[26]. On its own, DOM acts as a stabilizer for colloidal plastics that favors continued contaminant transport, however, this effect may be countered by divalent cations (Ca^{2+}, Mg^{2+}) that can facilitate bridging between negatively charged end groups[26,27]. Ultimately, the concentration of DOM is critical when evaluating colloidal plastics as steric and electrostatic stabilization have been observed in laboratory studies which could lead to enhanced transport in aquatic environments.

The final influence mentioned here is the role of biological factors on MP/NPs as it pertains to the transport, fate, and behavior of these contaminants. Bacteria and other simple organisms are thought to immediately interact with MP/NPs in an effort to colonize the new environment[35,46]. This has led to a buildup of microorganisms upon the polymer's surface that alter surface chemistry and particle buoyancy[10,17,40,48]. This behavior results in a variation of vertical transport pathways where lighter polymers and smaller particles can decrease in buoyancy, while heavier polymers become more buoyant resulting in upward transport. A multitude of factors can lead to the loss and reemergence of microbial colonies further complicating vertical transport cycles[40,48]. In

contrast to particulates or dissolved substances, attachment of microorganisms increase MP/NP heteroaggregation due to the release of extracellular polymeric substances that form a sticky media[26,40]. The impact of a microorganism assemblage on to MP/NP's surface can lead to altered physical properties, changes in vertical transport and chemical release, and can lead to bioaccumulation and trophic transfer[40]. All of this alters the fate and transport of MP/NPs in aquatic systems.

In addition to microorganisms, the trophic transfer and accidental ingestion of MP/NPs has been widely observed[10,20,29,35]. The retention rate for MP/NPs within an organism is a function of size where smaller particles are retained for an extended period and can penetrate deeper within the body[36,38,49]. This raises concerns about MP/NP toxicity as it relates to chronic exposure, bioaccumulation and biomagnification, and the partitioning of secondary contaminants (i.e. additives, metals, and other persistent organic pollutants)[6,10,23,25]. As MP/NPs traverse the trophic levels, the contaminant load also rises thus subjecting higher-level organisms to greater MP/NP burdens[20,23,50]. This creates further pressure on these organisms and offers another pathway to human exposure through seafood consumption[19,23,35,51].

1.5 Analytical Detection of MP/NPs

The complexity in MP/NP transport, fate, and behavior is influenced by a variety of physical, environmental, and biological factors as detailed above. The extent to which these factors interact with each other and with MP/NPs is not fully understood and require new techniques and instruments capable of investigating these behaviors in complex environments. To address these uncertainties, numerous studies have emerged that have focused on the abundance, persistence, mobility, and interactions of these pollutants. A significant hurdle in the assessment of MP/NPs concerns the small size of these particles and the ability to distinguish them from complex

environmental and biological media. Standard protocols are still being developed and have mostly focused on larger sized microplastics, while analytical methods fall short in addressing both MP/NPs[9,20,21,52].

Many MP/NPs analyses are focused on particle size, behavior, and their association with the environmental and biological matrices. Most studies have focused on larger sized particles and tend to underreport morphological and chemical information[21,42,52]. This lack of information stems from current sampling protocols and analytical techniques that are largely incapable of addressing NPs and are not suited to provide physical and chemical information. Particle identification and distinction is further complicated with a reduction in size causing most analytical methods to be insufficient[21,53]. Fully characterizing MP/NPs requires multiple analytical instruments to contribute a more complete understanding of these contaminants[52,53].

A common approach to assess MP/NP morphology is via particle visualization through light and electron microscopy. Both of these methods provide different aspects for particle detection and topographic analysis but largely fail at distinguishing natural and synthetic particles or confirming chemical identity. For optical microscopy, a significant limitation is with particle size detection and resolution[20,21,52]. Analyses that use light microscopy were found to have a high rate of misidentified particles and this type of visualization was limited to larger MPs[20,21,52]. Electron microscopy provides a means to visualize particles on the nanoscale, however, chemical identification is limited, and the sample preparation results in a wealth of analytical artifacts[21,52].

For the chemical analysis and confirmation of MPs, Fourier-Transform Infrared (FTIR) and Raman spectroscopy are two nondestructive techniques often coupled with optical microscopy[17,21]. In this coupled approach, the physical and chemical aspects of MPs are obtained enabling a more complete analysis of the contaminant. In FTIR, the sample is irradiated by infrared

radiation leading to an increase in energy expressed as unique molecular vibrations. Likewise, Raman spectroscopy involves the use of a laser to produce scattered photons that provide a molecular fingerprint. These instruments enable the detection and analysis of a bulk sample to single particles with detection limits of 10 µm and 1 µm for FTIR and Raman respectively[21,52,54]. Aside from size limitations, FTIR and Raman are afflicted by polymer surface modifications that can complicate chemical identification, sample preparation can be strenuous, and these instruments can fail to provide information on additives or adsorbed chemicals[17,21,52,54]. All things considered, the use of FTIR and Raman spectroscopy are excellent for the chemical analysis of MPs from biological or environmental matrices but are incapable of assessing individual NPs[21].

In the analysis of either MPs or NPs, spectrometric techniques offer a mechanism for chemical analysis and quantification but often fall short of providing morphological information. Mass spectrometric instruments such as pyrolysis gas chromatography-mass spectrometry (Py-GC-MS), thermal extraction desorption gas chromatography mass spectrometry (TED-GC-MS), and matrix assisted laser desorption ionization time-of-flight mass spectrometry (MALDI-TOF MS) are capable of MP/NP analysis and quantification but they are destructive techniques with limitations in terms of reproducibility[17,21,53,54]. Alongside established analytical methodologies and instruments, several novel techniques have been, and continue to be, developed or repurposed with the aim to improve the identification and quantification of MP/NPs. Direct analysis in real time-high resolution mass spectrometry (DART-MS), operates at ambient temperatures using chemi-ionization and an orbitrap mass analyzer thus providing a more rapid and accurate chemical analysis although it remains a destructive analysis[55,56]. Owing to their potential, these instrumental techniques are relatively new in addressing MP/NPs and remain to be further explored and perfected.

In parallel with instrumental advancements, the extraction of MP/NPs from complex media at environmentally relevant concentrations is still a significant research need. Most conventional extraction methods have relied on polymer density for isolation, and other techniques, such as the one described by Zhou et al., utilize surfactants to perform cloud-point extraction (CPE) of PS and polymethyl methacrylate (PMMA) NPs[54]. CPE uses surfactants that effectively isolate and concentrate NPs from aqueous environment allowing for analysis by mass spectrometry. The viability of this method was further demonstrated with its applicability to a complex media, WWTP effluent, while being reproducible with a high rate of recovery[54]. Extending the application of CPE, future studies should be able to use this cost-effective strategy to effectively isolate and detect previously unobtainable plastics from complex environmental samples at relevant concentrations.

To overcome some of these challenges, the development of tracer polymers has provided a mechanism to access particle transport, fate, and behavior by providing a distinguishable signature to the MP/NP. In the development of these MP/NP tracers, unique artifacts are incorporated into the particle such as fluorescent tags, isotopic elements, or trace metals. Fluorescent tags are the most commonly used artifact to trace MPs, with Nile Red as a popular choice as it adsorbs to most polymers based on hydrophobicity while fluorescence is quenched in most polar environments. In addition to Nile Red dye, Karakolis et al. 2019 identified alternative, commercially available dyes for various MP polymers that offered a wider fluorescent spectrum, higher fluorescent stability, are more robust to digestive procedures, and are cost-effective[57]. The use of fluorescent dyes with MP/NPs has enabled polymer identification and rapid screening of environmental and biological samples but may be limited in these applications due to low light emission per molecule, the photostability of the dye, and sample complexity[21,58,59]. This has limited

fluorescent tracer studies to specific size or concentration regimes that often exceed environmental relevance[60]. The drawback to using fluorescence labels is that polymer size and concentration control detection making the method not viable for addressing smaller MP/NPs at environmental relevant concentrations[36,61].

Isotopic labelling of plastics is another method to trace MP/NPs with the advantage of being able to address contaminant transport and transformations[62-64]. Often with the incorporation of ^{13}C-enriched monomers, MP/NPs with isotopic signatures that can be isolated and quantified with minimal interference using ionization-based instruments[65,66]. This provides a mechanism to accurately trace the cycling of anthropogenic carbon in the environment as it relates to the degradation of polymers and carbon cycling[64,65]. In addition, the use of stable isotopic labeling potentially reduces the physical and chemical discrepancies between the tracers and their corresponding MP/NPs relative to other polymer proxies. As it currently stands, isotopic tracing of synthetic MP/NPs is a viable approach that has been minimally explored in the literature, is expensive, and instrumentational analysis is yet to be perfected and widely adopted for this purpose.

As an alternative tagging strategy to fluorescence and isotopic labels, trace metals have been explored as a means to trace and detect MP/NPs in complex media. Metal-doped plastics typically require a shelling process to provide the desired polymer surface and encapsulate the metal particles embedded within the polymer matrix. Following the work of Keller et al. 2020, PS NP and PET microfiber proxies were synthesized with palladium and indium oxide respectively[30]. These proxy NPs and microfibers were deployed in laboratory studies that simulated polymer transport in sewage sludge, followed by detection using inductively coupled plasma mass spectrometry (ICP-MS). As the trace metal are used to distinguish MP/NPs from the environment,

ICP-MS provides a fast and reliable mechanism to quantify trace metal concentrations that serve as a proxy for MP detection[30]. Expanding upon the metal-doped NP approach, research performed by Jiménez-Lamana et al., Curtis et al., and Rauschendorfer et al. demonstrated the ability to distinguish individual polymers via single particle ICP-MS (spICP-MS) using PS shelled NPs with Au nanoparticle tags[67-69]. The advantage of a discrete approach in addressing NPs is that the individual dynamics of a polymer suspension can be determined through an intractable, quantitative assessment[30,58]. This would allow for data collection that reflects the complexity of NP transport, fate, and behavior at environmentally relevant concentrations.

The current shortcomings with metal-doped polymers are limited polymer selection, applicable metal tags, and development of a proxy that is an accurate representation of the corresponding MP/NPs. Regarding physical representation, metal-doped proxies are synthesized with a defined shape and a density that may not reflect that of a pure plastic material. The inability to align the proxy's physical parameters with that of environmentally relevant plastic particles would limit comparability. A further limitation of this approach is that particle stability and degradation over extended periods have been minimally studied or reported. However, though still in its infancy, metal-doped MP/NPs offer an approach to quantitatively assess the fate, transport, and behavior of elusive contaminants without the concern of high background interference; and future developments are likely to increase proxy applicability and popularity in addressing MP/NPs[30,58,70].

1.6 Project Design and Significance

The purpose of this study was to investigate the dynamics of NPs within estuarine environments using Au-doped PS proxies through spICP-MS detection. Using this approach, particle aggregation and partitioning between media were evaluated based on environmental

factors associated with the collected sediment and water type. Experimental results obtained from this study were used to better understand the behavior, transport, and potential fate of PS NPs in aquatic environments.

The justification for using PS-based proxies is that PS is a high-use consumer plastic that is environmentally relevant in aquatic and coastal zones[10,19,70]. In addition, PS materials are prone to photodegradation resulting in potential toxicological impacts at various particle size regimes[9,12,37,39]. This study aimed to assess the behavior of these proxies in an estuarine environment, a likely sink for these materials as they traverse from terrestrial use, to riparian systems, and ultimately into marine environments.

The Nooksack River Estuary was viewed as an optimal aquatic environment for its role as the intersection between freshwater, marine, and recreational influences[71,72]. Like many Pacific Northwest estuarine systems, this region is a host to a diverse ecological system yet remains continuously pressured by anthropogenic factors including plastic debris[19,71]. As such, it is critical to understand the environmental mechanisms that influence the transport and retention of plastic particles and the related stress MP/NPs entail on these systems.

Bellingham Bay is situated to the north of Puget Sound and is comprised of more than 64 km^2 of sub and intertidal habitat[72]. The bay itself is a mix of urban and undeveloped regions with the eastern shore containing the major port, industrial, and commercial structures while the northern-most shorelines remain relatively undeveloped. The Nooksack River is the most prominent freshwater input to the Bay affecting salinity, suspended solids, and sediment deposition. Along with this, adsorption to sediment can favor the deposition and retention of MP/NPs in aquatics systems based on sediment parameters (grain size, metal content, and carbon species and content). The combination of these factors, in tandem with weak marine currents,

would favor the estuary as a high depositional region for MP/NPs[72]. To investigate the role of sediment and how it can influence the transport and fate of MP/NPs, sediment samples were collected with the goal of capturing the variability in physical and chemical attributes. The key attributes highlighted in this study were sediment grain size, metal content and speciation, and carbon content and speciation.

As a central focus of this project pertains to NP suspension and stability, the role of salinity and dissolved organic carbon (DOC) on PS tracer stability was investigated. This test followed an increasing gradient in salt and DOC concentration followed by spICP-MS detection. The question here was how PS tracer stability and suspension would be affected by increasing DOC and salinity. It was hypothesized that, based on colloidal stability, an increase in salinity would favor PS tracer aggregation and deposition due to the electrical double layer compression. This would imply that the transition from a freshwater environment to a marine environment would cause MP/NPs to aggregate and deposit within estuarine systems. Conversely, it was hypothesized that DOC would adsorb to the PS tracers leading to stabilization due to steric and electrostatic repulsion between colloidal particles. This would imply that the DOC would generate a sufficient negative surface charge across the PS tracer and would coat the PS tracers leading to repulsive forces associated with steric stabilization. As the concentration of DOC increases, MP/NPs are anticipated to be more stable in aquatic environments leading to enhanced transport, however, the concentration of divalent cations could complicate this through cation bridging.

To address NP partitioning between the water and sediment, an experiment based on NP proxy-sediment equilibration was performed. Sediment from each site along with two distinct water types were used to develop slurries that were spiked with the PS tracers. Analysis of the PS tracers was performed through spICP-MS where the PS tracers were defined by fractions:

suspended, loosely bound, and sediment bound. It was hypothesized that, upon equilibration, the PS tracers will primarily partition to the sediment and that the strength of this association will be reflected in the sediment and water attributes. With this, smaller sediment particles and higher concentrations of metals are expected to play a role in tracer deposition while the water parameters will hold the same effect previously hypothesized in the aggregation and equilibration experiments. Additionally, sediment carbon content is anticipated to have a profound effect on PS tracer retention with higher total carbon concentrations and higher black carbon concentrations are expected to play a role in PS tracer deposition. The experimental design to examine the partitioning behavior of the PS tracers between water and sediment is depicted in Figure 1.

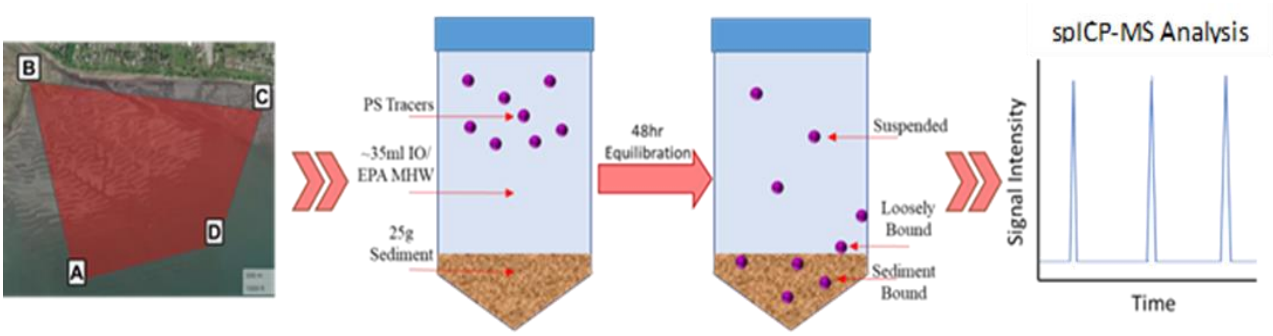

Figure 1. Experimental design for the PS tracer partitioning experiments between water and sediment. The sediment collected from each sample site was paired with either EPA moderately hard water (EPA MHW) or Instant Ocean (IO), spiked with PS tracers, and thoroughly mixed to reach equilibration. The suspended and loosely bound PS tracers were analyzed for each sample by spICP-MS.

Chapter 2: Methods

2.1 Study Region/Sediment Collection

Northern Bellingham Bay is defined by the estuary formed from where the Nooksack River outlet meets the marine water of the Salish Sea. A popular access point to this area is Locust Beach (48.77, -122.53) where the flood plains extend to the Nooksack River outlet and the floodplain is readily accessible during low tide. In this study, sediment samples were collected on August 19,

2020 at low tide following a path preset using the smartphone app "GPS Fields Area Measure" developed by Farmis that offered the global position and coordinates. Four sites were evaluated that encompassed an area of $1km^2$ and the top 10cm of sediment was collected in triplicate using a sediment core sampler, a stainless-steel trowel, and a plastic container at each site. The collected sediment was transported back to the laboratory and stored in a refrigerator at 4°C. The study site is depicted in Figure 1A. and each site is assigned a label (A-D). The coordinates for each site following the lettered labelling scheme are presented in Table 1.

Table 1. Global coordinates of the Bellingham Bay study region designated by each sediment sample site (A-D).

Site	Longitude	Latitude
A	48.767	-122.560
B	48.776	-122.564
C	48.776	-122.544
D	48.769	-122.548

2.2 Sediment Preparation

The sediment samples were thoroughly mixed to achieve homogenization. For this purpose, the sediment samples were individually transferred to a large stainless-steel bowl and the sediment was mixed with gloved hands. Large, unrepresentative artifacts were removed during this process, and the mixed sediment was returned to its original container then stored in the refrigerator. For experiments that required dried sediment, sediment samples were placed on aluminum trays and set in an oven at 60°C for 48 hours.

2.3 Characterization of Sediment

2.3.1 Physical Characterization of Sediment

The sediment samples were characterized by their particle grain sizes. Dried sediment was disrupted with a pestle to ensure reduce particle agglomeration and then the mass was obtained

using an analytical balance (VWR-124B2). The sediment was then passed through a stainless-steel sieve with mesh sizes of 2000, 500, 250, 125, and 63 μm. A top and bottom cover were placed on the sieve stack and the entire apparatus was manually shaken for a summed total of 15 min. The mass of each fraction was obtained, and the grain size percentage was calculated from the total mass.

2.3.2 Chemical Characterization of Sediment

The collected sediment samples were characterized by their chemical composition with an emphasis on carbon speciation and environmentally available metals. The instrumental techniques used to determine chemical composition were ICP-MS, flame atomic absorption spectrometer (FAAS), and elemental analysis (EA). These instrumental techniques enabled the detection of trace metals, major metals, and carbon content respectively.

To determine the concentration of environmentally available metals, the sediment samples were dried then digested following EPA Method 3050B where the trace metals were analyzed via ICP-MS following EPA Method 200.8 and the major metals were analyzed by FAAS following EPA Method 7000B. Au was the exception to these methods and was prepared following EPA Method 3050B with the exception of using an aqua regia solution (4:1 HCl/HNO_3) to favor Au dissolution. The distinction in metal analysis was based on abundance where the trace metals were analyzed using ICP-MS and FAAS was reserved for the more abundant metals.

For trace metal analysis, two calibration standards were used with ICP-MS-6020-CAL-R-1 (AccuStandard®) used for the analysis of Al, V, Mn, Co, Ni, Co, Ni, Cu, Zn, and Cd while an Au standard (SPEX CertiPrep® Claritas PPT®) was used in the analysis of Au analytes. A quadrupole ICP-MS (Agilent 7500ce), with a MicroMist glass concentric nebulizer and a Quartz

Scott-type spray chamber, was used for the detection of metal analytes following instrument operating conditions described in the Appendix (Table 1A). Likewise, metal analysis by FAAS was performed by Western Washington University's Scientific Technical Services using a Varian SpectrAA 220 FS Atomic Absorption Spectrometer.

Carbon content and speciation followed a chemo-thermal oxidation (CTO) method that differentiated total carbon (TC) into labile carbon (LC), black carbon (BC), and inorganic carbon (IC) fractions. The carbon speciation method performed was an adaptation of the CTO methods described by Caria et al. (2011), Elmquist et al. (2004), and Gustafsson et al. (2001)[73-75]. The sediment samples were dried at 60°C for over 24 hrs while empty aluminum trays were placed in a muffle furnace at 550°C for 8 hrs. A portion of the dried sediment was saved for TC analysis. The dried sediment was transferred to the aluminum trays and the mass was obtained before being placed in the muffle furnace at 375°C for over 18 hrs. The mass loss for each sample was attributed to the LC fraction and a portion of the sample was saved for BC and IC analysis. Finally, the sediment was transferred to ceramic dishes and acidified with enough 1M HCl to fully saturate each sample. These samples were covered with a ceramic lid and left to acidify overnight to remove all IC sources. Ultrapure water (herein referred to as MilliQ water) was added to the acidified samples and where then filtered through Whatman #2 filter paper (8 µm pore size) and washed by two additional aliquots of milliQ water. This step was performed to prevent an additional mass increase from HCl residue when the sediment was dried. The sediment was returned to the ceramic dishes using milliQ water for the transfer, and the sediment was dried at 80°C for 24 hrs.

Carbon content analysis was performed using a Thermo Fisher Scientific Flash EA 1112 NC Soil Analyzer that operated through the combustion of dried sediment. An atropine standard

was used to quantify carbon content based on the ratio of carbon to nitrogen. All samples were packed and sealed in aluminum capsules and the mass was obtained before analysis.

2.4 PS Tracer Synthesis and Characterization

2.4.1 PS Tracer Synthesis

The PS tracers were procured from Dr. David Rider's research group; part of the Department of Chemistry, Western Washington University. These PS tracers are comprised of a core, polymer shell, and internalized AuNPs and the methods used for synthesis are described in Curtis et al. and Rauschendorfer et al. Briefly, PS tracer synthesis starts with the styrene (20%) and 2-vinylpyridine (80%) to form a polystyrene-poly(2-vinylpyridine) co-polymer (PS-co-P2VP) core[67,68]. The core was then covered by a selected polymer shell and for this study PS was selected as the shelling polymer. Formation of internalized metallic nanoparticles has been performed through the electrostatic binding of metallic ions with the protonated pyridine group followed by photoreduction to yield nanoparticles. This technique has been demonstrated with Au, preformed Ag, Pd, and Pt, all of which offer a trace metallic signature in most environments[67]. The PS tracers deployed in this study for environmental assessment utilized AuNPs for ICP-MS detection. The synthesis scheme is illustrated in Figure 2.

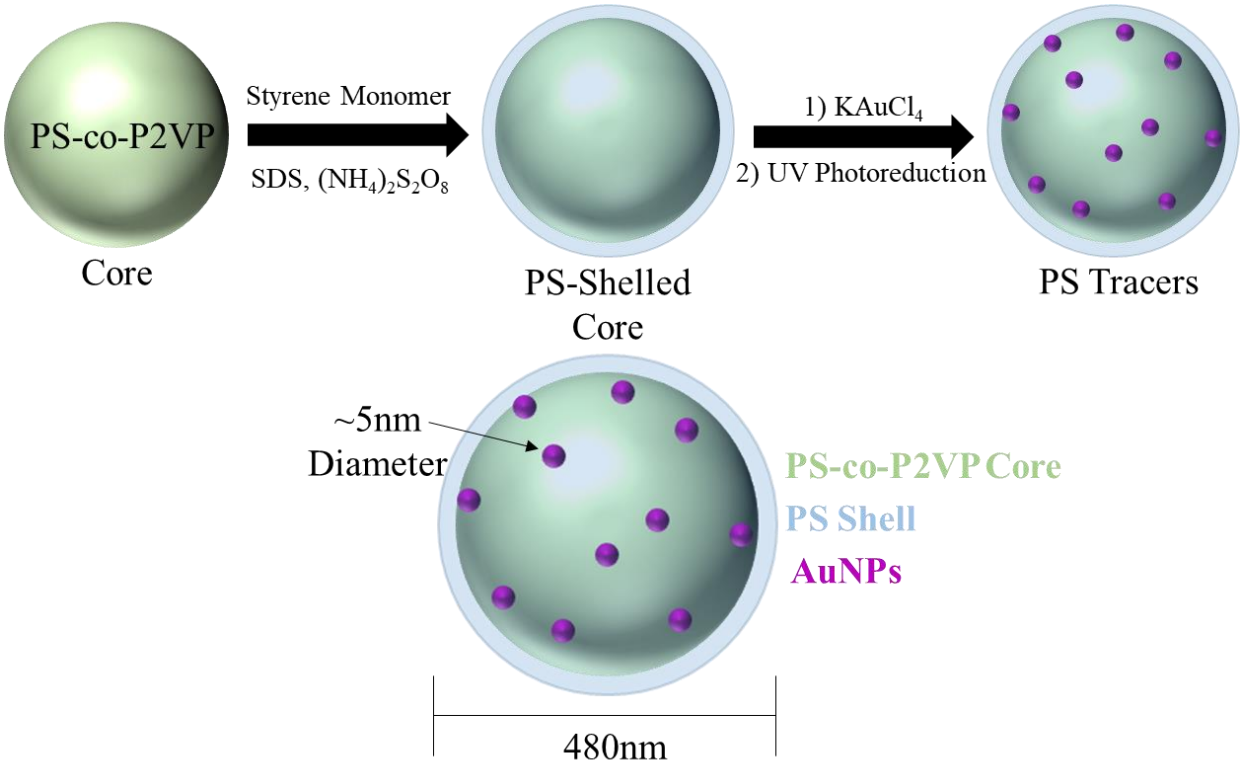

Figure 2. PS Tracer synthesis scheme starting from the PS-co-P2VP core and ending with the addition of the AuNPs. The diagram of the PS tracer provides the particle's diameter (480 nm) along with the approximate diameter (~5 nm) of the AuNPs.

2.4.2 PS Tracer Physical Characterization

The PS tracers were physically evaluated on the basis of particle size distribution, metallic nanoparticle content and distribution, density, and zeta potential. The evaluation of particle size and metallic nanoparticle distribution was performed by Dr.Rider's research group using Dynamic Light Scattering (DLS) (Delsa Nano HC, Beckman Coulter), tapping-mode Atomic Force Microscopy (AFM) (Bioscope Catalyst, Bruker), and scanning transmission electron microscopy (STEM; JSM-7200F field emission microscope, JEOL)[67].

To determine the metallic nanoparticle content for the PS tracers, spICP-MS was employed, and the corresponding signal intensity distribution reflected metallic nanoparticle content. The standard operating conditions for the ICP-MS in single particle mode is provided in

the Appendix (Table 1A). For the analysis of AuNPs, an AuNP standard (60 nm Gold Nanospheres, Bare (citrate) nanoComposix®) and an Au solution standard (SPEX CertiPrep® Claritas PPT®) were used.

Assessment of PS tracer density was performed by Postnova Analytics Inc. using Sedimentation Field Flow Fractionation (Sed-FFF) with a UV detector and a 512 nm diameter PS standard. The standard operating conditions for the Sed-FFF are available in the Appendix (Table 2A).

To assess PS tracer charge, zeta potential measurements were collected in aquatic media at varying salinity and DOC concentrations. Zeta potential measurements were determined through the use of a Malvern Zetasizer (Malvern Panalytics) and were performed by Professor James Ranville at the Colorado School of Mines.

2.4.3 PS Tracer Chemical Characterization

The chemical characterization of the PS tracers was performed by Dr. Rider's group who compared PS-co-P2VP cores, PS-shelled cores, PS tracers, and virgin PS using FTIR (Nicolet iS10 FT-IR spectrometer), Raman spectroscopy (Renishaw inVia Qontor Raman microscope), and thermogravimetric analysis (TGA) (TA Instruments Q500). FTIR and Raman spectroscopy were used to confirm the core identity and the attachment of PS shell to the cores. The acquisition parameters for the Raman microscope are detailed in the Appendix (Table 3A). The use of TGA to assess all particles through combustion was done to find evidence of metallic nanoparticles associated with the tracers. In conjunction with TGA, this study used spICP-MS to provide further evidence of metallic nanoparticles associated with PS tracers as described in section 2.4.2.

2.5 PS Tracer Stock Concentration

The concentration of the PS tracer stock solution was determined via spICP-MS with five replicate samples. The solution was sonicated for a minimum of 30 minutes before being diluted by a factor of 2, 5, and 10 million. The samples continued to be sonicated up until analysis by ICP-MS. To analyze the Au labelled PS tracers, an AuNP standard (60 nm Gold Nanospheres, Bare (citrate) nanoComposix®) and an Au solution standard (SPEX CertiPrep® Claritas PPT®) were used to determine the transport efficiency (equation 1A) and enable PS tracer quantification (equation 2A). In addition to determining the PS tracer stock concentration, the total Au mass (equation 3A) and the number of AuNPs per PS tracer (equation 4A) were determined following the assumptions of total sample ionization (100% ionization efficiency), a standard AuNP diameter of 5 nm, and that all particles can be accurately described as spheres[76]. All equations are located in the Appendix. Operational conditions for spICP-MS are presented in the Appendix (Table 1A).

2.6 PS Tracer Ruggedness

The ruggedness of the PS tracers was assessed on the basis of changes in AuNP detection in MilliQ, EPA moderately hard water (EPA MHW), and Instant Ocean (IO) at different times. The EPA MHW and the IO were used as synthetic substitutes for fresh and marine water respectively; with the goal of representing the extreme aquatic differences experienced in estuarine systems. For this, two treatments of each water type were prepared where one treatment was spiked with PS tracers (10.6 mg/L) and all samples were mixed for 48hrs using a shaker table. After the mixing period, the samples without PS tracers were spiked at a concentration of 10.6 mg/L and all samples were sonicated for a minimum of 30 min. All samples were filtered through a Fisherbrand™ 0.22 µm mixed cellulose ester syringe filter aimed at separating PS tracers from loose AuNPs. A portion of the filtered solutions (9 ml) was acidified with a 1:4 HNO_3/HCl solution

(1 ml) for at least 24hrs. The final samples were brought to a final 50x dilution using MilliQ water before analysis by ICP-MS. An Au solution standard (SPEX CertiPrep® Claritas PPT®) was used for calibration while the operational conditions for the ICP-MS are presented in the Appendix (Table 1A).

2.7 PS Tracer Stability and Suspension

The colloidal stability of the PS tracers was assessed using aqueous solutions at varying NaCl (0, 1, 5, 15, 30 g/L) and DOC (0, 1.5, 3 mg/L) concentrations. The aqueous solutions were made using MilliQ water, sodium chloride (purity 99%; Fisher Chemical), and Suwannee River humic acid (SRHA). The use of NaCl to represent salinity followed that NaCl is a monovalent salt that is usually the most abundant salt in aquatic systems. Five salinity treatments and three DOC treatments were used in this experiment and the PS tracers were sonicated then spiked into each sample at a final concentration of 10.6 mg/L. The pH of each solution was recorded using a calibrated HQ411d pH-meter and the probe was rinsed after each read using MilliQ water. Each solution was secured to the shaker table with the vials arranged in a similar orientation and light exposure was minimized. The samples were left to shake for approximately 48 hrs at 330 RPM to establish equilibrium. After mixing was achieved, the samples were stood upright, and the particles were allowed to settle for 45 min. The top portion (1 cm depth) of the solution was extracted and this was used to prepare diluted samples for spICP-MS. A standard MilliQ sample and controls (same water chemistry without PS tracers) were made the same day spICP-MS analysis was performed. All samples were continuously sonicated right before uptake by the autosampler connected to the ICP-MS. For calibration, an AuNP standard (60 nm Gold Nanospheres, Bare (citrate) nanoComposix®) and an Au solution standard (SPEX CertiPrep® Claritas PPT®) were used while instrument operating conditions are presented in the Appendix (Table 1A).

2.8 PS Tracer Partitioning

The partitioning behavior of the PS tracers was evaluated using the sediment collected from sample sites (A-D) paired with either synthetic fresh or marine water. The sediment (25g) was loaded into the sample chambers using a centrifuge (Thermo Scientific™ Sorvall™ Legend™ XFR Centrifuge) at 3000 RPM and -4 °C for 1hr. None of the samples displayed excess water to be removed so 35 ml of EPA MHW or IO with the PS tracer solution (10.6 mg/L) was added. The concentration of the PS tracers spiked into each sample was based on the concentration of the PS tracer stock solution. These samples were subject to 48 hr mixing period using a shaker table with minimal light exposure. Control samples of PS tracer spiked EPA MHW and IO without sediment were ran with each site and were subject to the same mixing conditions. Additionally, PS tracer spiked MilliQ samples were prepared the same day sample analysis by spICP-MS was performed.

After mixing was achieved, all samples were allowed a settling period of 1 hr before preparing diluted suspend PS tracer samples for spICP-MS analysis. The suspended PS tracer samples were prepared by collecting a 100 μL aliquot from the top portion (2 cm depth) followed by dilution. After the suspended PS tracer samples were prepared, the mixed samples were sonicated for at least 30 min before loosely bound PS tracer samples were prepared for spICP-MS analysis following the same procedure used for the suspended PS tracer samples. All samples required a two-step dilution process to be viable for spICP-MS analysis. All intermediate dilution samples and controls were sonicated for at least 30 min before the final dilution was prepared. The final diluted samples and controls remained sonicated right up until sample analysis by the ICP-MS. For calibration and particle quantification, an AuNP standard (60 nm Gold Nanospheres, Bare (citrate) nanoComposix®) and an Au solution standard (SPEX CertiPrep® Claritas PPT®) were used while instrument operating conditions are presented in the Appendix (Table 1A).

An acid digestion of the water and sediment using an aqua regia solution (4:1 HCl/HNO_3) was used to determine the concentration of Au partitioned to each fraction. This test was performed to evaluate sediment partitioning of the PS tracers based a calculated mass balance. For this, 1g of dried sediment from each sample was digested using 5 mL of aqua regia and following EPA method 3050B then analysis by ICP-MS following EPA method 200.8. For the water samples, 2 mL of aqua regia was added to 25 mL of the sample water followed by analysis using ICP-MS following EPA method 200.8.

2.9 Statistical Analyses

The statistical analyses performed in this study were used to distinguish the sampled sites as well as the PS tracer spiked samples for the various experiments performed. For all statistical analyses, a significance level was set to $\alpha = 0.05$ while normality and homogeneity of variance were evaluated using the Shapiro-Wilk test and Levene's test respectively. Multivariate and univariate statistical analyses were performed followed by post hoc analyses for each experiment. For the measured sediment variables, linear correlations were investigated. All statistical evaluations were performed using RStudio and packages used for statistical analyses are provided in the Appendix (R Packages).

The statistical analyses for sediment the sample sites were compared based on sediment grain size, carbon content and speciation, and metal content and speciation. The types of statistical tests performed were MANOVA, ANOVA, and Tukey's Honest Significant Difference (HSD) tests as a post hoc analysis. Statistically different variables for each sample site were identified using Tukey's HSD tests and assigned a group based on this difference. All variables were assessed for linear correlation to determine variable dependence and reduce redundancies in modelling.

The ruggedness of the PS tracers as well as their stability and suspension in the presence of NaCl and DOC was evaluated through ANOVA with Tukey's HSD post hoc tests. The ruggedness of the PS tracers was statistically compared across water types and before and after 48 hr mixing. For the PS tracer stability and suspension experiment, statistical analyses were made for either varying salinity at a constant DOC concentration or for varying DOC at a constant salinity.

For the PS tracer partitioning experiments, several statical comparisons were performed that included a water type comparison, water versus sediment comparison, and a sediment sample site comparison. ANOVA with Fisher's Least Significant Difference (LSD) post hoc tests were performed for the comparisons between water types and the comparison between sample site sediment. To compare suspended and suspended and loosely bound treatments, a pairwise t-test was performed. To statistical evaluate the comparison of water samples versus sediment samples, a Welch's ANOVA with a post hoc Games-Howell pairwise comparison tests were performed. These analyses were used as the data was not found to have equal variance while departures in normality were observed but anticipated to have a minimal impact on the corresponding *F*-test.

Chapter 3: Results

3.1 Sediment Site Characterization

To examine the impact of aquatic systems on the transport of MP/NPs, sediment was collected from sample sites and categorized by sediment grain size, metal content, and carbon content to build a sediment profile for each site. In the analysis of sediment grain size, each site was characterized by five size regimes that spanned from coarse sand (2000-500 μm) to silts and clays (<63 μm). The average grain size by percent mass was determined for each sediment class

to build a grain size profile for each site and significance was indicated through grouped letter assignment for each sediment class (Table 2 and Figure 3).

Table 2. Sediment grain size percentage by mass for the sample sites (A-D). There were five sediment classes ranging from coarse sand to silts and clays. These sediment classes created a sediment profile for each sample site (Mean ± SD; n=3).

Site	Percent Coarse Sand (2000-500 µm)	Percent Medium Sand (500-250 µm)	Percent Fine Sand (250-125 µm)	Percent Very Fine Sand (125-63 µm)	Percent Silt & Clay (<63 µm)
A	0.5 ± 0.07	13.8 ± 2.0	72.5 ± 1.3	11.4 ± 2.4	1.8 ± 0.8
B	2.5 ± 1.2	26.0 ± 4.4	51.2 ± 12.4	15.9 ± 9.1	4.4 ± 3.4
C	0.8 ± 0.3	1.0 ± 0.4	1.8 ± 0.3	16.8 ± 1.6	79.5 ± 1.0
D	0.4 ± 0.02	6.0 ± 0.4	34.8 ± 1.0	48.5 ± 1.0	10.2 ± 0.4

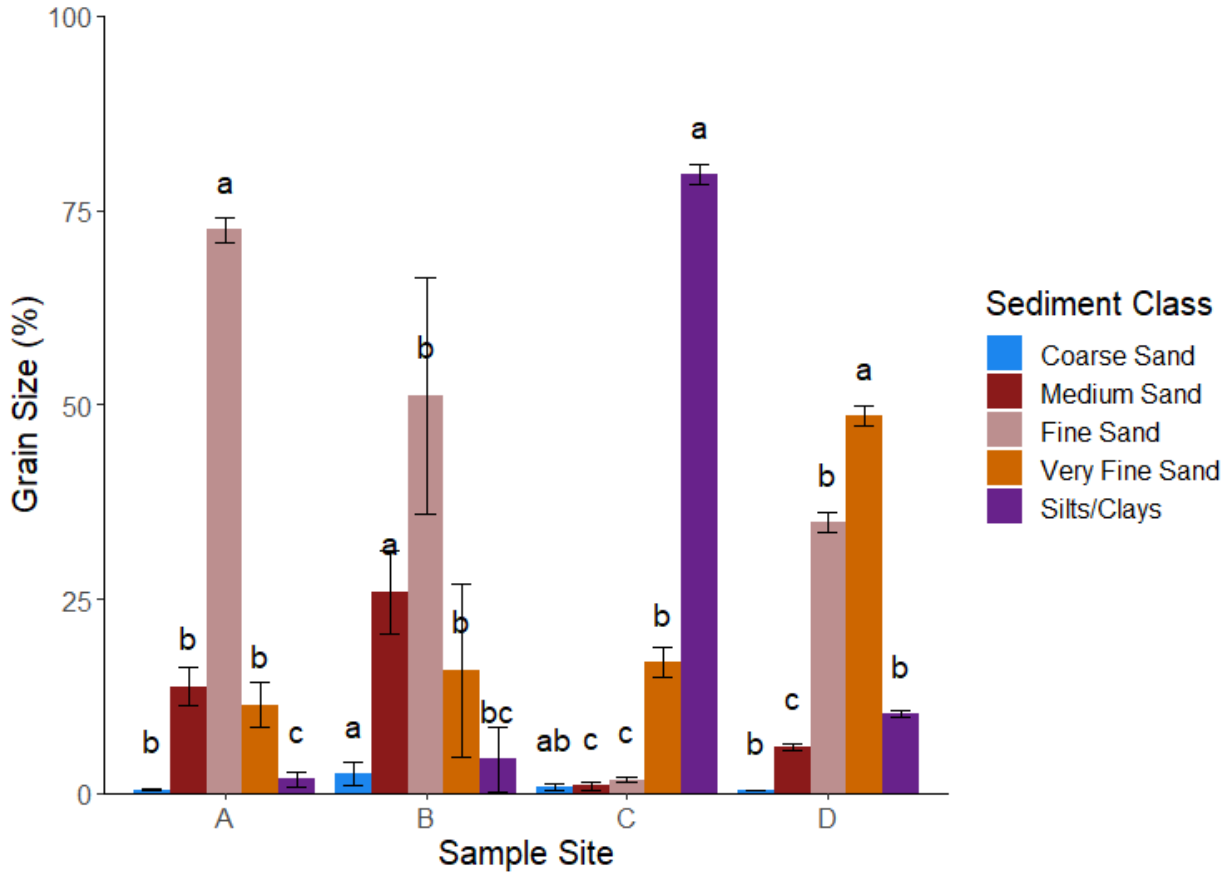

Figure 3. Sediment grain size percentage by mass for the sample sites (A-D). The sediment grains were categorized into five size classes: Coarse Sand (2000-500 µm), Medium Sand (500-250 µm), Fine Sand (250-125 µm), Very Fine Sand (125-63 µm), and Silts & Clays (<63 µm). Post hoc tests were performed between sites on all sediment classes with a significance level of .05. Sites with classes that were significantly different were designated a group letter (a-c) where classes sharing similar letters were not significantly different (Mean ± SD; n=3). This figure was generated using R software.

3.1.1 Sediment Grain Size

Comparing the sample sites by grain size classes indicated that significant differences were present using MANOVA ($F_{3,8}$ = 24.84, $P < 0.001$) and ANOVA tests was found to be significant for coarse sand ($F_{3,8}$ = 5.19, $P < 0.05$), medium sand ($F_{3,8}$ = 40.91, $P < 0.001$), fine sand ($F_{3,8}$ = 45.41, $P < 0.001$), very fine sand ($F_{3,8}$ = 25.32, $P < 0.001$), and silts and clays ($F_{3,8}$ = 834.05, $P < 0.001$) (Table 4A). Further analysis using Tukey's HSD provided individual site comparisons by a single grain size class (Table 5A). For coarse sand, site B (2.5 ± 1.2%; group a) had the highest mass percentage and could be distinguished from sites A (0.5 ± 0.07%; group b) and D (0.4 ± 0.02%; group b) while site C (0.8 ± 0.3%; group ab) was indistinguishable from any site. For medium sand, site B (26.0 ± 4.4%; group a) had the highest mass percentage followed by site A (13.8 ± 2.0%; group b) then sites C (1.0 ± 0.4%; group c) and D (6.0 ± 0.4%; group c). Distinctions between sites for fine sand indicated that site A (72.5 ± 1.3%; group a) had the highest mass percentage followed by sites B (51.2 ± 12.4%; group b) and D (34.8 ± 1.0%; group b) and then site C (1.8 ± 0.3%; group c) with the lowest fine sand content. Very fine sand content was the highest with site D (48.5 ± 1.0%; group a) while sites A, B, and C (group b) were indistinguishable from each other. With the last category of silts and clays, site C (79.5 ± 1.0%; group a) had the highest percentage followed by site D (10.2 ± 0.4%; group b), then site B (4.4 ± 3.4%; group bc), and lastly site A (1.8 ± 0.8%; group c). The amount of silt and clay associated with Site B was indistinguishable from sites A and D.

3.1.2 Sediment Carbon Speciation

Comparisons between sites based on carbon content were evaluated on the basis of TC as well as speciation between LC, BC, and IC. The distinction in carbon species provide the categories for characterizing each site by a carbon profile where LC comprised the majority of the

TC content at all sites, BC was minimal, and IC was found to be negligible (Table 3 and Figure 4). In addition, all sites were compared by carbon species and species found to be significantly different were alphabetically grouped. Site C had a significantly higher TC, LC, and BC from all other sites while sites A, B, and C were indistinguishable by all carbon species.

Table 3. Sediment carbon concentrations (g/kg) for each sample site (A-D). The total carbon concentration and the concentrations of the labile, black, and inorganic carbon species were reported (Mean ± SD; n = 3).

Site	Total Carbon (g/kg)	Labile Carbon (g/kg)	Black Carbon (g/kg)	Inorganic Carbon (g/kg)
A	1.44 ± 0.05	1.38 ± 0.06	0.04 ± 0.01	0.01± 0.01
B	1.61 ± 0.18	1.54 ± 0.17	0.07 ± 0.03	0.00 ± 0.04
C	6.47 ± 0.50	6.18 ± 0.48	0.22 ± 0.02	0.07 ± 0.03
D	2.21 ± 0.09	2.10 ± 0.10	0.09 ± 0.02	0.03 ± 0.03

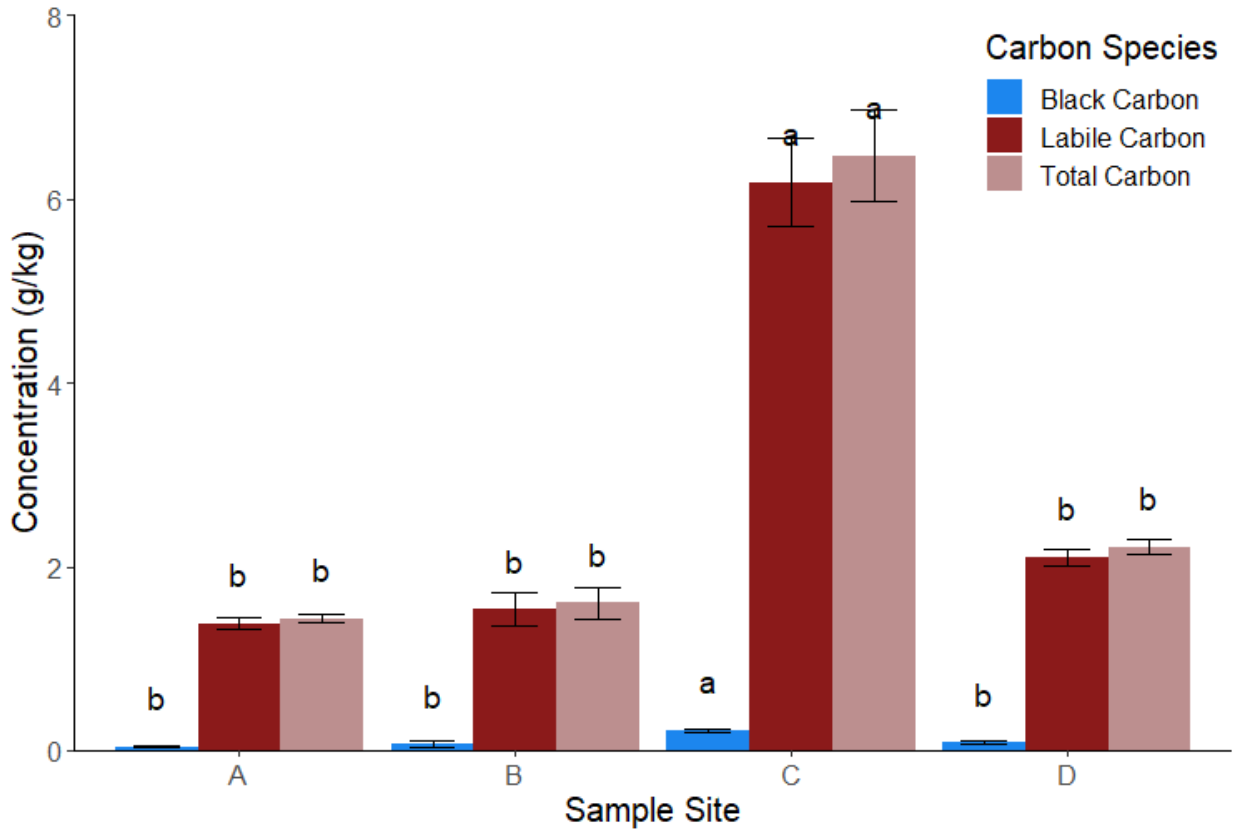

Figure 4. Sediment carbon concentration for each sample site (A-D). The concentration of TC, LC, and BC were reported along with a site comparison and grouping determined by a post hoc analysis. The letter designation compares specific carbon species between sample sites (Mean ± SD; n=3). This figure was generated using R software.

Sediment carbon species content was analyzed using MANOVA and ANOVA tests. The analyses were significant for MANOVA ($F_{3,8} = 2.54, P < 0.05$) and the ANOVA tests for TC ($F_{3,8} = 158.1, P < 0.001$), LC ($F_{3,8} = 150.2, P < 0.001$), and BC ($F_{3,8} = 30.29, P < 0.001$) (Table 6A). The performed Post Hoc tests established that site C had significantly more TC, LC, and BC than all other sites while sites A, B, and C were indistinguishable from each other (Table 7A).

3.1.3 Sediment Metal Speciation

To further develop a sediment profile for each site, the concentration of metals was determined through FAAS (Al, Ca, Fe, K, Mg, and Na) and ICP-MS (Co, Cr, Cu, Mn, Ni, V, and Zn) analysis. The FAAS metals present at higher concentrations than the trace metals analyzed with ICP-MS, however, only Al and Na were significantly different between sample sites (Table 8A and Figure 2A). A post hoc analysis was performed on Al and Na at a significance level set to $\alpha = 0.05$. The analysis indicated a significant difference in Al concentration between sites C (29.76 ± 2.10 g/kg; group a) and A (21.65 ± 1.92 g/kg; group b) while sites B (21.74 ± 2.51 g/kg, group ab) and D (23.35 ± 3.29 g/kg; group ab) could not be distinguished from any other sample. For Na, site C (7.61 ± 0.77 g/kg; group a) had a significantly higher concentration while sites A (5.28 ± 0.32 g/kg; group b), B (5.18 ± 0.64; group b), and D (5.56 ± 0.28 g/kg; group b) were indistinguishable from each other. More information on the statistical analyses that included MANOVA, ANOVA, and Tukey's HSD are provided in the Appendix section (Table 9A and Table 10A).

Trace metal concentrations were determined for each site along with statistical comparisons between sites (Table 4 and Figure 3A). Through post hoc analyses, the sample sites were found to be statistically different based on Cr, Cu, Mn, and Zn concentrations. For Cr, site C (group a) could be differentiated from sites A (group b) and B (group b) but not site D (group ab)

which was indistinguishable from all other sites. The concentration of Cu was statistically higher in site C (group a) while sites A, B, and D were indistinguishable (group b). Mn was the most abundant trace metal detected and was statistically different for all sites being highest at site A (group a) followed by site D (group b), site C (group c), and finally site B (group d). For Zn, site C (group a) had the highest concentration followed by sites D (group b) and A (group bc), and finally site B (group c). For site A, the concentration of Zn was statistically comparable with sites B and D. Further statistical analyses that include MANOVA, ANOVA, and Tukey's HSD is available in the Appendix (Table 11A and Table 12A).

Table 4. Sediment trace metal concentration(g/kg) for each site (A-D) (Mean ± SD; n = 3).

Site	V (mg/kg)	Cr (mg/kg)	Mn (mg/kg)	Co (mg/kg)	Ni (mg/kg)	Cu (mg/kg)	Zn (g/kg)
A	38.59 ± 1.73	35.23 ± 0.98	451.33 ± 5.89	13.49 ± 0.78	128.58 ± 14.82	25.72 ± 1.35	43.69 ± 1.64
B	42.34 ± 1.03	36.16 ± 2.11	267.19 ± 11.36	11.54 ± 1.08	120.59 ± 18.37	24.00 ± 2.45	41.61 ± 1.94
C	40.57 ± 1.46	54.99 ± 10.70	319.38 ± 10.46	12.61 ± 0.17	98.54 ± 0.69	40.11 ± 3.32	58.11 ± 1.00
D	40.42 ± 2.66	40.79 ± 0.96	350.41 ± 5.04	12.94 ± 0.21	117.64 ± 3.49	26.93 ± 3.66	48.04 ± 0.88

3.1.4 Sediment Variable correlation

To investigate the role of sediment variables in relation to each other, a correlation table and figure provided variable comparisons (Table 13A and Figure 4A). Comparing all the variables to each other revealed correlations between grain size and the concentration of carbon and metal species. These correlations indicate that these variables are not independent from each other indicating a possible relationship. Additionally, variables such as Mn did not display a simple correlation with sediment grain size or carbon content allowing for sample sites to be discernable by this variable.

3.2 PS Tracer Characterization

3.2.1 PS Tracer Physical Characterization

The physical attributes characterized for the PS tracers were particle size, density, and zeta potential. For size evaluation, DLS, AFM, and STEM visual confirmation was employed that revealed a PS tracer diameter of 480 ± 26 nm (Table 5 and Figure 5). Likewise, an increase in particle diameter was observed with the addition of a PS shell to the PS-co-P2VP core while no diameter increase was observed with the formation of AuNPs using STEM. PS tracer visualization using STEM did provide information on AuNP formation including confirmation of that the majority of the AuNPs residing below the PS shell.

Table 5. Particle diameter size for the PS-co-P2VP cores, PS-shelled cores, and the PS tracers as determined by SEM, DLS, and AFM.

Sample	SEM size (nm)	DLS size (nm)	AFM size (nm)	MP Conc. (MP/mL)
PS-co-P2VP Core	325 ± 11	367 ± 28	269 ± 15	---
PS-Shelled Core	457 ± 13	441 ± 47	442 ± 51	---
AuNP-PS Tracers	477 ± 25	446 ± 195	480 ± 26	$(2.65 \pm 0.28)*10^{11}$

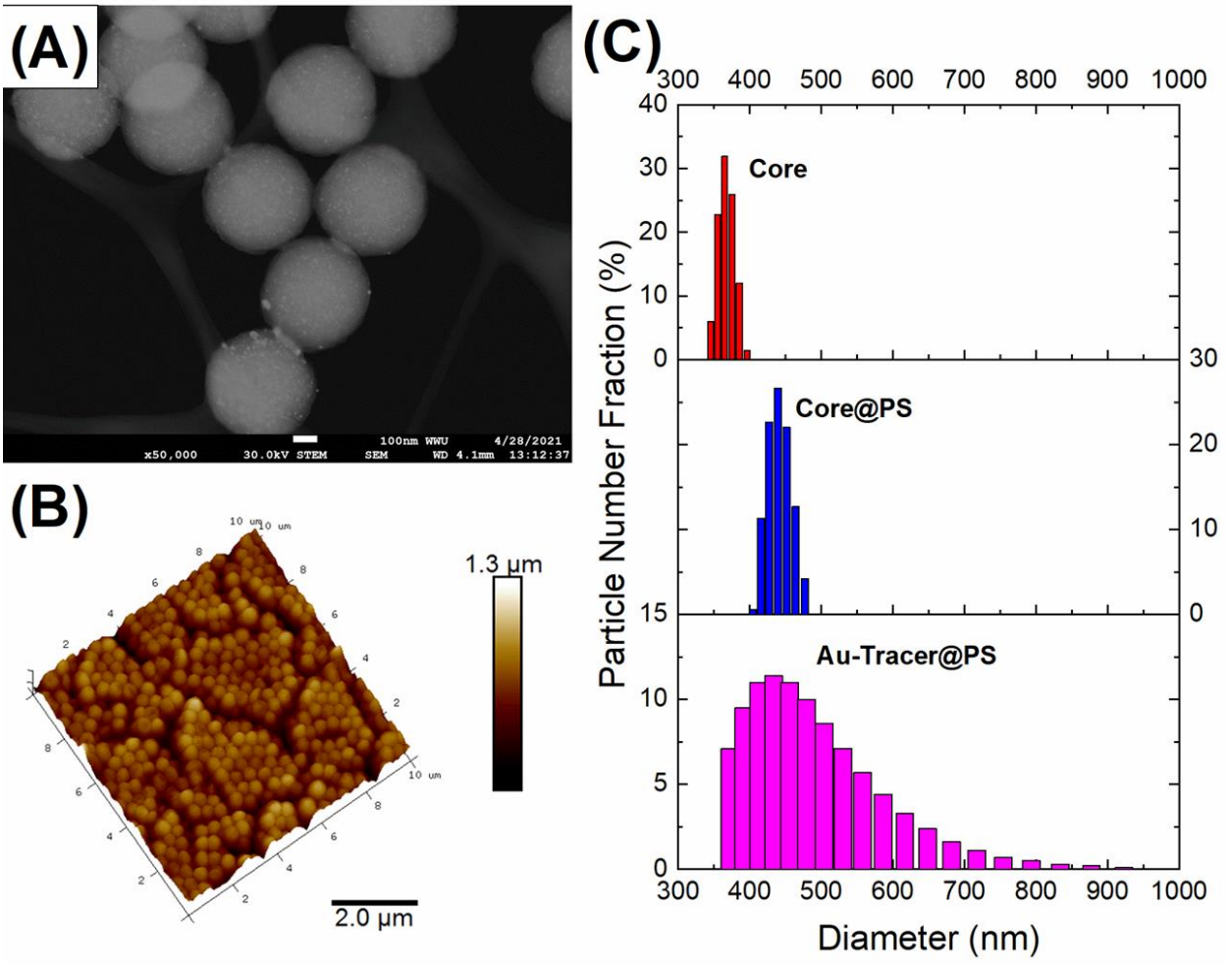

Figure 5. Physical characterization of the PS tracers by (A) STEM, (B) Tapping-Mode AFM, and (C) DLS detailing the size distribution in the PS-co-P2VP core (top), the PS-shelled cores (middle), and the fully synthesized PS tracers (bottom). This figure was adapted from Rauschendorfer et al, 2021.

The density of the PS tracers was assessed using Sed-FFF. Comparing the PS tracers with a PS standard revealed a notable difference in density where the PS tracers eluted later than the PS standard (Figure 5A). The calculated density of the PS tracers was 1160 ± 182 kg/m^3 based on the Sed-FFF data which was slightly higher than a standard PS particle density (1045 kg/m^3) (Table 6). The data and density calculations were generated by PostNova Analytics Inc. following procedures described by Tadjiki et al[77].

Table 6. Calculated density of the PS tracers using Sed-FFF and a 512 ± 7 nm PS standard.

Sample	Particle Density (kg/m^3)
PS Standard	1045 ± 43
PS Tracer	1160 ± 182

The zeta potential of the PS tracers was evaluated at varying salinity (0-30 g/L) and DOC concentrations (0-3 mg/L) in MilliQ water (Table 7). In pure MilliQ water, the zeta potential of the PS tracers was 28.6 ± 0.5 mV. As salinity was increased, the zeta potential of the PS tracers approached zero and became slightly negative at 30 g/L NaCl (-0.7 ± 1.2 mV). The addition of DOC to the MilliQ water resulted in a decrease of positive zeta potential going from 28.6 ± 0.5 mV at 0 mg/L DOC to 7.9 ± 0.1 mV at 3 mg/L DOC. When DOC was coupled with salinity, negative zeta potentials were recorded with salinity at 5 g/L resulting in -4.76 mV (DOC = 1.5 mg/L) and -2.14 mV (DOC = 3 mg/L) and salinity at 30 g/L resulting in zeta potentials of -1.06 mV (DOC = 1.5 mg/L) and -2.8 mV (DOC = 3 mg/L).

Table 7. Zeta potential measurements of the PS tracers in various aquatic media comprised of MilliQ water, NaCl, and humic acid (Mean and SD; n = 2). All zeta potential measurements were reported in mV. The asterisk (*) indicates a single measurement was collected. This data was collected by Professor James Ranville of the Colorado School of Mines. This table was provided by Rauschendorfer et al, 2021.

Salinity (g/L)	DOC Conc. (mg/L) 0	1.5	3.0
0	28.6 ± 0.5	16.4 ± 0.7	7.9 ± 0.1
1	19.5 ± 0.4	---	---
5	6.8 ± 2.3	-4.76*	-2.14*
30	-0.7 ± 1.2	-1.06*	-2.8*

3.2.2 PS Tracer Chemical Characterization

As the synthesis of the PS tracers required the formation of a PS-co-P2VP cores, a PS shell to cover the core, and the coordination of Au ions to form AuNPs, the tracers were chemically characterized throughout this process. With the use of FTIR and Raman spectroscopy, the PS-co-

P2VP cores, the PS shelled cores, and the fully synthesized PS tracers were compared to a PS standard to reveal successful PS tracer shelling (Figure 6). The assignment of Raman bands to atomic movements is made available in the Appendix (Table 14A).

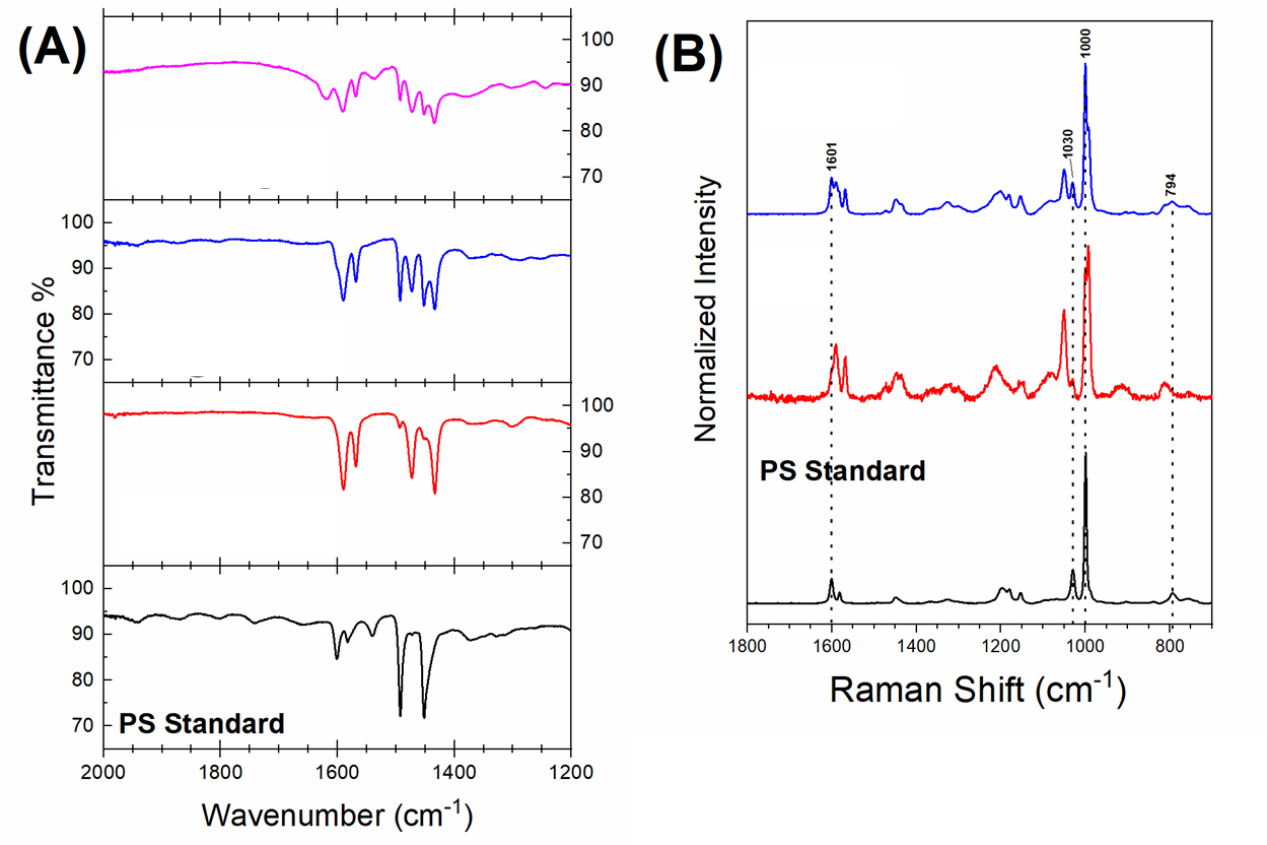

Figure 6. Chemical characterization of the PS-co-P2VP cores (Red), the PS-shelled cores (Blue), and the PS tracers (Pink) through (A) FTIR and (B) Raman spectroscopy. This figure was adapted from Rauschendorfer et al, 2021.

Additional confirmation of AuNPs associated with the PS tracers was performed through TGA, spICP-MS, and STEM. Using TGA, the PS-co-P2VP cores and the PS shelled cores displayed total combustion as the temperature approached 500°C while PS tracers retained a mass well above 600°C (Figure 6A). With spICP-MS, PS tracer detection relied on the abundance of AuNP that were associated with the PS tracer. This enabled the detection and distinction of PS tracers from unbound AuNPs based on the distribution in signal intensity (Figure 7A). With this, a conservative approach was taken to define the PS tracers in regard to signal intensity.

3.2.3 PS Tracer Stock Concentration

The concentration of the working PS tracer stock solution was determined using spICP-MS on highly diluted PS tracer solutions. Particle events were based on signal intensity and a particle number concentration was calculated based on the frequency of signal events, particle transport efficiency, sample flow rate, and analysis time (equation 1A). The average PS tracer concentration was estimated to be $(2.65 \pm 0.28)*10^{11}$ MP/mL (Table 8). The comparison of PS tracer stock concentrations at varying dilutions is available in the Appendix (Figure 8A).

Table 8. PS tracer concentration of the stock batch using spICP-MS. The concentration was determined by calculating the number of particles per volume (MP/mL). The calculations involved dividing the signal frequency by the transport efficiency, analysis time, and flow rate to yield a particle count per volume (MP count/mL). Accounting for the dilution factor, the stock concentration was determined (Mean ± SD; n=5).

Replicate Number	Signal Frequency	MP Count/mL	Dilution Factor	Stock Conc. (MP/mL)	Average Conc. (MP/mL)
01	159	$2.34*10^4$	$1*10^7$	$2.34*10^{11}$	
02	193	$2.84*10^4$	$1*10^7$	$2.84*10^{11}$	
03	210	$3.09*10^4$	$1*10^7$	$3.09*10^{11}$	$(2.65 \pm 0.28)*10^{11}$
04	175	$2.58*10^4$	$1*10^7$	$2.58*10^{11}$	
05	163	$2.40*10^4$	$1*10^7$	$2.40*10^{11}$	

3.2.4 PS Tracer Ruggedness

Due to concerns over potential leaching of gold nanoparticles from the tracers, the ruggedness of the PS tracers was evaluated in MilliQ, EPA MHW, and IO water after 48 hrs to evaluate the potential leachability of gold that would be indicated by a loss of mass over time. Comparing the three water types, there is a significant difference in the concentration of Au detected in the EPA MHW (group b) treatments compared to the MilliQ (group a) and IO (group a) treatments (Table 15A and Figure 7). Comparing the concentration of Au over time revealed no statistical difference between freshly prepared and 48 hr mixed treatments for all water types.

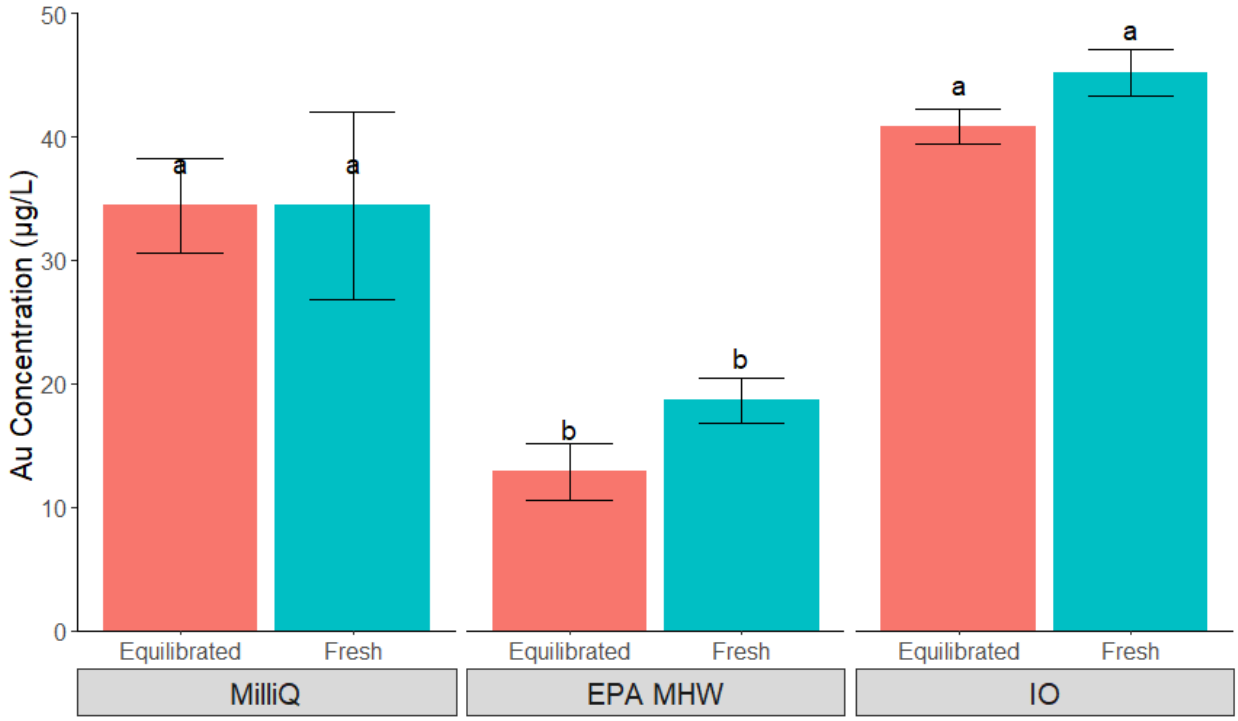

Figure 7. Evaluation of PS tracer ruggedness in varying aquatic media. The tracers' ruggedness was evaluated over time with initial media exposure (Fresh) and after 48 hr equilibration (Equilibrated). The Au concentration was reported along with a designated group based upon a post hoc analysis (Mean ± SD; n = 3). This figure was generated using R software.

3.3 PS Tracer Stability and Suspension

The impact of water chemistry on PS tracer colloidal stability and suspension was evaluated using varying concentrations of NaCl and humic acid to represent changes in salinity and DOC respectively. By coupling salinity with DOC, the influence of both factors was observed where a decrease in suspended PS tracers with increasing salinity at similar DOC concentrations. Likewise, a higher percent of PS tracers was detected at the highest DOC concentration used compared to samples without DOC at the same salinity (Table 9 and Figure 8).

Table 9. PS tracer stability and suspension at varying NaCl and SRHA concentrations. The percent of PS tracers was based on the number of PS tracers detected through spICP-MS divided by the calculated number of PS tracers spiked into each sample. An increase in NaCl concentrations, at constant SRHA concentrations, coincided with a decrease in the percent of suspended PS tracers. The concentration of SRHA, compared across similar NaCl concentrations, coincided with an initial decrease then an increase in the percent of suspended PS tracers (Mean ± SD; n=3).

NaCl (g/L)	SRHA (mg/L)	PS Tracer Conc. (MP/mL)	Percent PS Tracer Detection (%)
0	0	$(1.11 \pm 0.15)*10^8$	72.44 ± 9.96
0	1.5	$(8.03 \pm 0.39)*10^7$	52.06 ± 2.53
0	3	$(1.35 \pm 0.12)*10^8$	87.66 ± 7.83
1	0	$(4.84 \pm 0.57)*10^7$	31.37 ± 3.72
1	1.5	$(4.44 \pm 0.24)*10^7$	28.75 ± 1.54
1	3	$(8.52 \pm 0.82)*10^7$	55.24 ± 5.34
5	0	$(3.73 \pm 0.11)*10^7$	24.21 ± 7.39
5	1.5	$(3.10 \pm 0.70)*10^7$	20.12 ± 4.55
5	3	$(1.03 \pm 0.14)*10^8$	66.80 ± 8.87
15	0	$(2.48 \pm 0.28)*10^7$	16.08 ± 1.80
15	1.5	$(3.16 \pm 0.27)*10^7$	20.47 ± 1.75
15	3	$(9.36 \pm 0.62)*10^7$	60.66 ± 3.99
30	0	$(1.82 \pm 0.57)*10^7$	11.81 ± 3.68
30	1.5	$(2.04 \pm 0.31)*10^7$	13.24 ± 1.98
30	3	$(8.14 \pm 0.10)*10^7$	52.77 ± 6.79

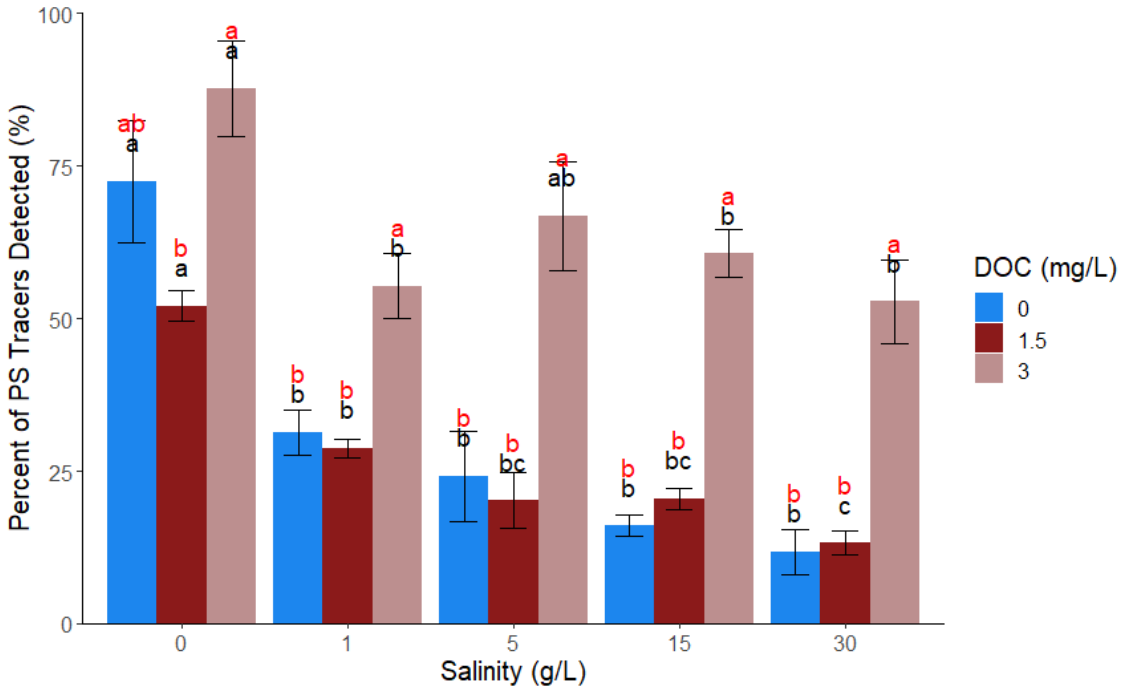

Figure 8. PS tracer stability and suspension in aqueous media of varying salinity and DOC concentrations. The percent of suspended PS tracers was reported along with an alphabetic group designation based on post hoc analysis (Mean ± SD; n=3). The group designation in red represents comparisons made based on the concentration of DOC while the group designation in black represents comparisons made based on salinity. This figure was generated using R software.

Comparisons between treatments of the same DOC concentrations and varying salinity were all found to be statistically different by ANOVA tests and samples were grouped using Tukey's HSD (Table 16A and Table 17A respectively). At DOC = 0 mg/L, the 0 g/L NaCl (72.44 ± 9.96%; group a) treatment was statistically different from the 1 (31.37 ± 3.72%; group b), 5 (24.21 ± 7.39%; group b), 15 (16.08 ± 1.80%; group b), and 30 g/L (11.81 ± 3.68%; group b) treatments. At DOC = 1.5 mg/L, the 0 g/L NaCl (52.06 ± 2.53%; group a) treatment had the highest PS tracer detection and was distinguishable from 1 (28.75 ± 1.54%; group b), 5 (20.12 ± 4.55%; group bc), 15 (20.47 ± 1.75%; group bc), and 30 g/L (13.24 ± 1.98%; group c) treatments. Finally, treatment comparisons at DOC = 3 mg/L found that the 0 g/L (87.66 ± 7.83%; group a) was statistically different from the 1 (55.24 ± 5.34%; group b), 15 (60.66 ± 3.99%; group b), and 30 g/L (52.77 ± 6.79%; group b) treatments, while the 5 g/L (66.80 ± 8.87%; group ab) treatment was indistinguishable from all other treatments.

Comparisons between treatments varying in DOC concentrations at constant salinity were statistically evaluated using ANOVA tests and Tukey's HSD tests to identify differences between treatments (Table 16A and Table 17A). For the treatments where salinity was 0 g/L, the 3 mg/L DOC (87.66 ± 7.83%; group a) treatment was distinguishable from the 1.5 mg/L (52.06 ± 2.53%; group b) treatment, while the 0 mg/L (72.44 ± 9.96%; group ab) treatment was indistinguishable from either treatment. As salinity was increased to 1, 5, 15, and 30 g/L, the 3 mg/L (group a) treatment had a significantly higher detection of suspended PS tracers while the 0 (group b) and 1.5 mg/L (group b) treatments were indistinguishable.

3.4 PS Tracer Partitioning

The partitioning behavior of the PS tracers in aquatic media was investigated through the pairing of sample site sediment with EPA MHW or IO. PS tracer detection was distinguished

between suspended and suspended and loosely bound particles for all samples. Statistical analyses were used to address the differences in water chemistry, compare the percent of suspended to suspended and loosely bound PS tracers, and compare the sample site sediments by the percent of PS tracer capture.

3.4.1 Suspended Vs. Suspended and Loosely Bound PS Tracers

A focus of this research was discerning between the PS tracers that remained suspended from the PS tracers that were loosely bound to the sediment and experimental chamber. Addressed through sample sonication, water and sediment/water treatments were compared based on water type using a pairwise t-test (Table 18A). All comparisons were only made between the same treatment (water vs. sediment/water) and water type (EPA MHW vs. IO). No statistical difference was found between the suspended PS tracers and the suspended and loosely bound PS tracers ($P > 0.05$).

3.4.2 PS Tracer Partitioning: Water

The impact of water chemistry on PS tracer stability was compared using EPA MHW and IO treatments equilibrated for 48 hrs followed by spICP-MS analysis. The percent of PS tracers that remained suspended in EPA MHW was 20.52 ± 9.55% and 7.21 ± 2.90% in IO. Likewise, the percent of suspended and loosely bound PS tracers was 24.77 ± 11.67% in EPA MHW and 10.78 ± 3.47% in IO (Table 10 and Figure 9). Statistical comparisons between the water types were performed using a pairwise t-test where a statistical difference was reported for the suspended treatment ($F_{1,6} = 6.68$; $P = 0.041$) and the loosely bound and suspended treatment ($F_{1,6} = 5.99$; $P = 0.05$) (Table 19A).

Table 10. Detection of suspended and loosely bound PS tracers after 48hr equilibration in EPA MHW and IO. Samples that were not sonicated treated as only suspended PS tracers while sonicated samples were treated as suspended and loosely bound PS tracers (Mean and SD; n=12).

Water Type	Sonicated	MP/mL	MP (%)
EPA MHW	No	$3.17*10^7$	20.52 ± 9.55
IO	No	$1.11*10^7$	7.21 ± 2.90
EPA MHW	Yes	$3.83*10^7$	24.77 ± 11.67
IO	Yes	$1.67*10^7$	10.78 ± 3.47

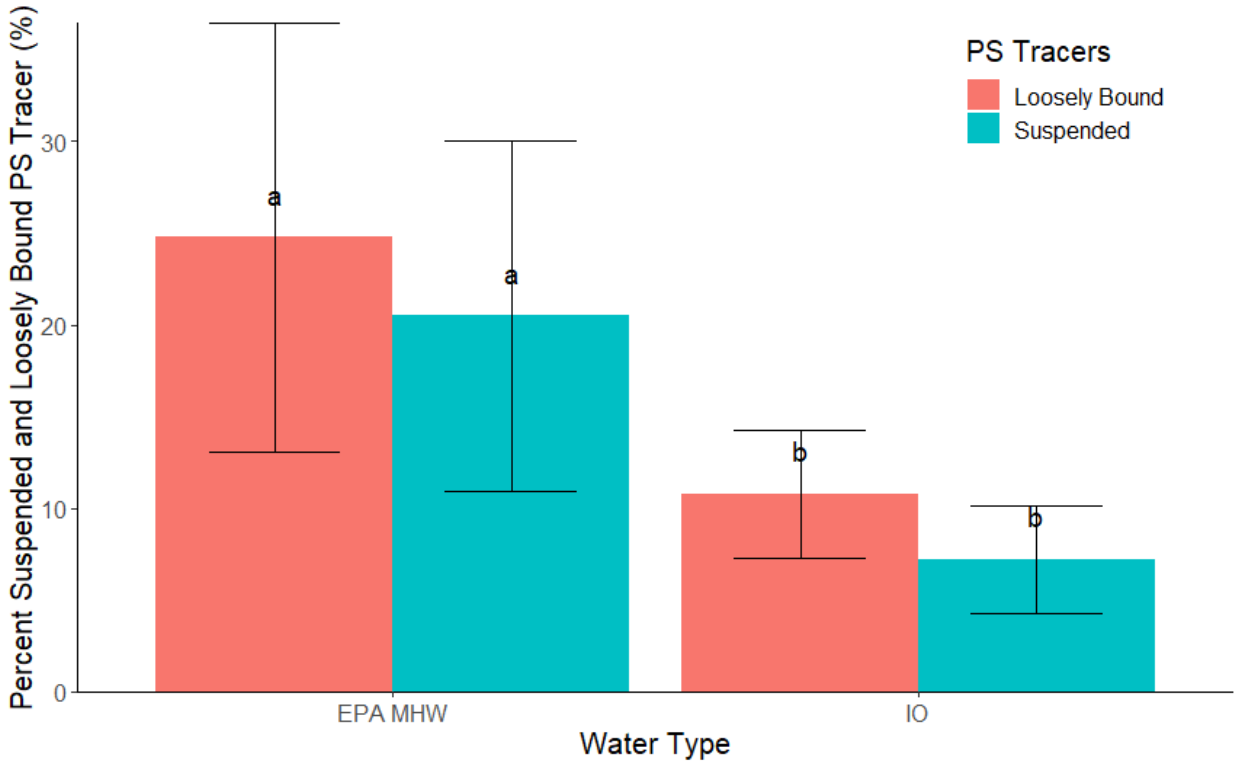

Figure 9. Comparing the percent of PS tracers detected as suspended particles and as loosely bound and suspended particles in EPA MHW and IO (Mean ± SD; n = 12). An alphabetic group assignment was performed based on a post hoc analysis. This figure was generated using R software.

3.4.3 PS Tracer Partitioning: Water and Sediment

To investigate the extent of PS tracer partitioning between water and sediment, comparisons between treatments of sediment/water were compared with water treatments. Sediment partitioning was compared with EPA MHW and IO for suspended PS tracers and loosely bound and suspended PS tracers where a profound effect was observed (Figure 10). For suspended PS tracers, the sediment paired with EPA MHW had a percent PS tracer suspension of 4.95 ±

3.75% and 5.62 ± 3.07% for sediment paired with IO (Table 11). For loosely bound and suspended PS tracers, sediment paired with EPA MHW had a percent PS detection of 5.62 ± 3.07% and sediment paired with IO had 2.06 ± 1.11% PS tracer detection (Table 11). Statistical evaluation of the suspended PS treatments found a significant difference ($P < 0.05$) for all samples except for the comparison of IO with sediment paired with EPA MHW ($P = 0.41$). For loosely bound and suspended PS tracers, all treatment comparisons were statistically different ($P = 0.05$) (Table 20A - Table 22A).

Table 11. Percent of suspended PS tracers detected after 48hr equilibration with environmental media. The environmental media was either water or sediment and water while the water type was either EPA MHW or IO. Samples were sonicated to account for the suspended and loosely bound PS tracers (Mean and SD; n=12).

Environmental Media	Water Type	Sonication	Suspended MP Percent (%)
Water	EPA	No	20.52 ± 9.55
Sediment/Water	EPA	No	4.95 ± 3.75
Water	EPA	Yes	24.77 ± 11.67
Sediment/Water	EPA	Yes	5.62 ± 3.07
Water	IO	No	7.21 ± 2.90
Sediment/Water	IO	No	2.06 ± 1.11
Water	IO	Yes	10.78 ± 3.47
Sediment/Water	IO	Yes	5.62 ± 3.07

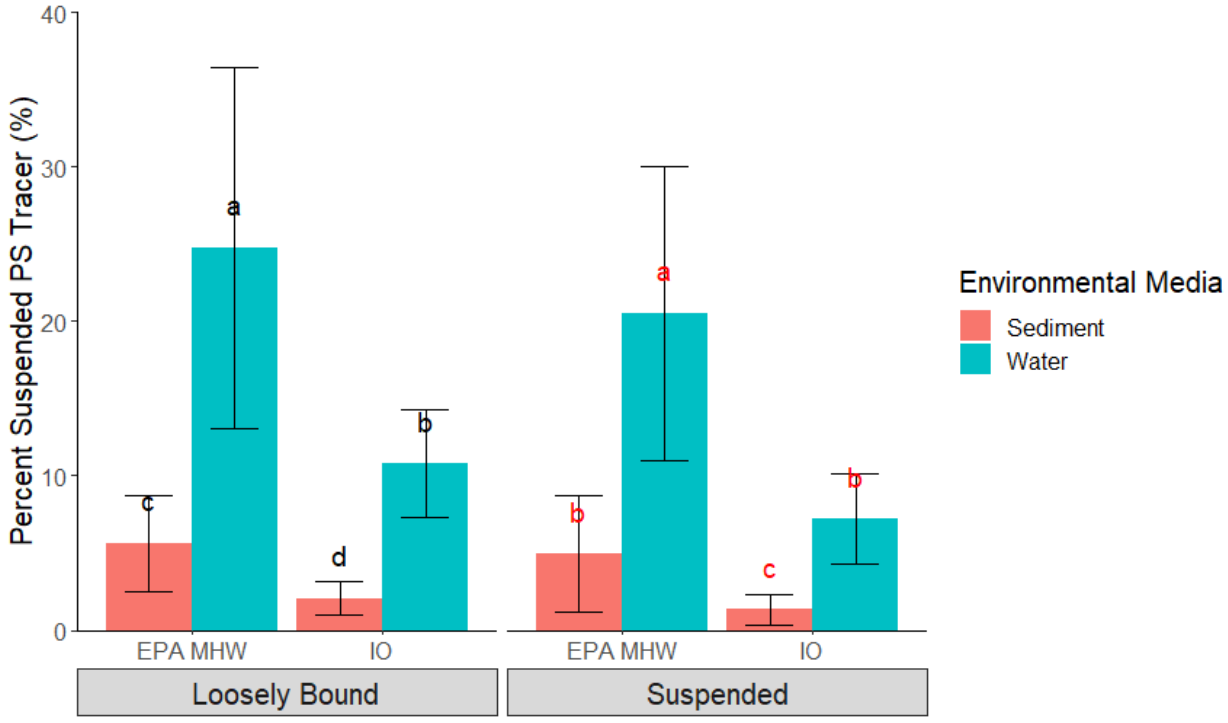

Figure 10. Comparing the percent of suspended PS tracers between samples containing water and samples containing water and sediment for both the suspended and suspended and loosely bound PS tracers (Mean ± SD; n = 12). These comparisons were made using EPA MHW and IO as the aqueous media and sediment from each of the sample sites (A-D). A post hoc comparison was used to alphabetically assign a group to compare with the black colored grouping comparing the percent of PS tracer detected in the suspended and loosely bound fraction. Likewise, a similar post hoc comparison was used to assign the red colored grouping that compared the percent of PS tracers in the suspended fraction. This figure was generated using R software.

3.4.4 PS Tracer Partitioning: Sediment Sites

As the impact of sediment was investigated with the comparison to water treatments, comparisons between each sample site sediment on PS tracer retention were performed. Comparisons were drawn between sediments in the same water type for suspended PS tracers and suspended and loosely bound PS tracers (Table 23A and Figure 11). Statistical comparisons for the percent of suspended PS tracers between sample site sediments were not found to be significant in EPA MHW (P = 0.44) or IO (P = 0.28) (Table 24A). For suspended and loosely bound PS

tracers, sample site sediments in IO were not significant (*P = 0.26*) while sample site sediments in EPA MHW initially indicated a difference, but a post hoc analysis revealed no significant difference (*P = 0.12*) (Table 24A and 25A).

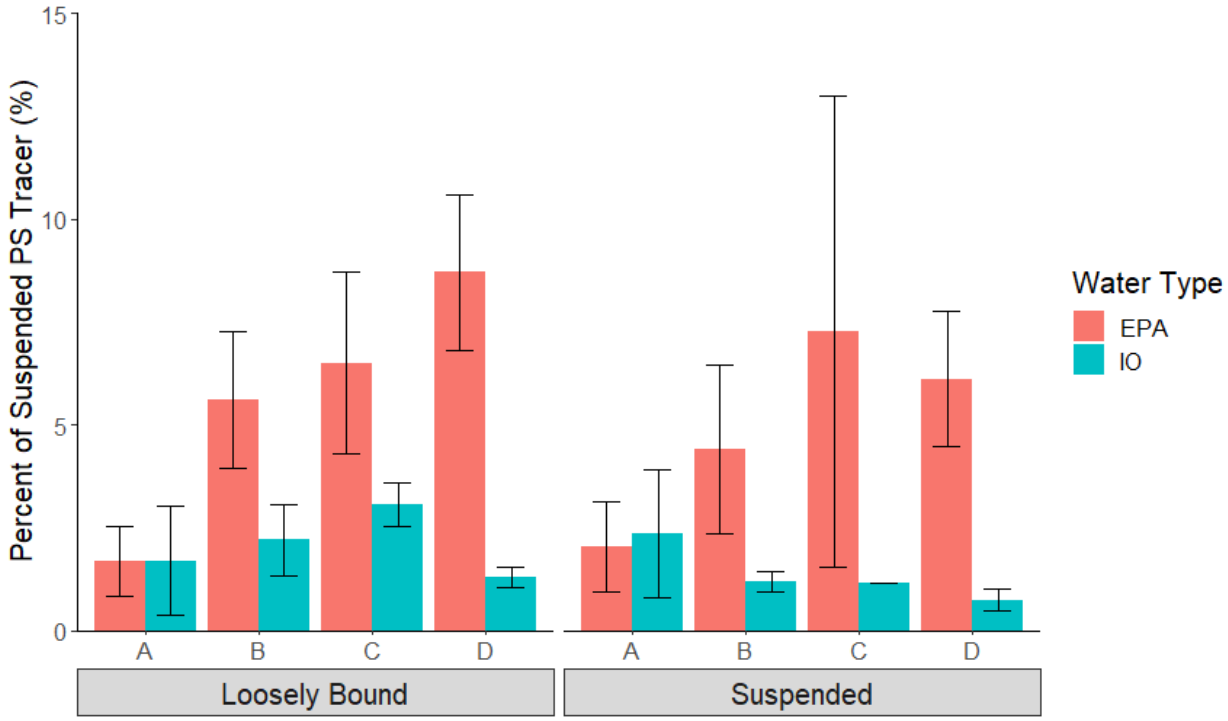

Figure 11. Comparing the percent of suspended PS tracers between sediment from the sample sites (A-D) (Mean ± SD; n = 3). These comparisons were made in EPA MHW and IO for the suspended and the suspended and loosely bound fractions. This figure was generated using R software.

3.4.5 PS Tracer Partitioning: Au Mass Association

The mass of Au associated with the water and the sediment portions were determined using ICP-MS. The total sum of Au exceeded the calculated Au value which was based on PS tracer concentration (10.6 mg/L). The mass of Au in each fraction is presented in Table 26A.

Chapter 4: Discussion and Conclusion

4.1 Sediment Profile

Classifying the sample sites by their physical and chemical characteristics revealed that sediment grain size, carbon content and speciation, and metal abundance were able to produce four distinct sites.

4.1.1 Sediment Grain Size

Comparisons by sediment grain size found that each site was primarily comprised of various sands, silts, and clays. This distinction is important as sediment particle size is tied to surface area, surface charge, cation exchange capacity, and particle settling velocity all of which influence the sediment's interactions with MP/NPs and transport in aquatic systems. In addition, sediment grain size correlated (Table 13A) with the metals Al, Cr, Cu, and Zn which were all statistically significant (Table 9A and Table 11A). The correlation of sediment grain size and Al was attributed to the presence of clay that has a size range below silt. As a result, sample sites recorded to have a higher concentration of particles below 63 μm are expected to have more clay particles and therefore a higher Al concentration. Sediment grain size correlation with Cr, Cu, and Zn is attributed to the intermolecular interactions between particles where smaller sediment grain sizes were observed to concentrate trace metals[78].

4.1.2 Sediment Carbon Analysis

Analysis of the sediment carbon content revealed that site C had the highest concentration of TC, LC, and BC compared to all other sites. Likewise, site D had the second highest LC concentration, but was not found to be statistically different from sites A and B. Comparing carbon content to sediment grain size revealed a strong positive correlation was observed with silt that

waned to a strong negative correlation with fine and medium sand (Table 13A). This trend has been observed in other studies where sediment grain size could be used as a key predictor for carbon content in estuaries with exceptions to areas with high sediment deposition, organic pollution, low-oxygen columns, or high seagrass-based carbon input[79-81].

The correlation of organic carbon with smaller grain sizes may be influenced by physical, chemical, and biological factors. The physical contributions to this correlation are associated with the fluid dynamics of the system and surface adsorption[79]. The transport and deposition of finer grain sediment and stable allochthonous carbon could both be influenced by the Nooksack River discharge and tidal actions resulting in a similar distribution[80]. Likewise, sediment surface area influences the adsorption of organic matter through electrostatic interactions with the mineral grain's surface[81]. In terms of chemical interactions, a ligand exchange/dehydration reaction may occur between hydroxyl groups associated with organic carbon compounds and the sediment surface. This would allow for the reversible, coordinated adsorption of organic carbon to the mineral surface that is directly influenced by sediment grain size[82]. The influence of biological factors for each sample site are expected to be minimal as the sites were mostly absent of seagrass and other major aquatic fauna[79]. As TC, LC, and BC had a strong correlation with sediment grain size, it was not possible to distinguish between these variables based on their interactions with the PS tracers. As such, this study focused on the role of sediment grain size as grain size appears to integrate most factors that include electrostatic forces and geochemical substrate concentrations[78].

4.1.3 Sediment Metal Analysis

Examining the sample sites by metal content, it was found that the statistically different metals were Cr, Cu, Mn, and Zn (Table 4), as well as Al and Na (Table 8A). Al, Cr, Cu, and Zn concentrations all showed a decrease in sediment grain size in line with previous studies[78]. The

higher concentrations of Na observed with site C was attributed to site location given its greater distance from a freshwater source. As the sediment was dried for analysis, an increase in Na concentration was expected. The concentration of Mn did not have an apparent correlation with sediment grain sizes but was significantly different at all sites (Table 13A). The differences in Mn concentrations are attributed to mineralogical differences within the study region. The difference in Mn concentrations was intriguing as this metal is often present as Mn oxides that usually exhibit negative surface charges. This has enabled Mn oxides to have a high sorption capacity for metal ions while it is expected to repel MP/NPs that hold a similar negative charge[83,84].

4.2 PS Tracer Characterization

4.2.1 PS Tracer Physical Characterization

The size of the PS tracer at all stages of synthesis were determined by DLS, AFM, and STEM where the addition of the PS shell was noted by a sizable increase in particle diameter from the core particles. Conversely, the addition of AuNPs to the PS-shelled cores did not significantly increase particle diameter. This provided evidence that the PS tracers were properly intercalated within the PS around the core and that the addition of AuNPs did not disrupt this process. The distribution in PS tracer size was reassuring as it was indicative of a reliable synthetic process that yields monodisperse PS tracers. From this, the size of the tracers used throughout this study was established.

The density of the PS traces was assessed through Sed-FFF with UV detection. The density of the PS tracers slightly exceeded that of pristine PS (1045-1100 kg/m^3) and thus shows an area where these tracers deviate from PS MP/NPs. Lowering the density of the PS tracers is a priority of ongoing research, but as it stands this is a weakness in the development of these tracers. Applied

as a PS MP/NP proxy, these PS tracers were viable as this study served as a proof-of-concept for the environmental application of labeled MP/NP tracers.

The associated charge of the PS tracers was investigated through the determination of the particle's zeta potential. In MilliQ water, the PS tracers held a positive charge with a zeta potential of 28.6 ± 0.5 mV which coincides with weak electrostatic colloidal stability[85]. The positive charge associated with the PS tracers could be attributed to excess pyridine groups of the PS-co-P2VP cores. Compared to the literature, the zeta potential for PS has been variable with size and associated functional groups, however, the zeta potential was recorded by Hwang et al. as close to 0 mV for 460 nm PS particles labelled with fluorescein isothiocyanate[86,87]. From this, the PS tracers did deviate in expressed surface charge, and aligning particle zeta potentials is a goal for future tracer development.

The addition of salinity and DOC on PS tracer zeta potential was also investigated and the results were similar to other scientific studies[26,88,89]. The addition of salinity was found to reduce PS tracer zeta potential and this effect was attributed to an increase in ionic strength compressing the electric double layer. The interaction of DOC with the PS tracers shifted the zeta potential more negative. This shift in zeta potential was attributed to the adsorption of DOC, a negatively charged molecule, that contributed to charge neutralization. Unlike salinity which suppressed coulombic forces, DOC contributes to the formation of a negative surface charge and can contribute to colloidal stability of neutral and negatively charged MP/NPs, however, this is not expected for the PS tracers due to their positive zeta potential[10,26].

4.2.2 PS Tracer Chemical Characterization

The chemical identity of the PS tracers was evaluated through FTIR and Raman spectroscopy and provided evidence that the tracers exhibited an exterior PS chemistry. This confirmed that the shelling approach for the PS tracers was correctly performed and provided confidence that the PS tracers would have similar chemical behavior to pristine PS MP/NPs. The addition of the AuNPs to the PS-shelled cores was confirmed through STEM, TGA, and spICP-MS. This provided the evidence that the AuNPs were internalized in the PS tracers and the dispersion in the number of AuNPs associated with a single tracer.

The chemical analysis of the PS tracers displayed a reliable synthesis approach where the PS tracers had an outward appearance of PS with an AuNP loading distribution of (2.75 ± 0.12)*10^3 to 344 ± 15 AuNP per PS tracer assuming a constant AuNP diameter of 5 to 10 nm (Table 8). Serving as a proxy, the PS tracers are chemically aligned with pure PS MP/NPs based on their outward appearance while the AuNPs enable precise analytical detection of the PS tracers.

4.2.3 PS Tracer Ruggedness

The ruggedness of the PS tracers was evaluated using varying water types to investigate AuNP retention. With these results, the PS tracers were concluded to be stable over time and in each of the water types. The discrepancies in Au concentrations between the water types were attributed to salinity causing PS tracer aggregation and adsorption to the sample chamber. This would explain the lower Au detection observed with the EPA MHW samples. The justification as to why this effect was not observed with the IO samples was based on sample-specific matrix effects affecting the ICP-MS internal standard recovery even after a 50x dilution factor was applied to all samples[90].

Comparing ruggedness over time indicated that the PS tracers did not leach gold as no statistical difference was observed. Additionally, all Au concentrations were lower in the equilibrated treatments compared to their freshly prepared counterparts. This indicated that any difference in the detected Au concentrations was the result of the immediate interactions between the PS tracers and water type and not degradation over time. For the sake of this study, the PS tracers were regarded as functionally stable as the Au concentration did not increase over time, spICP-MS does not rely on an internal standard for quantification, and all samples were heavily diluted (>1000x) for spICP-MS analysis.

4.3 PS Tracer Stability and Suspension

The stability of the PS tracers was evaluated using SRHA as the DOC and NaCl for salinity with concentrations reflecting a range recorded for Bellingham Bay[91]. The observed trend for increasing salinity in the absence of DOC was a significant decrease in the number of suspended PS tracers (Figure 8). The loss to colloidal stability is attributed to the increased ion presence compressing the electric double layer. This would suppress the electrostatic forces between particles leading to PS tracer aggregation and deposition. The decrease in colloidal stability of the PS tracers due to salinity parallels research into MP/NP stability in aquatic systems[26,88,89].

The impact of DOC on the PS tracers' colloidal stability was more complex than the impact of salinity as stability trends varied with increasing humic acid concentrations. The 3 mg/L DOC treatments displayed a stabilizing effect with the highest suspended PS tracer percentage compared to the 0 and 1.5 mg/L treatments. The observed stabilizing effect for the 3 mg/L DOC treatments was attributed to steric repulsion between DOC coated polymers while electrostatic forces are thought to have a minimal impact based on measured zeta potential.

For the 1.5 mg/L DOC treatments, a stabilizing effect was not observed with an initial decrease in the percent of suspended PS tracers compared to the 0 mg/L DOC treatments. This observation was attributed to incomplete polymer coating with DOC leading to hydrophobic aggregation and weakened electrostatic forces. As a complex organic molecule, humic acid is comprised of hydrophobic (aromatic and aliphatic carbons) and hydrophilic (hydroxyl groups and carboxylates) moieties that enable interactions with the polymers while remaining dissolved in aqueous media. The interaction of DOC with the PS tracers and the experimental chamber would adhere to the hydrophobic effect to create a more energetically stable system favoring indiscriminate adsorption to the PE, PP, or PS surfaces. At lower concentrations, it is theorized that the DOC would cause incomplete coating of the polymer surfaces encouraging a bridging effect between the PS tracers and the chamber. Additionally, the attachment of DOC to the PS tracers was found to contribute to a more negatively charged particle. As the PS tracers were found to have a positive surface charge, the addition of DOC would weaken these electric forces thus promoting aggregation and deposition.

Comparing the findings of this experiment to other studies, a similar effect was observed where salinity favored the aggregation and deposition of MP/NPs while DOC had a more stabilizing role by causing steric repulsion between PS tracers[26]. Extending these observations of salinity and DOC to natural systems, the role of salinity is expected to cause MP/NP aggregation while DOC would have a more complicated behavior. With salinity, the suppression of the coulombic forces is anticipated favoring MP/NP aggregation and deposition, however, in a natural system this effect would be added by the presence of divalent cations. The impact of DOC on MP/NP stability is expected to diverge from the observations made in this study as the system would be immensely larger and the sheer quantity of DOC would be orders of magnitude higher

than that of the MP/NPs. As such, DOC is expected to readily adsorb to the MP/NPs forming stable colloidal complexes. In addition, natural systems would have divalent cations that could lead to aggregation through cation bridging and the presence of natural particles can have a variety of effects on MP/NPs not explored in this experiment. With this, the stability and suspension of the PS tracers was comparable to other MP/NP studies that used a simplistic aquatic system but the behavior of the tracers in a natural system remains to be explored.

4.4 PS Tracer Partitioning

4.4.1 PS Tracer Partitioning: Water

The role of EPA MHW and IO on PS tracer suspension after equilibration was found to have a profound influence on PS tracer stability. The percent of suspended PS tracers associated with EPA MHW was 20.52 ± 9.55% and IO was 7.21 ± 2.90% indicating a clear distinction between the two water types (Table 10 and Figure 9). This distinction was attributed to the increased salinity associated with IO and is in accordance with the findings from the Stability and Suspension experiments. Comparing the percent of suspended particles to that of suspended and loosely bound particles did show an increase in the average percent of detected PS tracers but it was not statistically significant (Figure 9). As such, the portion of loosely bound PS tracers was considered negligible in this experiment.

4.4.2 PS Tracer Partitioning: Water and Sediment

Comparing the percent of suspended PS tracers between treatments that contained water versus water and sediment revealed that sediment had a significant impact on decreasing PS tracer suspension (Figure 10). Compared to their water counterparts, sediment with EPA MHW had a suspended PS tracer percentage of 4.95 ± 3.75 % (EPA MHW only: 20.52 ± 9.55%) and sediment

with IO water had a PS tracer percentage of 1.36 ± 1.01% (IO only: 7.21 ± 2.90%) (Table 11). This indicated that sediment had a meaningful impact on PS tracer suspension leading to a near total capture. These results parallel what has been reported in the literature where the majority of MP/NPs were found to adsorb to sediments and biosolids. The implications of these findings are that MP/NPs are highly retained to environmental particulates due to adsorption and Heteroaggregation thus limiting transport and often favoring deposition.

4.4.3 PS Tracer Partitioning: Sediment Sites

Comparing the different sediment from the sample sites indicated that there was no statistical difference in the percent of suspended or suspended and loosely bound PS tracers between sites in either EPA MHW or IO water (Table 23A and Figure 11). This inability to distinguish between the different sediments was due to the near total partitioning of the PS tracers to the sediment. As a result, differences in grain size, carbon content, and metal content could not be properly compared in this study and thus no conclusion can be drawn at this time.

Visual observation indicated that treatments containing sediment from sites C and D did have a slower settling velocity compared to sites A and B in EPA MHW. This factor likely contributed to the increasing trend in percent of suspended PS tracers observed in Figure 11. This trend was not observed in the IO water treatments likely due to the higher salinity. Extending this observation to natural systems, the heteroaggregation of MP/NPs with sediment is expected to impact contaminant transport where larger sediment grain sizes have faster settling velocities. This would impact MP/NP transport allowing for greater dispersion in aquatic environments.

4.5 PS Tracer Partitioning: Au Mass Association

The mass of Au associated with the sediment portion exceeded 95% for all samples when compared with the corresponding water fraction. The mass of Au detected did exceed the theoretically determined Au mass and this was attributed to excess Au not associated with the PS tracers but still present in the PS tracer stock solution. Although a similar trend in partitioning was observed, the advantage of single particle analysis becomes apparent as PS tracer events were able to be distinguished from other Au artifacts.

4.6 Conclusion and Future Applications

Coupling metallically-labeled MP/NP tracers with spICP-MS has provided an analytical mechanism to investigate the transport, fate, and behavior of MP/NPs in environmental systems. As a major analytical challenge is often in discerning MP/NPs from complex carbonaceous matrices, ICP-MS quantification of a trace metal transcends this issue. Further to this, single particle analysis allows for a rapid, individualized approach to analysis that can discern between labelled plastics and free Au NP events. This rapid quantification has allowed for the application of the PS tracers viable for use in environmental studies that probe MP/NP transport, fate, and behavior. As this study only addressed an initial application and the similarities to MP/NPs being mimicked, expansion in the application of PS tracers for environmental and toxicological is warranted with further study.

A major advantage to the synthetic approach used for the PS tracers was independence of the PS-co-P2V cores from the PS-shell and AuNPs. This has allowed for substitutions of the polymer shell and of the metallic nanoparticles which has been demonstrated[67,68]. Alterations to the synthetic approach would improve versatility allowing for a broader spectrum of polymers to

be explored. Substitutions to the metallic nanoparticles has been explored that would allow for a closer density match and it has been proposed that the use of magnetic nanoparticles could favor MP/NP recapture after deployment. Adaptations to tracer synthesis has allowed for a variety of metallically-labelled MP/NP tracers to be developed that can address complex questions related to MP/NPs, however, each of these tracers would need to be robust.

The ruggedness of the PS tracers was addressed to meet the needs of this study and was not tested beyond this extent. In this pursuit, the PS tracers did not leach AuNPs over time or in varying water types, however for studies with harsher environmental conditions (heat, UV, pH, etc.), a full sweep of ruggedness should be performed to determine applicability. To this purpose, determining the range of pH, temperature, time, and UV exposure is critical while exposure to different media should be explored. These benchmark tests would set the stage in guiding future environmental and biological studies.

Building upon the findings in this study, experiments could be tailored to address specific environmental factors without interference. As no significant differences were found between the sediment samples, studies that reevaluate the experimental design and more detailed individual comparison of carbon content, sediment grain sizes, and metal species would provide insight into role these factors have on MP/NPs. Taken further, the settling rate of the tracers, the partitioning coefficient, and tracer resuspension could be explored to a greater extent. Expanding on the applications of using metallically-labeled MP/NP tracers to investigate MP/NP transport, fate, and behavior, future studies can be tailored for specific environmental and toxicological purposes. These applications could include scenarios that mimic landfills, WWTPs, and applied sludge allowing for contaminant transport, fate, and behavior to be investigated. For toxicological purposes, the use of these traces could expand our understanding of MP/NP accumulation and

concentration to specific tissues. This would prove useful for studies that are investigating MP/NP interactions with flora or fauna and could employ analytical techniques that exploit the tracer's trace metal signature.

This study set the foundation for the use of our metallically-labeled MP/NP tracers in environmental applications and displayed the versatility of single particle analysis for this purpose. Evaluation of the PS tracers used in this study found that the tracers chemically resembled pure PS but did deviate in material density. Although future work aims to address this, the PS tracers displayed similar behavior and partitioning that has been recorded with other studies. In terms of detection, these tracers can be rapidly quantified and distinguished at low concentrations using ICP-MS. When the tracers are analyzed on a single particle basis, spICP-MS provides a higher degree of certainty in particle events providing confidence in the detection of the tracers from impurities and background events. Further development of these tracers is expected to increase their versatility with alterations to the polymer shell and trace metal nanoparticles and in the use of these tracers for more complex environmental and toxicological studies.

Citations

1. Andrady, A. L.; Neal, M. A. Applications and Societal Benefits of Plastics. *Philos. Trans. R. Soc. Lond. B. Biol. Sci.* **2009**, *364* (1526), 1977–1984. DOI: 10.1098/rstb.2008.0304
2. Smith, P. H. Plastics Come of Age. *Sci. Am.* **1935**, *152* (1), 5–7.
3. Hahladakis, J. N.; Velis, C. A.; Weber, R.; Iacovidou, E.; Purnell, P. An Overview of Chemical Additives Present in Plastics: Migration, Release, Fate and Environmental Impact during Their Use, Disposal and Recycling. *J. Hazard. Mater.* **2018**, *344*, 179–199. DOI: 10.1016/j.jhazmat.2017.10.014
4. Wessel, C. C.; Lockridge, G. R.; Battiste, D.; Cebrian, J. Abundance and Characteristics of Microplastics in Beach Sediments: Insights into Microplastic Accumulation in Northern Gulf of Mexico Estuaries. *Mar. Pollut. Bull.* **2016**, *109* (1), 178–183. DOI: 10.1016/j.marpolbul.2016.06.002
5. Geyer, R.; Jambeck, J. R.; Law, K. L. Production, Use, and Fate of All Plastics Ever Made. *Sci. Adv.* **2017**, *3* (7), 1704–1724. DOI: 10.1126/sciadv.1700782
6. Oliveira, M.; Ribeiro, A.; Hylland, K.; Guilhermino, L. Single and Combined Effects of Microplastics and Pyrene on Juveniles (0+ Group) of the Common Goby Pomatoschistus Microps (Teleostei, Gobiidae). *Ecol. Indic.* **2013**, *34*, 641–647. DOI: 10.1016/j.ecolind.2013.06.019
7. Danso, D.; Chow, J.; Streit, W. R. Plastics: Environmental and Biotechnological Perspectives on Microbial Degradation. *Appl. Environ. Microbiol.* **2019**, *85* (19), e01095-19. DOI: 10.1128/AEM.01095-19
8. Ebnesajjad, S. Introduction to Plastics. In *Chemical Resistance of Commodity Thermoplastics*, Baur, E., Ruhrberg, K., Woishnis, W., Eds.; William Andrew Publishing, 2016, pp 13–25. DOI: 10.1016/B978-0-323-47358-3.00017-X
9. Mattsson, K.; Jocic, S.; Doverbratt, I.; Hansson, L. A. Chapter 13 - Nanoplastics in the Aquatic Environment. In *An Emerging Matter of Environmental Urgency*, Zeng, E., Ed.; Elsevier, 2018; pp 379–399. DOI: 10.1016/B978-0-12-813747-5.00013-8
10. Alimi, O.; Farner Budarz, J.; M. Hernandez, L.; Tufenkji, N. Microplastics and Nanoplastics in Aquatic Environments: Aggregation, Deposition, and Enhanced Contaminant Transport. *Environ. Sci. & Technol.* **2018**, *52* (4), 1704–1724. DOI: 10.1021/acs.est.7b05559
11. Hopewell, J.; Dvorak, R.; Kosior, E. Plastics Recycling: Challenges and Opportunities. *Philos. Trans. R. Soc. B Biol. Sci.* **2009**, *364* (1526), 2115–2126. DOI: 10.1098/rstb.2008.0311
12. Weinstein, J. E.; Crocker, B. K.; Gray, A. D. From Macroplastic to Microplastic: Degradation of High-Density Polyethylene, Polypropylene, and Polystyrene in a Salt Marsh Habitat. *Environ. Toxicol. Chem.* **2016**, *35* (7), 1632–1640. DOI: 10.1002/etc.3432
13. Young, R.; Sullivan, L.; Schwartz, E.; Kramer, F. Frontline: Plastic Wars. *Public Broadcasting Station*, March 31, **2020**. https://www.pbs.org/wgbh/frontline/film/plastic-wars/ (Accessed April 2020)
14. Verma, R.; Vinoda, K. S.; Papireddy, M.; Gowda, A. N. S. Toxic Pollutants from Plastic Waste- A Review. *Procedia Environ. Sci.* **2016**, *35*, 701–708. DOI: 10.1016/j.proenv.2016.07.069
15. Katz, C. Piling Up: How China's Ban on Importing Waste Has Stalled Global Recycling. *Yale Environment 360 (New Haven, CT)*, March 7, **2019**.

https://e360.yale.edu/features/piling-up-how-chinas-ban-on-importing-waste-has-stalled-global-recycling (Accessed May 2020)
16. Joyce, C. Where Will Your Plastic Trash Go Now That China Doesn't Want It?. *National Public Radio (Chicago, IL)*, March 13, 2019. https://www.npr.org/sections/goatsandsoda/2019/03/13/702501726/where-will-your-plastic-trash-go-now-that-china-doesnt-want-it (Accessed May 2020)
17. Prata, J. C.; da Costa, J. P.; Duarte, A. C.; Rocha-Santos, T. Methods for Sampling and Detection of Microplastics in Water and Sediment: A Critical Review. *TrAC Trends Anal. Chem.* **2019**, *110*, 150–159. DOI: 10.1016/j.trac.2018.10.029
18. Li, Y.; Zhang, H.; Tang, C. A Review of Possible Pathways of Marine Microplastics Transport in the Ocean. *Anthr. Coasts* **2020**, *3* (1), 6–13. DOI: 10.1139/anc-2018-0030
19. Gray, A. D.; Wertz, H.; Leads, R. R.; Weinstein, J. E. Microplastic in Two South Carolina Estuaries: Occurrence, Distribution, and Composition. *Mar. Pollut. Bull.* **2018**, *128*, 223–233. DOI: 10.1016/j.marpolbul.2018.01.030
20. Picó, Y.; Barceló, D. Analysis and Prevention of Microplastics Pollution in Water: Current Perspectives and Future Directions. *ACS Omega.* **2019**, *4* (4), 6709–6719. DOI: 10.1021/acsomega.9b00222
21. Huppertsberg, S.; Knepper, T. P. Instrumental Analysis of Microplastics—Benefits and Challenges. *Anal. Bioanal. Chem.* **2018**, *410* (25), 6343–6352. DOI: 10.1007/s00216-018-1210-8
22. Lebreton, L.; Slat, B.; Ferrari, F.; Sainte-Rose, B.; Aitken, J.; Marthouse, R.; Hajbane, S.; Cunsolo, S.; Schwarz, A.; Levivier, A.; Noble, K.; Debelijak, P.; Maral, H.; Schoeneich-Argent, R.; Brambini, R.; Reisser, J. Evidence That the Great Pacific Garbage Patch Is Rapidly Accumulating Plastic. *Sci. Rep.* **2018**, *8* (1), 1-15. DOI: 10.1038/s41598-018-22939-w
23. Naqash, N.; Prakash, S.; Kapoor, D.; Singh, R. Interaction of Freshwater Microplastics with Biota and Heavy Metals: A Review. *Environ. Chem. Lett.* **2020**, *18* (6), 1813–1824. DOI: 10.1007/s10311-020-01044-3
24. Teuten, E. L.; Saquing, J. M.; Knappe, D. R. U.; Barlaz, M. A.; Jonsson, S.; Björn, A.; Rowland, S. J.; Thompson, R. C.; Galloway, T. S.; Yamashita, R.; et al. Transport and Release of Chemicals from Plastics to the Environment and to Wildlife. *Philos. Trans. R. Soc. B Biol. Sci.* **2009**, *364* (1526), 2027–2045. DOI: 10.1098/rstb.2008.0284
25. Singh, N.; Khandelwal, N.; Tiwari, E.; Naskar, N.; Lahiri, S.; Lützenkirchen, J.; Darbha, G. K. Interaction of Metal Oxide Nanoparticles with Microplastics: Impact of Weathering under Riverine Conditions. *Water Res.* **2021**, *189*, 1-13. DOI: 10.1016/j.watres.2020.116622
26. Singh, N.; Tiwari, E.; Khandelwal, N.; Darbha, G. K. Understanding the Stability of Nanoplastics in Aqueous Environments: Effect of Ionic Strength, Temperature, Dissolved Organic Matter, Clay, and Heavy Metals. *Environ. Sci. Nano* **2019**, *6* (10), 2968–2976. DOI: 10.1039/C9EN00557A
27. Fadare, O. O.; Wan, B.; Guo, L.-H.; Xin, Y.; Qin, W.; Yang, Y. Humic Acid Alleviates the Toxicity of Polystyrene Nanoplastic Particles to Daphnia Magna. *Environ. Sci. Nano* **2019**, *6*, 1466–1477. DOI: 10.1039/C8EN01457D
28. Salama, A. I. A. Mechanical Techniques: Particle Size Separation. In *Encyclopedia of Seperation Science*; Wilson, I., Eds.; Academic Press: Oxford, 2000; pp 3277–3289. DOI: 10.1016/B0-12-226770-2/07641-9

29. Stapleton, P. A. Toxicological Considerations of Nano-Sized Plastics. *AIMS Environ. Sci.* **2019**, *6* (5), 367–378. DOI: 10.3934/environsci.2019.5.367
30. Keller, A. S.; Jimenez-Martinez, J.; Mitrano, D. M. Transport of Nano- and Microplastic through Unsaturated Porous Media from Sewage Sludge Application. *Environ. Sci. Technol.* **2020**, *54* (2), 911–920. DOI: 10.1021/acs.est.9b06483
31. Corradini, F.; Meza, P.; Eguiluz, R.; Casado, F.; Huerta-Lwanga, E.; Geissen, V. Evidence of Microplastic Accumulation in Agricultural Soils from Sewage Sludge Disposal. *Sci. Total Environ.* **2019**, *671*, 411–420. DOI: 10.1016/j.scitotenv.2019.03.368
32. *United States Environmental Protection Agency* Basic Information about Biosolids. https://www.epa.gov/biosolids/basic-information-about-biosolids (Accessed August 2020)
33. Li, L.; Zhou, Q.; Yin, N.; Tu, C.; Luo, Y. Uptake and Accumulation of Microplastics in an Edible Plant. *Chinese Sci. Bull.* **2019**, *64* (9), 928–934. DOI: 10.1360/N972018-00845
34. Koelmans, A. A.; Mohamed Nor, N. H.; Hermsen, E.; Kooi, M.; Mintenig, S. M.; De France, J. Microplastics in Freshwaters and Drinking Water: Critical Review and Assessment of Data Quality. *Water Res.* **2019**, *155*, 410–422. DOI: 10.1016/j.watres.2019.02.054
35. Van Cauwenberghe, L.; Devriese, L.; Galgani, F.; Robbens, J.; Janssen, C. R. Microplastics in Sediments: A Review of Techniques, Occurrence and Effects. *Mar. Environ. Res.* **2015**, *111*, 5–17. DOI: 10.1016/j.marenvres.2015.06.007
36. Okubo, N.; Takahashi, S.; Nakano, Y. Microplastics Disturb the Anthozoan-Algae Symbiotic Relationship. *Mar. Pollut. Bull.* **2018**, *135*, 83–89. DOI: 10.1016/j.marpolbul.2018.07.016
37. Limonta, G.; Mancia, A.; Benkhalqui, A.; Bertolucci, C.; Abelli, L.; Fossi, M. C.; Panti, C. Microplastics Induce Transcriptional Changes, Immune Response and Behavioral Alterations in Adult Zebrafish. *Sci. Rep.* **2019**, *9* (1), 15775. DOI: 10.1038/s41598-019-52292-5
38. von Moos, N.; Burkhardt-Holm, P.; Köhler, A. Uptake and Effects of Microplastics on Cells and Tissue of the Blue Mussel Mytilus Edulis L. after an Experimental Exposure. *Environ. Sci. Technol.* **2012**, *46* (20), 11327–11335. DOI: 10.1021/es302332w
39. Watts, A. J. R.; Urbina, M. A.; Goodhead, R.; Moger, J.; Lewis, C.; Galloway, T. S. Effect of Microplastic on the Gills of the Shore Crab Carcinus Maenas. *Environ. Sci. Technol.* **2016**, *50* (10), 5364–5369. DOI: 10.1021/acs.est.6b01187
40. Rummel, C. D.; Jahnke, A.; Gorokhova, E.; Kühnel, D.; Schmitt-Jansen, M. Impacts of Biofilm Formation on the Fate and Potential Effects of Microplastic in the Aquatic Environment. *Environ. Sci. Technol. Lett.* **2017**, *4* (7), 258–267. DOI: 10.1021/acs.estlett.7b00164
41. Kowalski, N.; Reichardt, A. M.; Waniek, J. J. Sinking Rates of Microplastics and Potential Implications of Their Alteration by Physical, Biological, and Chemical Factors. *Mar. Pollut. Bull.* **2016**, *109* (1), 310–319. DOI: 10.1016/j.marpolbul.2016.05.064
42. Naji, A.; Esmaili, Z.; Khan, F. R. Plastic Debris and Microplastics along the Beaches of the Strait of Hormuz, Persian Gulf. *Mar. Pollut. Bull.* **2017**, *114* (2), 1057–1062. DOI: 10.1016/j.marpolbul.2016.11.032
43. Li, M.; He, L.; Zhang, M.; Liu, X.; Tong, M.; Kim, H. Cotransport and Deposition of Iron Oxides with Different-Sized Plastic Particles in Saturated Quartz Sand. *Environ. Sci. Technol.* **2019**, *53* (7), 3547–3557. DOI: 10.1021/acs.est.8b06904

44. Thwar, P. K.; Velegol, D. Force Measurements between Weakly Attractive Polystyrene Particles. *Langmuir* **2002**, *18* (20), 7328–7333. DOI: 10.1021/la025680t
45. Ife, A. F.; Harding, I. H.; Shah, R. M.; Palombo, E. A.; Eldridge, D. S. Effect of PH and Electrolytes on the Colloidal Stability of Stearic Acid–Based Lipid Nanoparticles. *J. Nanoparticle Res.* **2018**, *20* (12), 318. DOI: 10.1007/s11051-018-4425-x
46. Leiser, R.; Wu, G.-M.; Neu, T. R.; Wendt-Potthoff, K. Biofouling, Metal Sorption and Aggregation Are Related to Sinking of Microplastics in a Stratified Reservoir. *Water Res.* **2020**, *176*, 115748. DOI: 10.1016/j.watres.2020.115748
47. Uddin, M. K. A Review on the Adsorption of Heavy Metals by Clay Minerals, with Special Focus on the Past Decade. *Chem. Eng. J.* **2017**, *308*, 438–462. DOI: 10.1016/j.cej.2016.09.029
48. Kooi, M.; Nes, E. H. van; Scheffer, M.; Koelmans, A. A. Ups and Downs in the Ocean: Effects of Biofouling on Vertical Transport of Microplastics. *Environ. Sci. Technol.* **2017**, *51* (14), 7963–7971. DOI: 10.1021/acs.est.6b04702
49. Hussain, N.; Jaitley, V.; Florence, A. T. Recent Advances in the Understanding of Uptake of Microparticulates across the Gastrointestinal Lymphatics. *Adv. Drug Deliv. Rev.* **2001**, *50* (1), 107–142. DOI: 10.1016/S0169-409X(01)00152-1
50. Yonkos, L. T.; Friedel, E. A.; Perez-Reyes, A. C.; Ghosal, S.; Arthur, C. D. Microplastics in Four Estuarine Rivers in the Chesapeake Bay, U.S.A. *Environ. Sci. Technol.* **2014**, *48* (24), 14195–14202. DOI: 10.1021/es5036317
51. Kontrick, A. V. Microplastics and Human Health: Our Great Future to Think About Now. *J. Med. Toxicol.* **2018**, *14* (2), 117–119. DOI: 10.1007/s13181-018-0661-9
52. Silva, A. B.; Bastos, A. S.; Justino, C. I. L.; da Costa, J. P.; Duarte, A. C.; Rocha-Santos, T. A. P. Microplastics in the Environment: Challenges in Analytical Chemistry - A Review. *Anal. Chim. Acta* **2018**, *1017*, 1–19. DOI: 10.1016/j.aca.2018.02.043
53. Lin, Y.; Huang, X.; Liu, Q.; Lin, Z.; Jiang, G. Thermal Fragmentation Enhanced Identification and Quantification of Polystyrene Micro/Nanoplastics in Complex Media. *Talanta* **2020**, *208*, 1-8. DOI: 10.1016/j.talanta.2019.120478
54. Zhou, X.; Hao, L.; Wang, H.; Li, Y.; Liu, J. Cloud-Point Extraction Combined with Thermal Degradation for Nanoplastic Analysis Using Pyrolysis Gas Chromatography–Mass Spectrometry. *Anal. Chem.* **2019**, *91* (3), 1785–1790. DOI: 10.1021/acs.analchem.8b04729
55. Zhang, X.; Mell, A.; Li, F.; Thaysen, C.; Musselman, B.; Tice, J.; Vukovic, D.; Rochman, C.; Helm, P. A.; Jobst, K. J. Rapid Fingerprinting of Source and Environmental Microplastics Using Direct Analysis in Real Time-High Resolution Mass Spectrometry. *Anal. Chim. Acta* **2020**, *1100*, 107–117. DOI: 10.1016/j.aca.2019.12.005
56. Doué, M.; Dervilly-Pinel, G.; Pouponneau, K.; Monteau, F.; Le Bizec, B. Direct Analysis in Real Time - High Resolution Mass Spectrometry (DART-HRMS): A High Throughput Strategy for Identification and Quantification of Anabolic Steroid Esters. *Drug Test. Anal.* **2015**, *7* (7), 603–608. DOI: 10.1002/dta.1727
57. Karakolis, E. G.; Nguyen, B.; You, J. B.; Rochman, C. M.; Sinton, D. Fluorescent Dyes for Visualizing Microplastic Particles and Fibers in Laboratory-Based Studies. *Environ. Sci. Technol. Lett.* **2019**, *6* (6), 334–340. DOI: 10.1021/acs.estlett.9b00241
58. Mitrano, D. M.; Beltzung, A.; Frehland, S.; Schmiedgruber, M.; Cingolani, A.; Schmidt, F. Synthesis of Metal-Doped Nanoplastics and Their Utility to Investigate Fate and

Behaviour in Complex Environmental Systems. *Nat. Nanotechnol.* **2019**, *14* (4), 362–368. DOI: 10.1038/s41565-018-0360-3
59. *Millipore Sigma Fluorescent Microparticles and Nanobeads*. https://www.sigmaaldrich.com/US/en/technical-documents/technical-article/materials-science-and-engineering/biosensors-and-imaging/fluorescent-microparticles (Accessed December 2020)
60. Capozzi, F.; Carotenuto, R.; Giordano, S.; Spagnuolo, V. Evidence on the Effectiveness of Mosses for Biomonitoring of Microplastics in Fresh Water Environment. *Chemosphere* **2018**, *205*, 1–7. DOI: 10.1016/j.chemosphere.2018.04.074
61. Maes, T.; Jessop, R.; Wellner, N.; Haupt, K.; Mayes, A. G. A Rapid-Screening Approach to Detect and Quantify Microplastics Based on Fluorescent Tagging with Nile Red. *Sci. Rep.* **2017**, *7* (1), 44501. DOI: 10.1038/srep44501
62. Sander, M.; Kohler, H.-P. E.; McNeill, K. Assessing the Environmental Transformation of Nanoplastic through 13C-Labelled Polymers. *Nat. Nanotechnol.* **2019**, *14* (4), 301–303. DOI: 10.1038/s41565-019-0420-3
63. Zumstein, M. T.; Schintlmeister, A.; Nelson, T. F.; Baumgartner, R.; Woebken, D.; Wagner, M.; Kohler, H.-P. E.; McNeill, K.; Sander, M. Biodegradation of Synthetic Polymers in Soils: Tracking Carbon into CO₂ and Microbial Biomass. *Sci. Adv.* **2018**, *4* (7), eaas9024. DOI: 10.1126/sciadv.aas9024
64. Taipale, S. J.; Peltomaa, E.; Kukkonen, J. V. K.; Kainz, M. J.; Kautonen, P.; Tiirola, M. Tracing the Fate of Microplastic Carbon in the Aquatic Food Web by Compound-Specific Isotope Analysis. *Sci. Rep.* **2019**, *9* (1), 19894. DOI: 10.1038/s41598-019-55990-2
65. Bol'shakov, A. A.; Mao, X.; González, J. J.; Russo, R. E. Laser Ablation Molecular Isotopic Spectrometry (LAMIS): Current State of the Art. *J. Anal. At. Spectrom.* **2016**, *31* (1), 119–134. DOI: 10.1039/C5JA00310E
66. Russo, R. E.; Bol'shakov, A. A.; Mao, X.; McKay, C. P.; Perry, D. L.; Sorkhabi, O. Laser Ablation Molecular Isotopic Spectrometry. *Spectrochim. Acta Part B At. Spectrosc.* **2011**, *66* (2), 99–104. DOI: 10.1016/j.sab.2011.01.007
67. Rauschendorfer, R.; Whitman, K.; Summer, S.; Patrick, S.; Pierce, A.; Sefi-Cyr, H.; Tadjiki, S.; Kraft, M.; Emory, S.; Rider, D.; et al. Development and Application of Au Nanoparticle-Nanopolymer Composite Spheres for Environmental Monitoring. *Front. Toxicol.* **2021 (Submitted)**.
68. Curtis, T.; Taylor, A. K.; Alden, S. E.; Swanson, C.; Lo, J.; Knight, L.; Silva, A.; Gates, B. D.; Emory, S. R.; Rider, D. A. Synthesis and Characterization of Tunable, PH-Responsive Nanoparticle–Microgel Composites for Surface-Enhanced Raman Scattering Detection. *ACS Omega* **2018**, *3* (9), 10572–10588. DOI: 10.1021/acsomega.8b01561
69. Jiménez-Lamana, J.; Marigliano, L.; Allouche, J.; Grassl, B.; Szpunar, J.; Reynaud, S. A Novel Strategy for the Detection and Quantification of Nanoplastics by Single Particle Inductively Coupled Plasma Mass Spectrometry (ICP-MS). *Anal. Chem.* **2020**, *92* (17), 11664–11672. DOI: 10.1021/acs.analchem.0c01536
70. Ivar do Sul, J. A.; Costa, M. F. Plastic Pollution Risks in an Estuarine Conservation Unit. *J. Coast. Res.* **2013**, 65 (10065), 48–53. DOI: 10.2112/SI65-009.1
71. Quinn, T. An Environmental and Historical Overview of the Puget Sound Ecosystem, In *Puget Sound Shorelines and the Impacts of Armoring—Proceedings of a State of the Science Workshop*; Scientific Investigations Report 2010-5254; U.S. Department of the

Interior and U.S. Geological Survey: Olympia, WA, **2010**; 11-18. https://pubs.usgs.gov/sir/2010/5254/pdf/sir20105254.pdf
72. Asher. C. *Bellingham Bay Regional Background Sediment Characterization: Bellingham, WA: Sampling and Analysis Plan*; 14-09-338; Department of Ecology, **2014**; 6-9. https://apps.ecology.wa.gov/publications/documents/1409338.pdf
73. Caria, G.; Arrouays, D.; Dubromel, E.; Jolivet, C.; Ratié, C.; Bernoux, M.; Barthès, B. G.; Brunet, D.; Grinand, C. Black Carbon Estimation in French Calcareous Soils Using Chemo-Thermal Oxidation Method. *Soil Use Manag.* **2011**, *27* (3), 333–339. DOI: 10.1111/j.1475-2743.2011.00349.x
74. Elmquist, M.; Gustafsson, Ö.; Andersson, P. Quantification of Sedimentary Black Carbon Using the Chemothermal Oxidation Method: An Evaluation of Ex Situ Pretreatments and Standard Additions Approaches. *Limnol. Oceanogr. Methods* **2004**, *2* (12), 417–427. DOI: 10.4319/lom.2004.2.417
75. Gustafsson, Ö.; Gschwend, P. M. Soot as a Strong Partition Medium for Polycyclic Aromatic Hydrocarbons in Aquatic Systems. *Molecular Markers in Environmental Geochemistry*; ACS Symposium Series; American Chemical Society, **1997**; 671, 24–365. DOI: 10.1021/bk-1997-0671.ch024
76. Pace, H. E.; Rogers, N. J.; Jarolimek, C.; Coleman, V. A.; Higgins, C. P.; Ranville, J. F. Determining Transport Efficiency for the Purpose of Counting and Sizing Nanoparticles via Single Particle Inductively Coupled Plasma Mass Spectrometry. *Anal. Chem.* **2011**, *83* (24), 9361–9369. DOI:10.1021/ac201952t
77. Tadjiki, S.; Montaño, M. D.; Assemi, S.; Barber, A.; Ranville, J.; Beckett, R. Measurement of the Density of Engineered Silver Nanoparticles Using Centrifugal FFF-TEM and Single Particle ICP-MS. *Anal. Chem.* **2017**, *89* (11), 6056–6064. DOI: 10.1021/acs.analchem.7b00652.
78. Horowitz, A. J. Physical and Chemical Factors Affecting Sediment-Trace Element Chemistry. In *A Primer on Sediment-Trace Element Chemistry*, 2nd ed.; 91-76; U.S. Geological Survey, **1991**; 16-42. DOI: 10.3133/ofr9176
79. Serrano, O.; Lavery, P. S.; Duarte, C. M.; Kendrick, G. A.; Calafat, A.; York, P. H.; Steven, A.; Macreadie, P. I. Can Mud (Silt and Clay) Concentration Be Used to Predict Soil Organic Carbon Content within Seagrass Ecosystems? *Biogeosciences* **2016**, *13* (17), 4915–4926. DOI: 10.5194/bg-13-4915-2016
80. Kelleway, J. J.; Saintilan, N.; Macreadie, P. I.; Ralph, P. J. Sedimentary Factors Are Key Predictors of Carbon Storage in SE Australian Saltmarshes. *Ecosystems* **2016**, *19* (5), 865–880. DOI: 10.1007/s10021-016-9972-3
81. Mayer, L. M. Surface Area Control of Organic Carbon Accumulation in Continental Shelf Sediments. *Geochim. Cosmochim. Acta* **1994**, *58* (4), 1271–1284. DOI: 10.1016/0016-7037(94)90381-6
82. Stumm, W. Chapter 4: Adsorption. In *Chemistry of the Solid-Water Interface: Processes at the Mineral-Water and Particle-Water Interface in Natural Systems*, 1st ed.; Wiley-Interscience, **1992**; pp 108-113
83. Post, J. E. Manganese Oxide Minerals: Crystal Structures and Economic and Environmental Significance. *Proc. Natl. Acad. Sci.* **1999**, *96* (7), 3447–3454. DOI: 10.1073/pnas.96.7.3447

84. Zou, W.; Zhang, J.; Li, K.; Han, P.; Han, R. Characterization of Manganese Oxide and the Adsorption of Copper(II) and Lead(II) Ions from Aqueous Solutions. *Adsorpt. Sci. Technol.* **2009**, *27* (6), 549–565. DOI: 10.1260/0263-6174.27.6.549
85. Joseph, E.; Singhvi, G. Chapter 4 - Multifunctional Nanocrystals for Cancer Therapy: A Potential Nanocarrier. In *Nanomaterials for Drug Delivery and Therapy*; Grumezescu, A., Ed.; William Andrew Publishing, **2019**; pp 91–116. DOI: 10.1016/B978-0-12-816505-8.00007-2
86. Hwang, J.; Choi, D.; Han, S.; Jung, S. Y.; Choi, J.; Hong, J. Potential Toxicity of Polystyrene Microplastic Particles. *Sci. Rep.* **2020**, *10* (1), 7391. DOI: 10.1038/s41598-020-64464-9
87. Ekvall, M. T.; Lundqvist, M.; Kelpsiene, E.; Šileikis, E.; Gunnarsson, S. B.; Cedervall, T. Nanoplastics Formed during the Mechanical Breakdown of Daily-Use Polystyrene Products. *Nanoscale Adv.* **2019**, *1* (3), 1055–1061. DOI: 10.1039/C8NA00210J
88. Derjaguin, B.; Landau, L. Theory of the Stability of Strongly Charged Lyophobic Sols and of the Adhesion of Strongly Charged Particles in Solutions of Electrolytes. *Prog. Surf. Sci.* **1993**, *43* (1), 30–59. DOI: 10.1016/0079-6816(93)90013-L
89. Segets, D.; Marczak, R.; Schäfer, S.; Paula, C.; Gnichwitz, J.-F.; Hirsch, A.; Peukert, W. Experimental and Theoretical Studies of the Colloidal Stability of Nanoparticles−A General Interpretation Based on Stability Maps. *ACS Nano* **2011**, *5* (6), 4658–4669. DOI: 10.1021/nn200465b
90. Wilschefski, S. C.; Baxter, M. R. Inductively Coupled Plasma Mass Spectrometry: Introduction to Analytical Aspects. *Clin. Biochem. Rev.* **2019**, *40* (3), 115–133. DOI: 10.33176/AACB-19-00024
91. Figueroa-Kaminsky, C.; Ahmed, A.; McCarthy, S.; Pelletier, G. J.; Mohamedali, T.; Gala, J. Predicting Puget Sound's Organic Carbon—and Why We Need Enhanced Monitoring. In *Salish Sea Ecosystem Conference*; Seattle, **2018**.

Appendix

Appendix: Figures

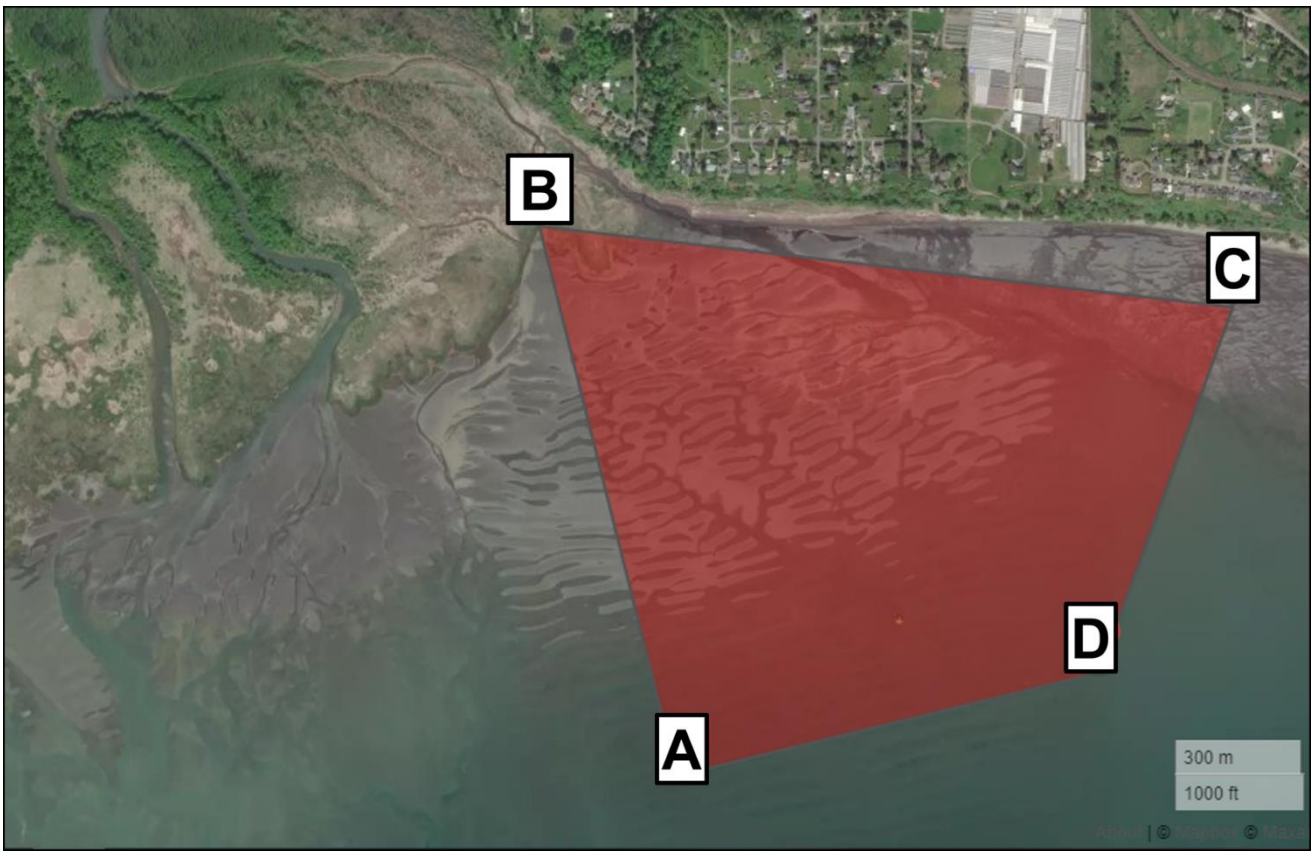

Figure 1A. Bellingham Bay study region where sediment was collected from four sample sites (A-D). Map generated using Geo JSON.

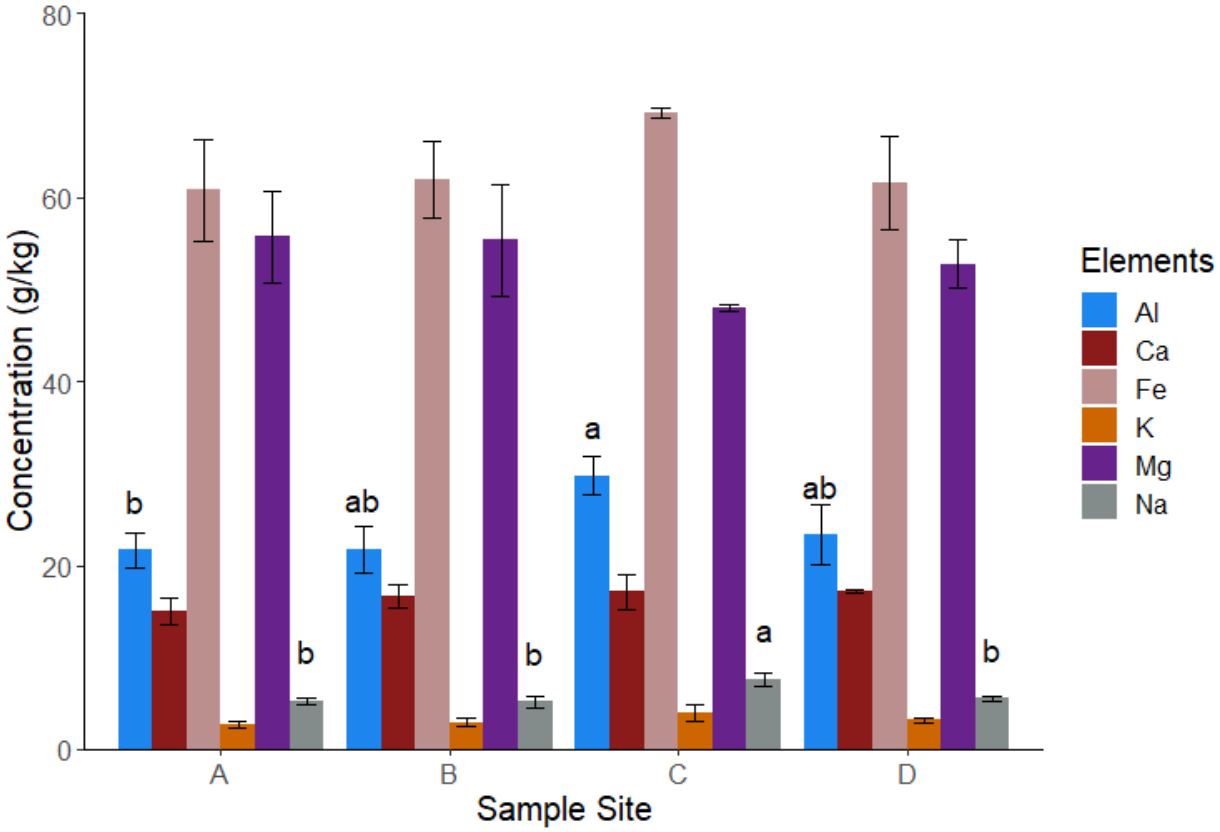

Figure 2A. Sediment major metal concentration for each sample site (A-D) as determined by FAAS analysis. Sites were compared and grouped based on a post hoc analysis and the assigned letters compare specific metals across sample sites. Metals without a designated letter group indicate that no statistical difference was determined (Mean ± SD; n = 3). This figure was generated using R software.

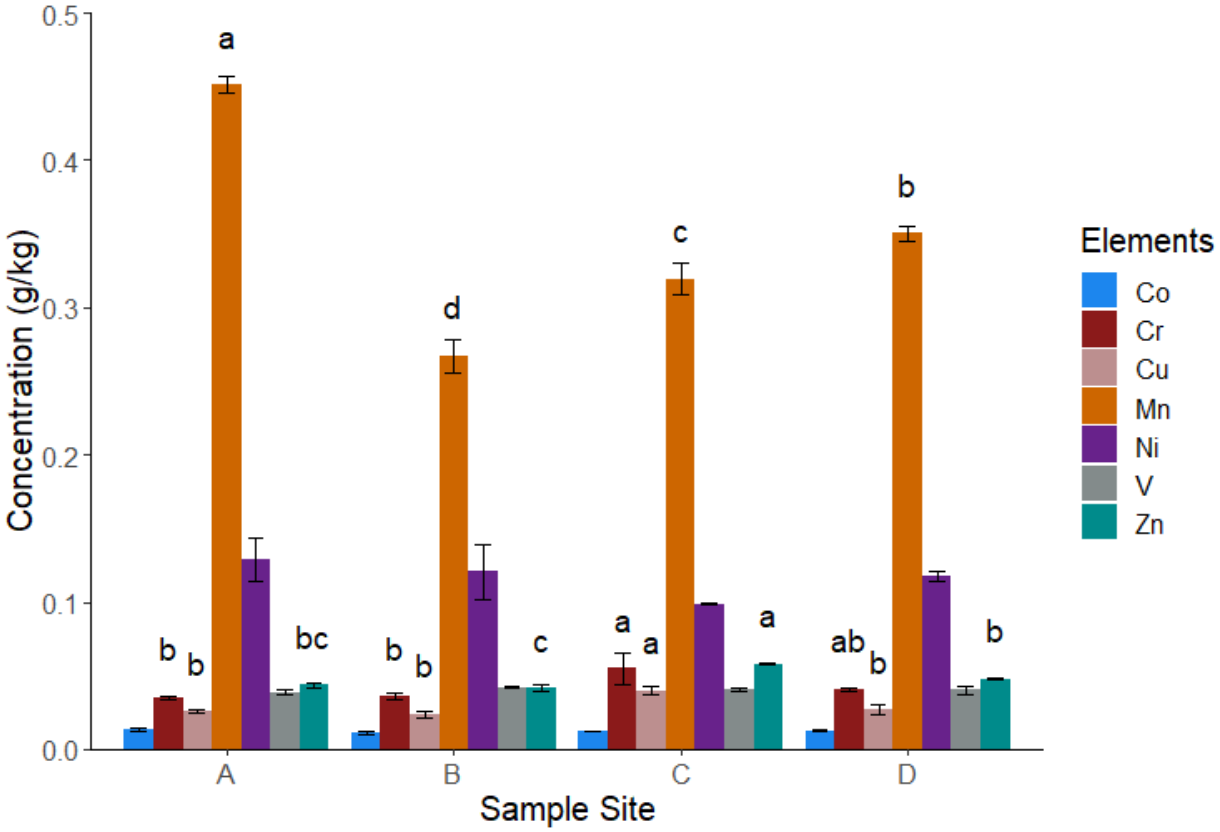

Figure 3A. The concentration of trace metals associated with the sediment for each sample site (A-D) as determined by ICP-MS. Sites were compared and grouped based on a post hoc analysis and the assigned letters compare specific metals across sample sites. Metals without a designated letter group indicate that no statistical difference was determined (Mean ± SD; n = 3). This figure was generated using R software.

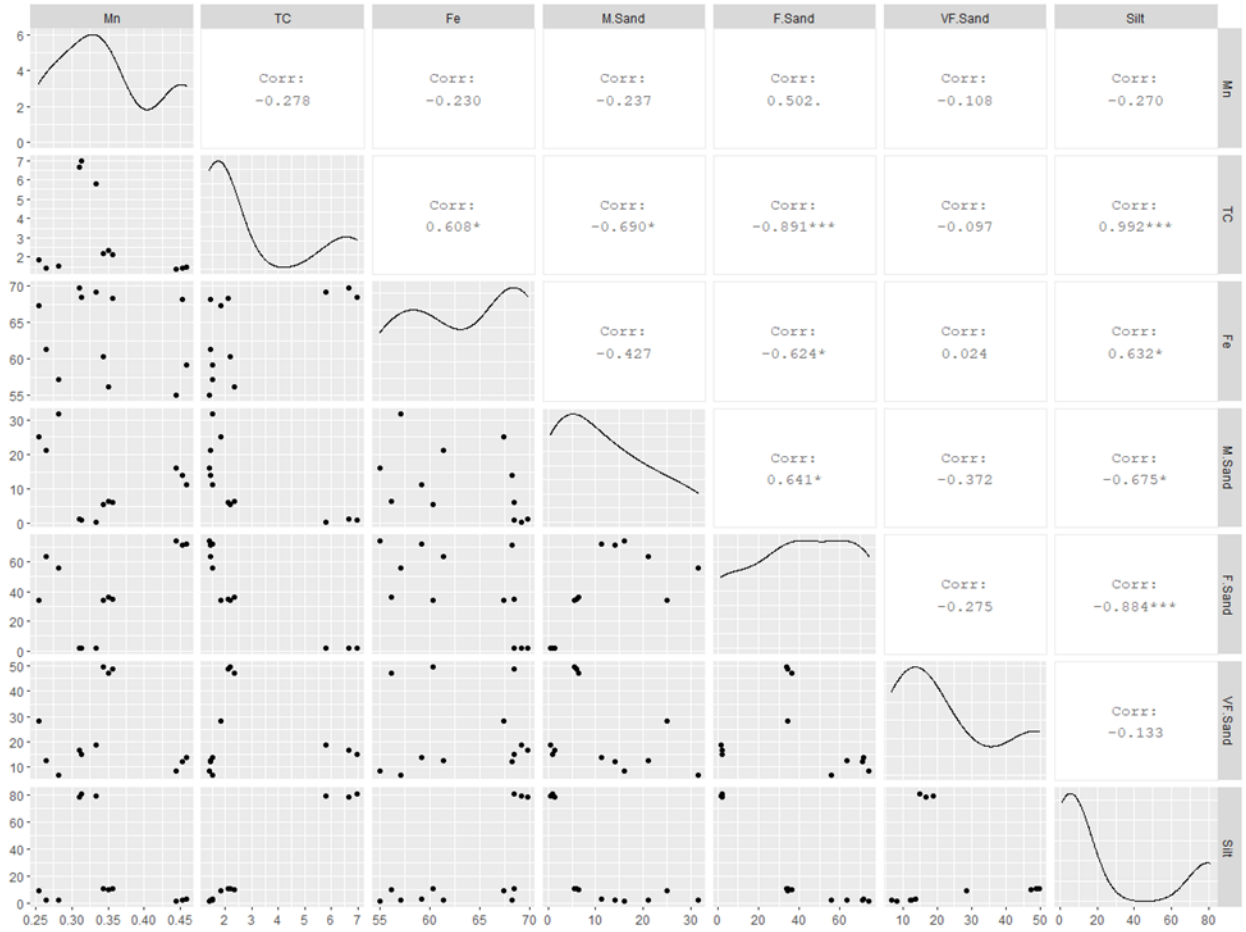

Figure 4A. Sediment variable correlation based on each sample site (A-D). The sediment grain sizes medium sand (M.Sand), fine sand (F.Sand), very fine sand (V. Sand), and silts and clays (Silt) were compared to the concentration of Mn, FE, and total carbon (TC) associated with each sample site. This figure was generated using R software.

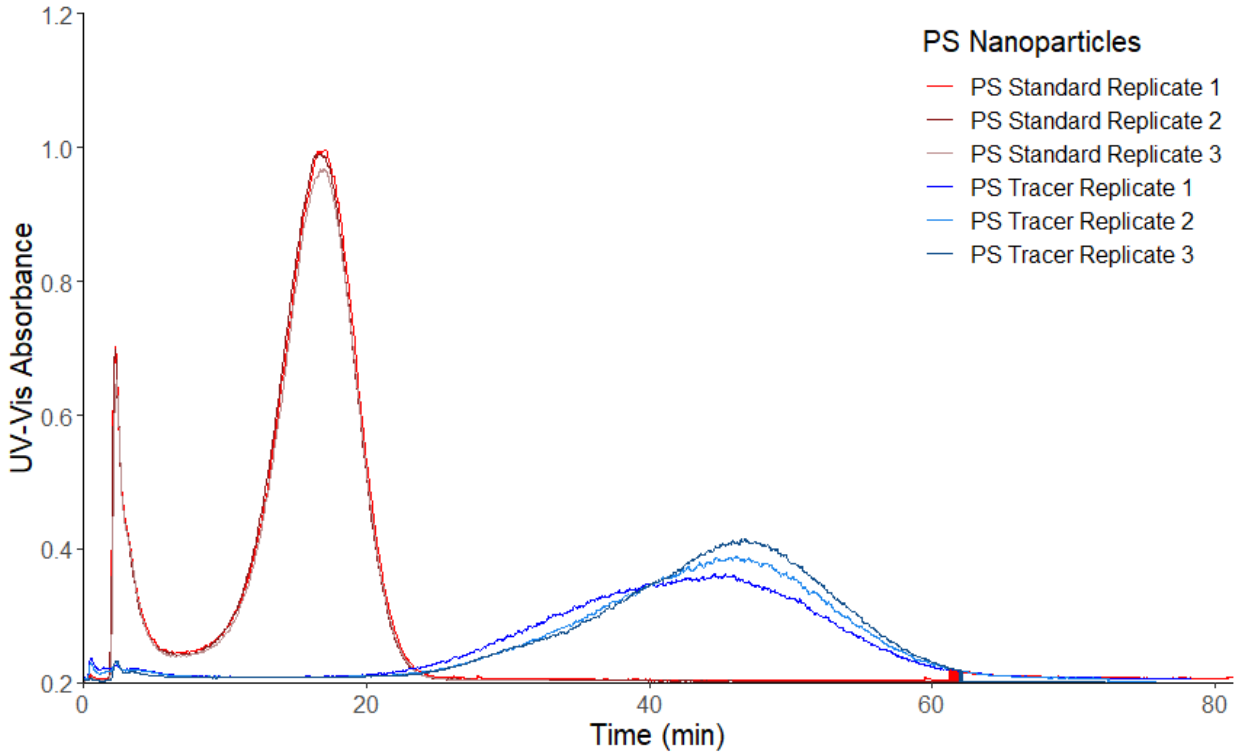

Figure 5A. Sed-FFF distribution and comparison of the PS tracers with a 512nm diameter PS standard. This figure was generated using R software.

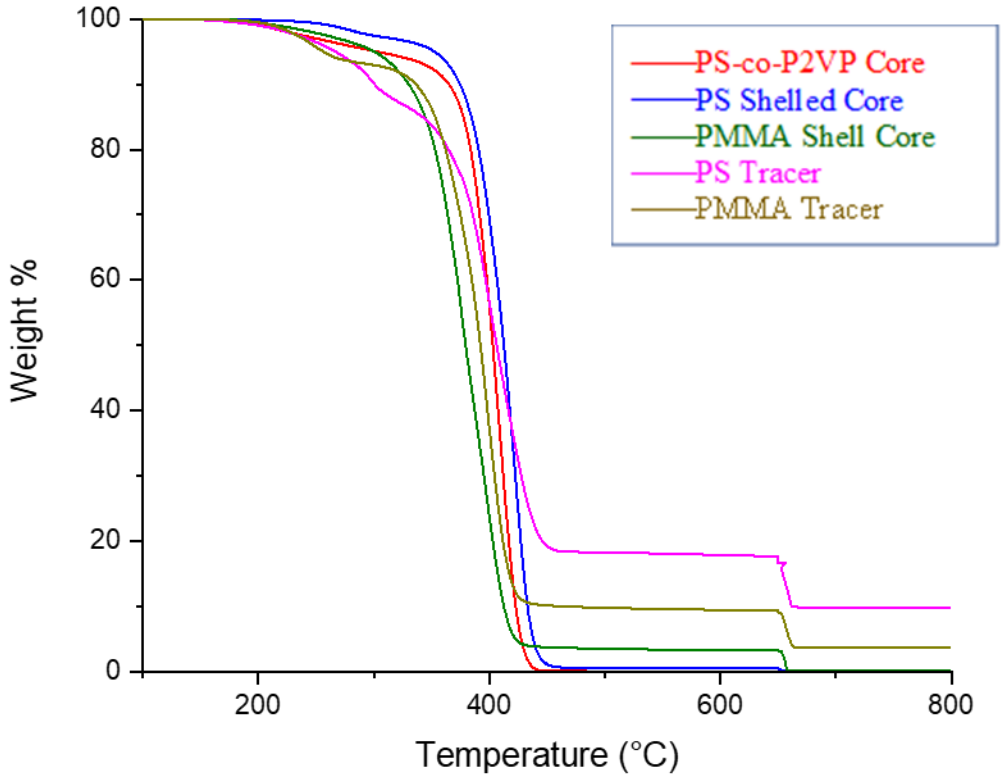

Figure 6A. Thermal degradation of the PS-co-P2V cores, PS shelled cores, and the PS tracers by TGA. Complete material combustion of the polymers was achieved by switching the purge gas from N_2 to air at a temperature of 650°C. The remaining mass after combustion of the organic material is representative of the AuNPs. This figure was redacted from Rauschendorfer et al 2021.

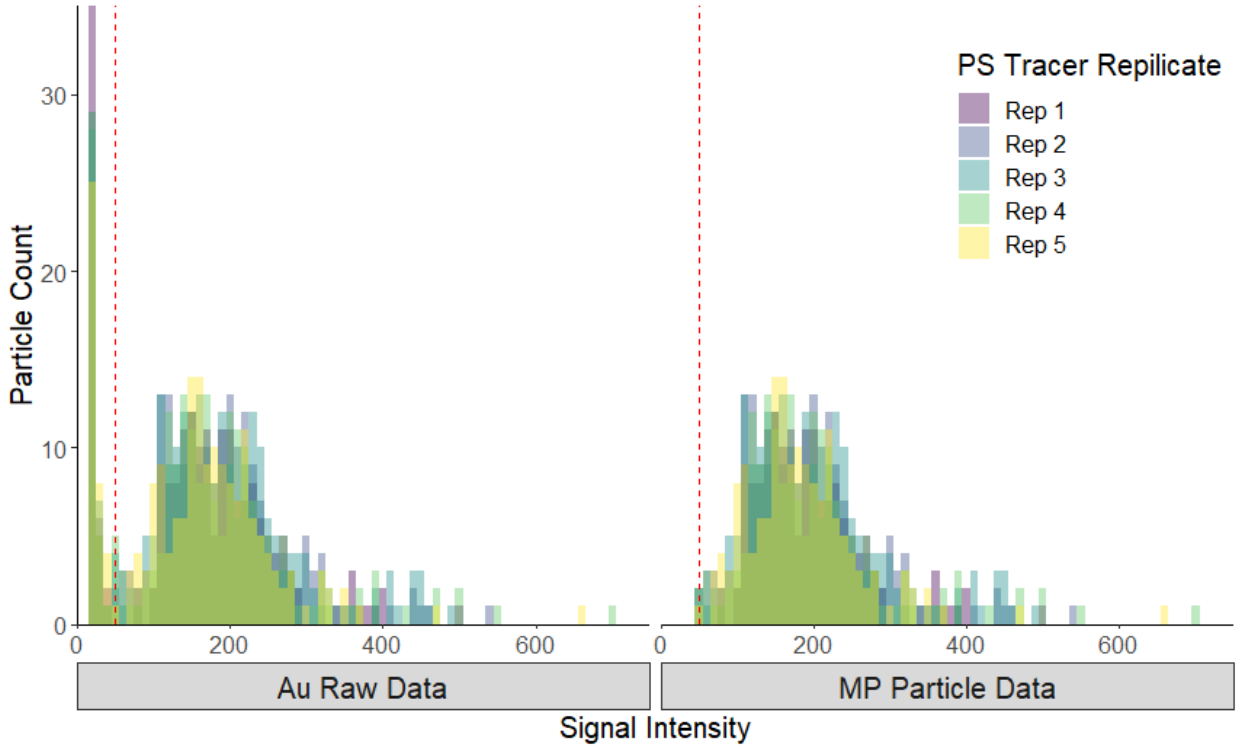

Figure 7A. Histogram distribution of the PS tracers showing relative monodispersity of the AuNP loading. The Au signal distribution is related to the mass of Au associated with a single PS tracer, free AuNP, or Au contaminant. A signal intensity cutoff of 70 was applied to ensure that Au background events were separated from PS tracer detection. The tailing effect for Au signal intensity is likely due to PS tracer aggregation and the detection of multiple particle events. This figure was generated using R software.

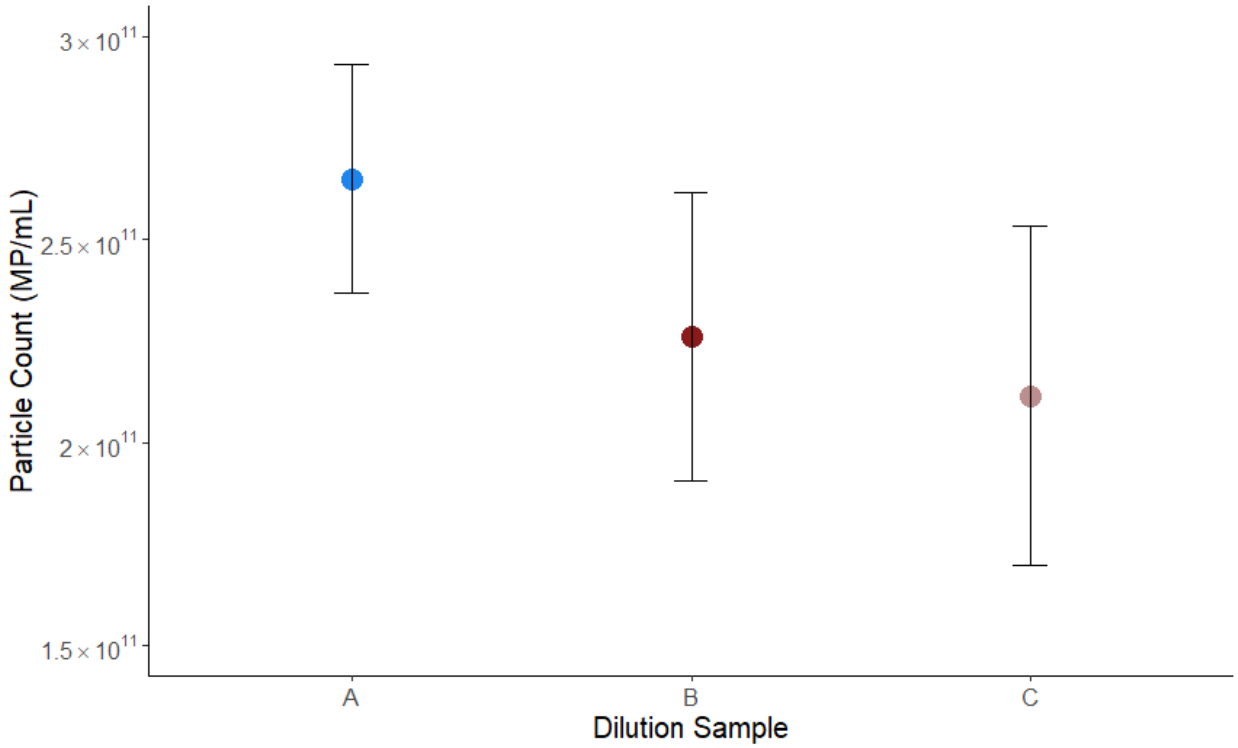

Figure 8A. spICP-MS measurements for PS tracer concentrations at stock dilutions of (A)10^7, (B) $5*10^6$, and (C) $2*10^6$ (n = 3). At a higher stock concentration, a lower particle count is observed, and this is attributed to coincidence events where multiple particles are detected at the same time causing an overlapped signal. This figure was generated using R software.

Appendix: Tables

Table 1A. Instrumental conditions for the Agilent 7500ce ICP-MS. The operational parameters for spICP-MS are provided which accounted for the analysis of nanoparticles and PS tracers.

Agilent 7500ce ICP-MS	
Instrument Parameters	**Value**
Nebulizer Gas Flow Rate	0.81 ml/min
Sample Flow Rate	0.34 ml/min
Spray Chamber	Scott Double Pass
ICP RF Power	1500 W
spICP-MS Operation	
Dwell time	10 ms
Transport efficiency	4-6%
Analyte	^{197}Au
Analysis Time	30 s

Table 2A. Instrumental conditions for Sedimentation Field Flow Fractionation (Sed-FFF). The analysis was performed by Postnova Analytics Inc, using a Sed-FFF model CF2000 with a UV detector attachment. This table was provided by Rauschendorfer et al, 2021.

Sedimentation Field Flow Fractionation (Sed-FFF)	
Postnova Analytics Instrument Parameter	**Model: CF2000 Value**
Field	1000 RPM
Channel Flow Rate	2 mL min^{-1}
Relaxation Time	5 min
Channel Thickness	131 μm
Injection Volume	50 μL
Carrier Solution	0.05% (v/v) FL-70 + 3 mM NaN_3

Table 3A. Operational conditions for the Renishaw inVia Qontor Raman Microscope.

Renishaw inVia Qontor Raman Microscope	
Parameter	**Setting**
Objective	Leica N Plan 50×L, NA = 0.50
Laser & Excitation Wavelength	HeNe, 632.8 nm
Spot Size on Sample	1.3 μm
Laser Power at Sample	5.0 mW
Power Density	3.8 mW/μm^2
Integration Time	10 sec
Spectra Averaged per Sample	12

Table 4A. Results for a MANOVA and one-way ANOVA tests used to determine if the sample sites were statistically different based on sediment grain size. The alpha value was set as $\alpha = 0.05$. The MANOVA test was significant ($F_{3,8} = 24.843$, $P < 0.001$) and each of the ANOVA tests were significant ($P < 0.05$ for all).

MANOVA	**$F_{3,8}$ value**	***p* value**
	24.84	$5.4*10^{-9}$
ANOVA	**$F_{3,8}$ value**	***p* value**
Coarse Sand	5.19	$2.8*10^{-2}$
Medium Sand	40.91	$3.4*10^{-5}$
Fine Sand	45.41	$2.3*10^{-5}$
Very Fine Sand	25.32	$2.0*10^{-4}$
Silt	834.05	$2.5*10^{-10}$

Table 5A. Results for Tukey's HSD test with $\alpha = 0.05$ based on sediment grain size. Tukey's HSD is a post hoc analysis that was used to compare each sample site by a specific grain size. Statistical differences between sites are indicated by grouping denoted alphabetically where group a represents the largest average mass percentage. Groups that share any of the same letter designations cannot be distinguished from each other.

Grain Type	Site	Average Mass Percentage (%)	SD	Grouping
Coarse Sand	A	0.52	0.089	b
Coarse Sand	B	2.55	1.45	a
Coarse Sand	C	0.82	0.42	ab
Coarse Sand	D	0.41	0.020	b
Medium Sand	A	13.77	2.41	b
Medium Sand	B	25.95	5.33	a
Medium Sand	C	0.96	0.48	c
Medium Sand	D	6.02	0.46	c
Fine Sand	A	72.46	1.65	a
Fine Sand	B	51.19	15.18	b
Fine Sand	C	1.80	0.31	c
Fine Sand	D	34.85	1.24	b
Very Fine Sand	A	11.43	2.88	b
Very Fine Sand	B	15.87	11.17	b
Very Fine Sand	C	16.84	1.91	b
Very Fine Sand	D	48.55	1.22	a
Silts and Clays	A	1.83	0.93	c
Silts and Clays	B	4.40	4.15	bc
Silts and Clays	C	79.54	1.28	a
Silts and Clays	D	10.18	0.44	b

Table 6A. Results for a MANOVA and one-way ANOVA tests used to determine if the sample sites were statistically different based on carbon concentration. The alpha value was set as $\alpha = 0.05$. The MANOVA test was significant ($F_{3,8} = 2.54$, $P < 0.01$) along with the ANOVA tests for Total Carbon (TC) ($F_{3,8} = 158.1$, $P < 0.001$), Labile Carbon (LC) ($F_{3,8} = 150.2$, $P < 0.001$), and Black Carbon (BC) ($F_{3,8} = 30.29$, $P < 0.001$). The Inorganic Carbon (IC) concentration was not significant ($P = 0.18$).

MANOVA	$F_{3,8}$ value	P value
	2.54	$3.3*10^{-2}$
ANOVA	**$F_{3,8}$ value**	**P value**
TC	158.1	$1.9*10^{-7}$
LC	150.2	$2.3*10^{-7}$
BC	30.29	$1.0*10^{-4}$
IC	2.06	0.18

Table 7A. Results for Tukey's HSD test based on carbon content with $\alpha = 0.05$. Tukey's HSD is a post hoc analysis that was used to compare each sample site by carbon species and concentration. Statistical differences between sites are indicated through grouping denoted alphabetically where group a represents the largest average concentration. Groups that share any of the same letter designations cannot be distinguished from each other. Site C was the only site that was significantly different from all other sites based on Total Carbon (TC), Labile Carbon (LC), and Black Carbon (BC).

Carbon Type	Site	Average Conc. (g/kg)	SD	Grouping
TC	A	1.44	$6.1*10^{-2}$	b
TC	B	1.61	0.22	b
TC	C	6.47	0.61	a
TC	D	2.21	0.11	b
LC	A	1.38	$6.7*10^{-2}$	b
LC	B	1.54	0.21	b
LC	C	6.18	0.59	a
LC	D	2.10	0.12	b
BC	A	$3.7*10^{-2}$	$9.1*10^{-3}$	b
BC	B	$6.9*10^{-2}$	$4.0*10^{-2}$	b
BC	C	0.22	$2.2*10^{-2}$	a
BC	D	$8.5*10^{-2}$	$2.1*10^{-2}$	b

Table 8A. Sediment metal concentrations (g/kg) for sample sites (A-D) as determined by FAAS (Mean ± SD; n = 3).

Site	Al Conc. (g/kg)	Mg Conc. (g/kg)	Fe Conc. (g/kg)	K Conc. (g/kg)	Na Conc. (g/kg)	Ca Conc. (g/kg)
A	21.65 ± 1.92	55.68 ± 4.91	60.76 ± 5.52	2.77 ± 0.39	5.28 ± 0.32	15.02 ± 1.47
B	21.74 ± 2.51	55.36 ± 6.10	61.93 ± 4.20	2.94 ± 0.47	5.18 ± 0.64	16.60 ± 1.29
C	29.76 ± 2.10	47.92 ± 0.35	69.15 ± 0.55	3.99 ± 0.86	7.61 ± 0.77	17.14 ± 1.94
D	23.35 ± 3.29	52.74 ± 2.65	61.63 ± 5.08	3.19 ± 0.29	5.56 ± 0.28	17.20 ± 0.24

Table 9A. Results for a MANOVA and ANOVA tests used to determine if the sample sites were statistically different based on sediment metal concentrations. The MANOVA test was not significant ($P < 0.49$) while the ANOVA tests were significant for Al ($F_{3,8} = 4.67$, $P < 0.05$) and Na ($F_{3,8} = 8.85$, $P < 0.01$). The metals Ca ($P = 0.41$), Fe ($P = 0.26$), K ($P = 0.20$), and Mg ($P = 0.29$) were not statistically significant by ANOVA.

MANOVA	$F_{3,8}$ value	P value
	1.02	0.49
ANOVA	**$F_{3,8}$ value**	**P value**
Al	4.67	0.036
Ca	1.08	0.41
Fe	1.63	0.26
K	1.98	0.20
Mg	1.50	0.29
Na	8.85	$6.4*10^{-3}$

Table 10A. Results for Tukey's HSD test based on sediment metal content with set to $\alpha = 0.05$. Tukey's HSD is a post hoc analysis that was used to compare each sample site by sediment metal concentration. Statistical differences between sites are indicated through grouping denoted alphabetically where group a represents the largest average concentration. Groups that share any of the same letter designations cannot be distinguished from each other.

Metal Species	Site	Average Conc. (g/kg)	SD	Grouping
Al	A	21.65	2.35	b
Al	B	21.74	3.08	ab
Al	C	29.76	2.57	a
Al	D	23.35	4.03	ab
Na	A	5.28	0.39	b
Na	B	5.18	0.79	b
Na	C	7.61	0.95	a
Na	D	5.56	0.34	b

Table 11A. Results for a MANOVA and ANOVA tests used to determine if the sample sites were statistically different based on sediment trace metal concentrations. The MANOVA test was significant ($F_{3,8} = 3.95$, $P < 0.001$) while the ANOVA tests were significant for Cr ($F_{3,8} = 5.51$, $P < 0.05$), Cu ($F_{3,8} = 13.51$, $p<0.01$), and Mn ($F_{3,8} = 161.1$, $P < 0.001$). The metals Co ($P = 0.10$), Ni ($P = 0.16$), and V ($P = 0.31$).

MANOVA	$F_{3,8}$ value	P value
	3.9532	$8.8*10^{-3}$
ANOVA	$F_{3,8}$ **value**	P **value**
Co	2.96	$9.8*10^{-2}$
Cr	5.51	$2.4*10^{-2}$
Cu	13.51	$1.7*10^{-3}$
Mn	161.1	$1.7*10^{-7}$
Ni	2.28	0.16
V	1.42	0.31
Zn	52.55	$1.3*10^{-5}$

Table 12A. Results from Tukey's HSD tests comparing sediment trace metal concentrations at each site (A-D). Site comparisons were made with set to $\alpha = 0.05$ which determined site grouping. Groups were assigned alphabetically with higher metal concentrations associated with site a. Sites with a common letter designation cannot be distinguished from each other based on that specific trace metal concentration.

Metal Species	Site	Average Conc. (g/kg)	SD	Grouping
Cr	A	$3.5*10^{-2}$	$1.2*10^{-3}$	b
Cr	B	$3.6*10^{-2}$	$2.6*10^{-3}$	b
Cr	C	$5.5*10^{-2}$	$1.3*10^{-2}$	a
Cr	D	$4.1*10^{-2}$	$1.2*10^{-3}$	ab
Cu	A	$2.6*10^{-2}$	$1.7*10^{-3}$	b
Cu	B	$2.4*10^{-2}$	$3.0*10^{-3}$	b
Cu	C	$4.0*10^{-2}$	$4.1*10^{-3}$	a
Cu	D	$2.7*10^{-2}$	$4.5*10^{-3}$	b
Mn	A	0.45	$7.2*10^{-3}$	a
Mn	B	0.27	$1.4*10^{-2}$	d
Mn	C	0.32	$1.3*10^{-2}$	c
Mn	D	0.35	$6.2*10^{-3}$	b
Zn	A	$4.4*10^{-2}$	$2.0*10^{-3}$	bc
Zn	B	$4.2*10^{-2}$	$2.4*10^{-3}$	c
Zn	C	$5.8*10^{-2}$	$1.2*10^{-3}$	a
Zn	D	$4.8*10^{-2}$	$1.1*10^{-3}$	b

Table 13A. Sediment predictor variable correlation. A value of 1.00 indicates a strong positive correlation, 0.00 indicates no correlation, and -1.00 indicates a strong negative correlation between variables. Sediment grain sizes were abbreviated as coarse sand (CS), medium sand (MS), fine sand (FS), very fine sand (VFS), and silts and clays (Silt). The correlation of carbon and metal species with sediment grain size were of particular interest as a high correlation would indicate that the individual influence of these species was indiscernible from grain size.

	V	Cr	Mn	Co	Ni	Cu	Zn	TC	LC	Al	Mg	Fe	K	Na	Ca	BC	IC	CS	MS	FS	VFS
V	1.00	-	-	-	-	-	-	-	-	-	-	-	-	-	-	-	-	-	-	-	-
Cr	0.07	1.00	-	-	-	-	-	-	-	-	-	-	-	-	-	-	-	-	-	-	-
Mn	-0.98	-0.28	1.00	-	-	-	-	-	-	-	-	-	-	-	-	-	-	-	-	-	-
Co	-0.97	0.00	0.93	1.00	-	-	-	-	-	-	-	-	-	-	-	-	-	-	-	-	-
Ni	-0.29	-0.98	0.48	0.21	1.00	-	-	-	-	-	-	-	-	-	-	-	-	-	-	-	-
Cu	-0.06	0.98	-0.15	0.10	-0.93	1.00	-	-	--	-	-	-	-	-	-	-	-	-	-	-	-
Zn	-0.09	0.98	-0.13	0.17	-0.93	0.97	1.00	-	-	-	-	-	-	-	-	-	-	-	-	-	-
TC	0.06	0.99	-0.27	-0.02	-0.97	0.99	0.97	1.00	-	-	-	-	-	-	-	-	-	-	-	-	-
LC	0.06	0.99	-0.27	-0.02	-0.96	0.99	0.97	1.00	1.00	-	-	-	-	-	-	-	-	-	-	-	--
Al	0.04	1.00	-0.25	0.01	-0.97	0.99	0.98	1.00	1.00	1.00	-	-	-	-	-	-	-	-	-	-	-
Mg	-0.07	-0.99	0.28	-0.03	0.97	-0.96	-0.99	-0.97	-0.97	-0.99	1.00	-	-	-	-	-	-	-	-	-	-
Fe	0.16	0.97	-0.36	-0.14	-0.96	0.97	0.92	0.99	0.99	0.98	-0.94	1.00	-	-	-	-	-	-	-	-	-
K	0.16	1.00	-0.37	-0.08	-1.00	0.96	0.97	0.98	0.98	0.99	-0.99	0.97	1.00	-	-	-	-	-	-	-	-
Na	0.00	0.99	-0.21	0.04	-0.95	1.00	0.97	1.00	1.00	1.00	-0.97	0.98	0.97	1.00	-	-	-	-	-	-	-
Ca	0.64	0.61	-0.75	-0.47	-0.73	0.45	0.55	0.53	0.53	0.55	-0.65	0.52	0.67	0.49	1.00	-	-	-	-	-	-
BC	0.19	0.98	-0.39	-0.14	-0.99	0.97	0.95	0.99	0.99	0.99	-0.98	0.99	0.99	0.98	0.63	1.00	-	-	-	-	-
IC	-0.17	0.97	-0.04	0.25	-0.89	0.97	1.00	0.95	0.95	0.97	-0.97	0.90	0.94	0.97	0.47	0.92	1.00	-	-	-	-
CS	0.83	-0.27	-0.74	-0.93	0.08	-0.31	-0.44	-0.21	-0.21	-0.26	0.32	-0.08	-0.20	0.11	-0.13	-0.50	0.79	1.00	-	-	-
MS	0.44	-0.77	-0.25	-0.57	0.65	-0.77	-0.87	-0.71	-0.71	-0.76	0.81	-0.62	-0.74	-0.38	-0.67	-0.89	0.36	0.81	1.00	-	-
FS	-0.32	-0.95	0.51	0.20	0.98	-0.87	-0.91	-0.91	-0.91	-0.93	0.96	-0.90	-0.97	-0.82	-0.96	-0.87	-0.40	0.13	0.68	1.00	-
VFS	0.08	0.02	-0.10	0.14	-0.04	-0.13	0.09	-0.11	-0.11	-0.05	-0.13	-0.20	0.06	0.58	-0.04	0.06	0.10	-0.38	-0.37	-0.23	1.00
Silt	0.06	0.98	-0.27	-0.03	-0.96	0.99	0.95	1.00	1.00	1.00	-0.96	0.99	0.97	0.50	0.99	0.94	0.14	-0.19	-0.69	-0.90	-0.16

Table 14A. Raman band assignments for the PS-co-P2VP cores and the PS-shelled cores. This table was adapted by Rauschendorfer et al, 2021.

PS-co-P2VP Core		PS-Shelled Core	
Raman Shift (cm^{-1})	**Assignment**	**Raman Shift (cm^{-1})**	**Assignment**
1601 (shoulder) (m)	PS ring stretch	1601 (s)	PS ring stretch
1590 (s)	P2VP ring stretch	1590 (m)	P2VP ring stretch
1567 (m)	PS ring stretch	-----	-----
-----	-----	1568 (m)	PS ring stretch
1447 (m)	P2VP ring stretch	1447 (m)	P2VP ring stretch
1330 (w)	PS/P2VP CH2 twist		
-----	-----	1328 (w)	PS/P2VP CH2 twist
1210 (m)	PS C=C of ring & backbone	-----	-----
-----	-----	1202 (m)	PS C=C of ring & backbone
-----	-----	1153 (m)	P2VP CH in plane bend
1149 (m)	P2VP CH in plane bend	-----	-----
1087 (w)	P2VP CH in plane bend	-----	-----
	-----	1051 (s)	PS CH in plane bend
1050 (s)	PS CH in plane bend	-----	-----
1030 (w)	PS CH in plane bend	1030 (m)	PS CH in plane bend
1000 (shoulder) (s)	PS/P2VP ring breathing	1000 (s)	PS/P2VP ring breathing
992 (s)	P2VP ring breathing	992 (shoulder) (s)	P2VP ring breathing
914 (w)	P2VP C-C vibrating	-----	-----
812 (w)	P2VP C=C of ring & backbone	-----	-----
-----	-----	794 (m)	PS C=C of ring & backbone

Table 15A. Evaluation of PS tracer ruggedness in various aquatic media. The concentration of free Au was compared in MilliQ, EPA MHW, and IO for freshly prepared and 48 hr equilibrated treatments (Mean and SD; n = 3). Each treatment was assigned to a lettered group based on a post hoc analysis.

Water Type	Equilibration Status	Au Concentration (µg/L)	Grouping
MilliQ	Freshly Prepared	34.42 ± 7.62	a
MilliQ	Equilibrated	34.43 ± 3.85	a
EPA MHW	Freshly Prepared	18.63 ± 1.83	b
EPA MHW	Equilibrated	12.86 ± 2.29	b
IO	Freshly Prepared	45.22 ± 1.87	a
IO	Equilibrated	40.81 ± 1.45	a

Table 16A. Results for ANOVA tests comparing (A) percent of suspended PS tracers with varying salinity at constant DOC concentrations and (B) percent of suspended PS tracers with varying DOC at constant salinity. The *F* and *P* values are provided. For A and B, all ANOVA comparisons indicated significant differences between treatments ($P = 0.01$).

(A) ANOVA: Salinity Comparison		
DOC Conc. (mg/L)	$F_{4,10}$ **value**	***P* value**
0	31.93	$1.1*10^{-5}$
1.5	62.36	$4.9*10^{-7}$
3	8.45	$3.0*10^{-3}$
(B) ANOVA: DOC Comparison		
Salinity (g/L)	$F_{2,6}$ **value**	***P* value**
0	11.47	$8.9*10^{-3}$
1	28.60	$8.6*10^{-4}$
5	26.03	$1.1*10^{-3}$
15	163.20	$5.9*10^{-6}$
30	50.93	$1.7*10^{-4}$

Table 17A. Results from Tukey's HSD tests comparing treatments at varying salinity and DOC concentrations. Treatment groups were alphabetically assigned with a representing the largest percent of PS tracers detected (n = 3).

Salinity (g/L)	DOC (mg/L)	Total MP Percent (%)	SD	Grouping
0	0	72.44	12.19	a
1	0	31.37	4.56	b
5	0	24.21	9.04	b
15	0	16.08	2.20	b
30	0	11.81	4.51	b
0	1.5	52.06	3.10	a
1	1.5	28.75	1.88	b
5	1.5	20.12	5.58	bc
15	1.5	20.47	2.14	bc
30	1.5	13.24	2.43	c
0	3	87.66	9.59	a
1	3	55.24	6.54	b
5	3	66.80	10.87	ab
15	3	60.66	4.89	b
30	3	52.77	8.32	b
0	0	72.44	12.19	ab
0	1.5	52.06	3.10	b
0	3	87.66	9.59	a
1	0	31.37	4.56	b
1	1.5	28.75	1.88	b
1	3	55.24	6.54	a
5	0	24.21	9.04	b
5	1.5	20.12	5.58	b
5	3	66.80	10.87	a
15	0	16.08	2.20	b
15	1.5	20.47	2.14	b
15	3	60.66	4.89	a
30	0	11.81	4.51	b
30	1.5	13.24	2.43	b
30	3	52.77	8.32	a

Table 18A. Results from a pairwise t-test comparing the percent of PS tracers detected before and after sonication. This comparison represents the portion of suspended PS tracers (before sonication) and the portion of suspended and loosely bound PS tracers (sonicated). A Bonferroni adjusted p value was used for all comparisons, however, no statistical difference ($P > 0.05$) was found for the water samples (A) or the water samples with sediment (B). The asterisk (*) denoted analyses that would not be appropriate for statistical comparisons by a pairwise t-test.

A. Water	EPA MHW	IO
EPA MHW Sonicated	1.00	*
IO Sonicated	*	0.095
B. Sediment	EPA MHW	IO
EPA MHW Sonicated	1.00	*
IO Sonicated	*	0.77

Table 19A. Pairwise comparisons of suspended PS tracers in EPA MHW and IO. Water type comparisons were made based on the suspended and suspended and loosely bound fractions with the *F* and *P* values provided.

Water Type Comparisons		
Pairwise t-test	$F_{1,6}$ **Value**	***P* Value**
Suspended	6.68	0.042
Loosely Bound	5.99	0.05

Table 20A. Results from Welch's ANOVA tests that compared the percent of suspended PS tracers detected after equilibration with water or water with sediment. The statistical tests were separated based on samples that contained suspended PS tracers and samples with suspended and loosely bound PS tracers. Both the suspended ($F_{3,20.52}$ = 27.15, $P < 0.001$) and suspended and loosely bound ($F_{3,20.52}$ = 34.21, $P < 0.001$) treatments were found to be significant.

Welch's ANOVA	$F_{3,20.52}$ **value**	***P* value**
Suspended	27.15	$2.6*10^{-7}$
Suspended & Loosely Bound	34.21	$3.6*10^{-8}$

Table 21A. Results of the Games-Howell pairwise comparison tests using a Bonferroni p value adjustment to compare (A) suspended PS tracers and (B) suspended and loosely bound PS tracers after equilibration in environmental media. All comparisons for the suspended PS tracers were significant ($P < 0.05$) with the exception of IO compared with Sediment and EPA MHW ($P = 0.41$). All the comparisons between the suspended and loosely bound PS tracer treatments were significant ($P < 0.05$).

A.	Sediment/EPA MHW	EPA MHW	IO
EPA MHW	$8.7*10^{-4}$	-	-
IO	0.41	$3.4*10^{-3}$	-
Sediment/IO	$4.1*10^{-2}$	$1.7*10^{-4}$	$1.1*10^{-4}$
B.	Sediment/EPA MHW	EPA MHW	IO
EPA MHW	$8.7*10^{-4}$	-	-
IO	$6.5*10^{-3}$	$1.0*10^{-2}$	-
Sediment/IO	$1.3*10^{-2}$	$2.3*10^{-4}$	$1.2*10^{-5}$

Table 22A. Games-Howell pairwise comparison tests using a Bonferroni p value adjustment grouping results for (A) percent suspended PS tracers and (B) percent of suspended and loosely bound PS tracers after equilibration in environmental media. Groups were designated letters alphabetically with group a indicating the highest percent of PS tracers detected.

A.	Average PS Tracer Percentage (%)	Group
EPA MHW	20.52 ± 9.97	a
Sediment/EPA MHW	4.95 ± 3.92	b
IO	7.21 ± 3.03	b
Sediment/IO	1.36 ± 1.05	c
B.	Average PS Tracer Percentage (%)	Group
EPA MHW	24.77 ± 12.19	a
Sediment/EPA MHW	5.62 ± 3.21	c
IO	10.78 ± 3.62	b
Sediment/IO	2.06 ± 1.12	d

Table 23A. Detection of suspended and loosely bound PS tracer detection after equilibration with site sediment and water. Sediment collected from the sample sites (A-D) was paired with either EPA MHW or IO and detected for suspended PS tracers using spICP-MS. These samples were also sonicated to determine the amount of suspended and loosely bound PS tracers associated with each treatment (Mean and SD; n = 3).

Site	Water Type	Sonicated	spICP-MS MP Average Count	PS Tracer Conc. (MP/ml)	Percent Suspended PS Tracers (%)
A	EPA MHW	No	34.67	$3.1*10^6$	2.02 ± 1.09
A	EPA MHW	Yes	52.00	$2.6*10^6$	1.69 ± 0.86
A	IO	No	14.00	$3.6*10^6$	2.36 ± 1.56
A	IO	Yes	23.33	$2.6*10^6$	1.69 ± 1.33
B	EPA MHW	No	29.67	$6.8*10^6$	4.41 ± 2.05
B	EPA MHW	Yes	30.67	$8.6*10^6$	5.60 ± 1.66
B	IO	No	8.67	$1.8*10^6$	1.19 ± 0.24
B	IO	Yes	17.00	$3.4*10^6$	2.20 ± 0.86
C	EPA MHW	No	61.67	$1.1*10^7$	7.26 ± 5.72
C	EPA MHW	Yes	69.33	$1.0*10^7$	6.50 ± 2.21
C	IO	No	18.00	$1.8*10^6$	1.15 ± 0.00
C	IO	Yes	25.33	$4.7*10^6$	3.06 ± 0.54
D	EPA MHW	No	25.33	$9.4*10^6$	6.11 ± 1.64
D	EPA MHW	Yes	31.33	$1.3*10^7$	8.70 ± 1.89
D	IO	No	12.67	$1.1*10^6$	0.74 ± 0.26
D	IO	Yes	14.67	$2.0*10^6$	1.30 ± 0.26

Table 24A. Results for the ANOVA tests comparing sediment collected from the sample sites (A-D) paired with either EPA MHW or IO. Analysis **(A)** compared each site by the percent of suspended PS tracers where either the EPA MHW ($P = 0.44$) or IO ($P = 0.28$) treatment were significant. Analysis **(B)** compared each site by the percent of PS tracers classified as suspended and loosely bound where the EPA MHW ($F_{3,8} = 5.74$, $P < 0.05$) treatment was significant while the IO ($P = 0.26$) treatment was not significant.

A.		
Water Type	***F*$_{3,8}$ value**	***P* value**
EPA MHW	1.02	0.44
IO	1.52	0.28
B.		
Water Type	***F*$_{3,8}$ value**	***P* value**
EPA MHW	5.74	0.022
IO	1.62	0.26

Table 25A. Results from Fisher's LSD with a Bonferroni adjusted *P* value that compared the sediment from each site by the percent of suspended and loosely bound PS tracers. All site comparisons were found to not be significant ($P > 0.05$).

Site	A	B	C
B	0.36	-	-
C	0.46	1.00	-
D	0.12	0.94	1.00

Table 26A. The mass of Au associated with the water and the sediment portions from the PS tracer partitioning experiments. Each portion was distinguished by sample site and the water paired with that sample (Mean and SD; n=3).

Site	Mass of Au (mg)			
	EPA MHW		IO	
	Water Portion	Sediment Portion	Water Portion	Sediment Portion
A	2.13 ± 0.47	136.77 ± 57.75	1.20 ± 0.10	120.68 ± 40.72
B	1.13 ± 0.17	124.16 ± 23.66	1.00 ± 0.13	94.95 ± 17.33
C	0.82 ± 0.10	137.54 ± 51.38	0.75 ± 0.06	85.65 ± 5.96
D	0.76 ± 0.08	112.81 ± 19.82	0.82 ± 0.11	103.88 ± 13.58

Appendix: Equations

equation 1A.

$$TE = \frac{\frac{STD_I}{STD_M}}{\frac{NP_I}{NP_M}}$$

TE: transport efficiency

STD_I: Standard solution signal

NP_I: Nanoparticle signal

NP_M: Nanoparticle mass

equation 2A.

$$N_p = \frac{f(I_p)}{q_{liq} * TE * t}$$

N_p: Particle number concentration (particles/ml)

$f(I_p)$: Frequency of signal events (particles)

q_{liq}: Sample flow rate (ml/s)

t: Sample analysis time (s)

equation 3A.

$$m_{Au} = f_a^{-1} * \left[\frac{I_p - I_{bgd}}{m * IE}\right]$$

m_{au}: Total gold mass

f_a: mass fraction

I_p: Pulse intensity

I_{bgd}: Background intensity

m: Intensity per mass

IE: Ionization efficiency

equation 4A.

$$NP_{Au} = \frac{m_{Au}}{\frac{\pi}{6} * (D_{AuNP})^3 * \rho}$$

NP_{Au}: Au nanoparticle concentration (particles/MP)

D_{AuNP}: Diameter of Au nanoparticle (cm)

ρ: Au Density (g/cm^3)

Appendix: R Packages

Function	Package	Citation
Tukey's HSD	agricolae	Felipe de Mendiburu (2020). agricolae: Statistical Procedures for Agricultural Research. R package version 1.3-2. https://CRAN.R-project.org/package=agricolae
Levene's Test for Equality of Variances	car	John Fox and Sanford Weisberg (2019). An {R} Companion to Applied Regression, Third Edition. Thousand Oaks CA: Sage. URL: https://socialsciences.mcmaster.ca/jfox/Books/Companion/
Games-Howell Pairwise Comparison	PMCMRplus	Thorsten Pohlert (2021). PMCMRplus: Calculate Pairwise Multiple Comparisons of Mean Rank Sums Extended. R package version 1.9.0. https://CRAN.R-project.org/package=PMCMRplus